Modelling of initiation of bone remodelling due to orthodontic treatment

Leder Horina, Jasna

University of Zagreb

Faculty of Mechanical Engineering and Naval Architecture

Jasna Leder Horina

Modelling of Initiation of Bone Remodelling due to Orthodontic Treatment

DOCTORAL THESIS

ZAGREB, 2015.

University of Zagreb

Faculty of Mechanical Engineering and Naval Architecture

Jasna Leder Horina

Modelling of Initiation of Bone Remodelling due to Orthodontic Treatment

DOCTORAL THESIS

Supervisors:

Tanja Jurčević Lulić, PhD, Full professor

Bert van Rietbergen, PhD, Associate professor

ZAGREB, 2015.

Sveučilište u Zagrebu

Fakultet strojarstva i brodogradnje

Jasna Leder Horina

Modeliranje iniciranja koštane pregradnje kod ortodontske terapije

DOKTORSKI RAD

Mentori:

Dr. sc. Tanja Jurčević Lulić, redoviti profesor

Dr. sc. Bert van Rietbergen, izvanredni profesor

ZAGREB, 2015.

BIBLIOGRAPHIC DATA

UDC	519.6:611.716:616.314
Keywords:	Tooth, orthodontic treatment, bone remodelling, numerical model
Scientific area:	Technical sciences
Scientific field:	Mechanical engineering
Institution:	Faculty of Mechanical Engineering and Naval Architecture (FMENA), University of Zagreb
Supervisors:	Tanja Jurčević Lulić, PhD, Full professor Bert van Rietbergen, PhD, Associate professor
Number of pages:	140
Number of pages (in total):	165
Number of figures:	72
Number of tables:	6
Number of references:	149
Date of oral examination:	01.04.2015
Committee members:	Ivica Smojver, PhD, Full professor Janoš Kodvanj, PhD, Full professor Tomislav Lauc, PhD, Assistant professor Tanja Jurčević Lulić, PhD, Full professor Bert van Rietbergen, PhD, Associate professor
Archive:	FMENA, University of Zagreb

Foreword/Acknowledgments

"Happiness can be found, even in the darkest of times,
if one only remembers to turn on the light."
Steve Kloves

During my studies at the Faculty of Mechanical Engineering and Naval Architecture I discovered the field of biomechanics, which sparked my research interest. Therefore, it was a logical step to do my master thesis in this field. I started to work on my thesis with Professor Tanja Jurčević Lulić, who was my thesis supervisor. We continued our collaboration when I enrolled in the PhD program. Since my master thesis was in the field of dental biomechanics, and during that period I had become familiar with dentistry, the next step was to use that knowledge and expand it to scientific research which has now been completed with this doctoral thesis.

During this period many people have had an influence on my research as well as on me. First I would like to express my gratitude to Professor Osman Muftić, who is no longer with us, but who had a huge influence on me during my studies and at the beginning of my research and work as a research assistant. His positive and open-minded approach opened my eyes not only in research, but in life as well. I would like to express my deepest gratitude to Professor Tanja Jurčević Lulić for her guidance, support, and all the discussions we had in this period. We started this journey many years ago, first with our collaboration on my master thesis, and then during my work on this thesis. I also deeply thank Professor Bert van Rietbergen for accepting me to his group and letting me be part of the University of Eindhoven. That period of time was a great experience for me and I have learned a lot from you. Thank you for your guidance and the discussions we had during my final period of research.

I am also thankful to the committee members, Professor Ivica Smojver, Professor Janoš Kodvanj and Professor Tomislav Lauc for finding time to review my thesis and provide valuable comments and encouragement needed for completing this work.

I also extend my gratitude to Marko Jokić and Boris Jalušić. Marko and Boris, you helped me as colleagues, scientists and friends during this period and I will always be thankful for that. Eduard, Zoran, Marijana and Lana, thank you for moral support, especially in the final period of research. My special appreciation goes to colleagues from 'Friday coffees' and to the rest of the Department of Applied Mechanics for their support.

A very special thank you goes to Monica, Michael and Mary - you have been more than friends to me, you have been my Dutch/Egyptian family. A special thank you also goes to Emanuela, whose advice helped me a lot. Jeroen, thank you is not enough, you have helped me a lot, and I cannot express my gratitude for your patience and help. Nilgoon, thank you for the discussions and for your moral support. Matilde, thank you for the discussions and conversations we had about work, science and life. Salman, thank you for all the help and for our office discussions about everything. Jose, thank you for opening my mind and helping me see the world from a different point of view. Francesca, among everything else , thank you for going to the sports centre. My special appreciation goes to Rody, Stefan, Tim (and Pinar) , Frank (and Elisa), Siavash, Maxime, Maqsood, and all the nice people who I met at TU/e, for their personal support and a friendly attitude. Thank you, Ana and Robi, for helping me at the beginning and during my whole stay in Eindhoven. Agata, thank you for being the best roommate. You all have certainly made my life, at TU/e and around it, easier.

A very special thank you goes to my closest friends, Maja, Martina, Slavica and Jana, for always being supportive, especially in this last period.

My special thanks goes to my parents and my sister. Thank you, mum and dad, for everything! You have been there my whole life as my parents and my friends, helping me and guiding me through life and always putting my needs in front of yours, wishing me all the happiness in the world. Thank you, I would not be here without you!

And last, but not least. My enormous thanks goes to my husband. Slaven, thank you for everything, for being my rock and for being there when I needed you. I could not have done it without your moral support. Thank you for your patience and understanding!

Jasna Leder Horina
Zagreb, March 2015

Contents

List of Figures

List of Tables

Nomenclature

Greek Symbols

α	- Constant characteristic for bone (Idhammad *et al.*), [-]
β	- Experimental data (Stanford), [-]
Γ_c^1 (solid 1), Γ_c^2	- Potentially in contact with boundary, [-]
δg, $\delta\xi^\beta$	- Tangential plane, [-]
ε	- Strain, [-]
θ	- Angle between x_3 in the Cartesian coordinate system and vector **n** (Adachi *et al.*), [rad]
$\hat{\lambda}$	- Lame parameter, [MPa]
λ_u, λ_l	- Index in the stimulus-remodelling rate relation, [-]
μ_x, μ_{water}, μ_{air}	- Linear attenuation coefficient, [-]
ρ	- Apparent density, [g/cm^3]
ρ_c	- Canalicular volume fraction (Adachi *et al.*), [1/rad]
$\dot{\rho}$	- Stress-induced density inhomogeneity, [g/cm^3]
σ	- Stress at the continuum level, [MPa]
σ_t	- Stress at the tissue level, [MPa]
τ	- Time constant, [g/(mm^2(J/g)month)]
$\tau\Delta t$	- Time step, [-]
τ_P	- Shear stress, [MPa]
ϕ	- Bone density (Idhammad *et al.*), [g/cm^3]
φ	- Angle between x_1 axis and the projection of **n** onto the x_1x_2-plane (Adachi *et al.*), [rad]
ψ_t	- Tissue level stimulus (Stanford), [MPa/day]
2ω	- Length of lazy zone (Stanford), [μm/MPa]
$\Delta\omega$	- Remodelling stimulus (Prendergast *et al*), [-]
ω, ω_{RE}	- Damage in the microstructure, [-]

Latin Symbols

AF	- Activation frequency of BMU, [1/t]
B	- Experimental parameter (Fernardez), [$(kg/m^2)^2$]
BV	- Total bone mass, [-]
c	- Constant characteristic for bone (Idhammad *et al.*), [-]
C	- Experimental data (Stanford), [-]
$\dot{\mathbf{C}}$	- Stress-induced anisotropy, [MPa]
D	- Damage variable, [-]
E_i	- Local elasticity modulus, [MPa]
F	- Object function, [MPa]
$f(x,x_i)$	- Decay in signal, [-]
$\hat{G}$	- Lame parameter, [MPa]
$\mathbf{H}$	- Remodelling tensor (Mengoni and Ponthot), [MPa]
HU	- Hounsfield Units
n	- Number of loading cases (Huiskes *et al.*), [-]
$\mathbf{n}$	- Vector (Adachi *et al.*), [-]
$\dot{r}$	- Remodelling rate (Stanford), [mm/s]
r_p	- Radius of osteocyte processes, [nm]
R	- Remodelling variable (Idhammad *et al.*), [MPa]
$R(x,t)$	- Signal that osteocytes sense (Ruimerman *et al.*), [$Jmm^{-3}s^{-1}$]
$2s$	- Length of lazy zone (Huiskes *et al.*), [-]
s, p	- Stress deviator and the pressure (Mengoni and Ponthot), [MPa]
S	- Remodelling stimulus (Huiskes *et al.*), [MPa]
S^j_{strain}	- Remodelling stimulus (McNamara and Prendergast), [-]
S_{oc}	- Remodelling stimulus (Adachi *et al.*), [nm/nm^3]
S_r	- Experimental parameter (Fernardez), [J/kg]
S_{ref}	- Referent value of remodelling stimulus (Huiskes *et al.*), [MPa]
$\overline{\mathbf{t_t}}$	- tangential contact stress, [MPa]
$\overline{u}$, $\overline{\delta\mathbf{u}}$	- Real and the virtual displacement field, [mm]
U_i	- Strain energy density in the bone, [MPa]
U^{ref}	- Change in strain energy density at location j (McNamara and Prendergast), [J/g]

U_{ref}	- Reference stimulus (McNamara and Prendergast), [J/g]
$V_{res},\ V_{form}$	- Volume of resorption cavity, [nm^3]
$W^{int}(\overline{\mathbf{u}})$	- Virtual work associated to the internal forces, [J]
$W^{ext}(\overline{\mathbf{u}})$	- Virtual work related to external forces expect the contact ones, [J]
$\mathbf{Y}$	- Remodelling stimulus (Doblaré and García), [MPa]

Summary

Owing to its interesting properties, bone has always been an appealing area of research. In addition, bone reacts to daily life activities to which it is constantly exposed and its properties are in turn affected. Over the last century, many attempts have been made to describe the mechanical behavior of bone. Different analytical and experimental approaches and later numerical techniques have been exploited in order to explain and understand bone properties. Bone remodelling is the process of resorption of bone tissue material and formation of new bone. These processes are triggered by daily loading and it is constantly happening in the human organism and to all human bones.

To explain the mechanical background of bone remodelling, many theories have been developed. First theories explained bone remodelling in the field of orthopedics, on the femur, where they admit to the existence of the mechanical stimulus. The mechanical stimulus represents the daily mechanical loading on bone. If the bone is in overloaded condition, then bone formation appears. On the other hand, if the bone is in underloaded condition, then bone resorption appears. Theories explaining bone remodelling in orthopedic biomechanics follow and confirm Wollf's Law.

In dental biomechanics, when orthodontic forces have been applied, bone remodelling appears in the alveolar bone. Since in orthodontics there are more tissues involved in bone remodelling in the alveolar bone, alternative theories have been made. These theories take into account the existence of the mechanical stimulus, but adjustments have been made because of the influence of the tooth and the periodontal ligament. Two approaches have been developed to explain bone remodelling in the alveolar bone. The first approach points out that the strains in the bone resulting from orthodontic force cause bone remodelling. The second approach points out that the deformities in PDL cause bone remodelling.

Even though the present orthodontic treatment strategies generally lead to satisfactory results, the biomechanical mechanism which leads to tooth movement is still not fully understood. A better understanding of this mechanism could lead to further optimization of the treatment. The goal of this research was to test whether tooth movement resulting from orthodontic force application can be predicted using load adaptive bone remodelling theories developed in previous studies when applied to the alveolar bone. The hypothesis

analyzed in this research is that the tooth is 'hanging' in the fibrous PDL when loaded by chewing forces, and that orthodontic forces would reduce the loading in the fibres on the side which the tooth is pushed towards and increase the loading in the fibres on the other side. To test this, patient-specific 3D models of tooth and the alveolar bone in combination with validated computational bone remodelling models were used. These models account for the cortical and cancellous bone, as well as the fibrous periodontal ligament. Chewing forces and orthodontic forces were applied as external forces and bone remodelling was predicted from changes in bone tissue loading, which was induced by the orthodontic forces.

In the research that was carried out, bone remodelling initiation caused by wearing a fixed orthodontic appliance was numerically described. Furthermore, the goal was to develop a numerical model that is patient-specific, which would result in a personalized orthodontic treatment. In the research, a single root tooth, the incisor, was used, and the tooth was loaded with the vertical force that describes the chewing force, as well as with the transversal force that describes the influence of the orthodontic force.

The research was carried out in four stages. The first stage was the development of a 2D model, and in this stage the focus was on the numerical description of the PDL and on quantifying the changes in bone loading due to the orthodontic and the chewing force. In the second stage of the research, the 3D geometry of the tooth, the PDL and the bone was defined. The geometry was based on 3D cone beam CT images of the patient. The geometry was obtained by using the Mimics software. In the third stage of the research analyses of the 3D model, obtained in the second stage, were made by using Marc Mentat, the software for finite element analysis. The finite element analysis was performed with three combinations of loads, so that the impact of the load on the model can be analyzed. The influence of the chewing force only, the influence of the orthodontic force only and the influence of both forces acting together was analyzed. The last stage of the research was the development of a bone remodelling algorithm in the Fortran programming language. The bone remodelling algorithm is implemented in Marc Mentat by using a special subroutine. This subroutine calculated the referent value of strain energy density, predicted bone formation, bone resorption and new apparent density as well.

The results confirmed the hypothesis and showed stress distribution and changes in strain energy density during bone remodelling initiation, by showing the underloading side of the bone and the overloading side of the bone, and by initiating bone resorption on the underloading side and bone formation on the overloading side of the bone.

Key words: tooth, orthodontic treatment, bone remodelling, numerical model

Prošireni sažetak

Uvod

Koštana pregradnja je proces kojim se kost trajno obnavlja. Osnovna zadaća koštane pregradnje je uklanjanje oštećenih dijelova kosti te održavanje ravnoteže kalcija u organizmu. Za održavanje normalne mikrostrukture kosti važno je da su u koštanoj pregradnji proces razgradnje i proces stvaranja nove kosti ravnomjerni [1]. Poznato je da mehaničko opterećenje igra važnu ulogu kod koštane pregradnje. Taj problem je prvi puta opisan pomoću Wolffovog zakona. Wolffov zakon kaže da će se kost formirati na mjestu gdje je povećano opterećenje (doći će do povećanja koštane mase), te resorbirati na mjestu gdje je smanjena razina opterećenja (smanjenje koštane mase). Wolffov zakon nije znanstveni zakon u tradicionalnom smislu, već kvalitativno zapažanje i očekivanje koje se odnosi na arhitekturu kosti i raspodjelu naprezanja [2].

Prvu veću nadogradnju Wolffovog zakona napravio je Frost [3, 4, 5, 6] koji je postavio matematičku i mehaničku formulaciju koštane pregradnje pretpostavljajući optimalnu razinu naprezanja iznad i ispod koje se događa pregradnja. On pretpostavlja da lokalna naprezanja reguliraju koštanu masu; ako je razina naprezanja dostigla referentno stanje, nova kost je formirana, a ako je razina naprezanja ispod te točke, kost se resorbira.

Razni istraživači su implementirali navedene zakone u numeričke modele. Modeli koji su se najčešće upotrebljavali su: model koji je razvijen na Sveučilištu u Stanfordu i model koji je razvijen na Sveučilištu u Nijmegenu. Osnovna razlika između modela je različit opis stimulusa pregradnje, a stimulus se može definirati kao skalarni prikaz primijenjenog mehaničkog opterećenja. S mehaničkog stajališta, izotropni Stanfordov model pretpostavlja da je konstitutivni zakon za kost na razini kontinuuma izotropno linearno elastičan, stoga se može zapisati u obliku Hookeovog zakona za male deformacije. Stanfordov model pretpostavlja da je kost potpuno kalcificirana (bez praznina). Resorpcija i formiranje kosti se pojavljuju na unutarnjoj površini, a stimulus je direktno povezan s brzinom pregradnje, te je definiran kao dnevna razina opterećenja tkiva [7, 8, 9, 10]. Nizozemska grupa uzima gustoću energije deformiranja (SED - strain energy density) kao stimulus pregradnje, pa je gustoća energije deformiranja upravljačka varijabla [11, 12, 13].

Prilikom nošenja ortodontskog aparata, da bi se omogućio pomak zuba u željenom smjeru,

treba se pregraditi alveolna kost.
Iako je s ortodontskog stajališta ortodontski tretman vrlo uspješan te vodi ka željenim rezultatima, biomehanička pozadina još uvijek nije u potpunosti opisana te su još uvijek nedovoljno istraženi mehanizmi koji uzrokuju pomak zuba. Bolje razumijevanje tih mehanizama može pridonijeti daljnjoj optimizaciji terapije.

Poticaj izradi ovoga rada su bili nedostaci uočeni u literaturi. Iz pregleda dostupne literature uočeno je da ima još otvorenih pitanja u području biomehanike ortodontskog pomaka zuba. Posljednjih dvadesetak godina područje ortodoncije je jako napredovalo: razvili su se novi materijali i ortodontski aparati su se unaprijedili. Provedeno je mnogo istraživanja s ciljem određivanja raspodjele naprezanja i deformacija u zubu, parodontnom ligamentu (PDL-u) i alveolnoj kosti kod različitih uvjeta opterećenja. Međutim, te analize su provedene uz velika pojednostavljenja geometrije i svojstva materijala. U dostupnoj literaturi moguće je pronaći samo nekoliko istraživanja provedenih u području analize ortodontskih pomaka zuba koja uzimaju u obzir teorije koštane pregradnje. Većina tih istraživanja imaju svoja ograničenja jer pojednostavljuju geometriju, te pojednostavljuju PDL ili ga u potpunosti zanemaruju.

Teorije koštane pregradnje koje se temelje na Wolffovom zakonu uspješno su primijenjene te opsežno istražene u području ortopedske biomehanike, ali navedene teorije nisu u uporabi u ortodonciji. U području ortodontske biomehanike, koriste se alternativne teorije da bi se opisao pomak zuba. Postojeći modeli koji opisuju proces koštane pregradnje alveolne kosti uvjetovane ortodontskom silom [14, 15, 16, 17] se uglavnom temelje na empirijskim pravilima, a ne na fundamentalnoj teoriji pregradnje koja se temelji na prilagodbi kosti opterećenju. Stoga, navedeni modeli nailaze na limite koji uglavnom proizlaze iz nedovoljno definirane geometrije, korištenja empirijski poznatih metoda, kao i nedovoljno objašnjenih mehanizama koji potiču proces pregradnje i pomak zuba. Postoji više pristupa opisu problema. Prvi se temelji na pretpostavci da je deformacija PDL-a ključni stimulus koji potiče koštanu pregradnju i time omogućuje pomicanje zuba. Drugi pristup se temelji na pretpostavci da su deformacije alveolne kosti glavni uzrok koštane pregradnje [18, 14, 16, 19, 20, 21, 22].

Ciljevi i hipoteza istraživanja

Wolffov zakon se ne može direktno primijeniti prilikom opisa koštane pregradnje koja je uvjetovana ortodontskom silom. Prema Wolffovom zakonu, za očekivati je da će se pojaviti

veće naprezanje na strani kosti na koju se zub potiskuje, te da će tu doći do formiranja kosti, ali kod djelovanja ortodontske sile, u smjeru djelovanja sile dolazi do resorpcije kosti, a na suprotnoj strani dolazi do formiranja kosti, što je zapravo u suprotnosti s Wolffovim zakonom.

Nije moguće da se pregradnja alveolne kosti odvija drugačije nego kod ostalih kostiju, a to neslaganje može se objasniti postojanjem PDL-a koji ima važnu ulogu u prijenosu opterećenja sa zuba na kost. PDL po svojoj strukturi spada u meka tkiva, te se sastoji od snopova vlakana zatim stanica koje izgrađuju PDL, kost i zub, međustanične tvari, krvnih i limfnih žila. Zbog svoje složene strukture te iznimne važnosti u samom procesu, PDL je vrlo teško opisati numerički. U literaturi su navedena dva pristupa opisa PDL-a, jedan pristup opisuje PDL samo kao vlakna, dok drugi pristup opisuje PDL kao kontinuum [23, 24, 25, 26, 27].

Cilj istraživanja provedenog u okviru disertacije je bio ispitati mogu li se ranije razvijene teorije koštane pregradnje koje se temelje na prilagodbi kosti opterećenju primijeniti na alveolnu kost prilikom opisa pomaka zuba uslijed djelovanja ortodontske sile. Postavljena je hipoteza da zub, kada je opterećen žvačnom silom, „visi“ između vlaknima obogaćenog PDL-a, a ortodontska sila smanjuje naprezanja u vlaknima na strani na koju se zub ”pritišće” (tlačno opterećena strana), te povećava naprezanja u vlaknima na suprotnoj strani (vlačno opterećena strana). Pretpostavljeno je da je moguće, u skladu s Wolffovim zakonom, uzimajući u obzir realniji opis parodontnog ligamenta, točnu geometriju sustava kost-ligament-zub te djelovanje ortodontske i žvačne sila, numerički opisati iniciranje koštane pregradnje gdje se na tlačno opterećenoj strani inicira resorpcija kosti, a na vlačno opterećenoj strani formiranje kosti. Također, pretpostavljeno je da će predloženi model iniciranja koštane pregradnje dati bolju fizikalnu sliku modelirane pojave, te omogućiti predviđanje iniciranja koštane pregradnje i pomaka zuba.

Metodologija istraživanja

U okviru istraživanja numerički je opisano iniciranje koštane pregradnje koja je uvjetovana nošenjem fiksnog ortodontskog aparata te model koji je svojstven za pojedinog pacijenta, čime je omogućen individualni pristup pacijentu tokom ortodontskog tretmana. Promatran je jednokorijenski zub, sjekutić, koji je opterećen vertikalnom silom, koja opisuje djelovanje žvačne sile, te poprečnom silom i momentom, koji opisuju djelovanje ortodontske sile. Ortodontske sile su razmjerno malog iznosa, svega nekoliko N, u usporedbi sa žvačnim silama koje mogu biti iznosa i do 100 N [24, 25, 18, 16, 22]. Ukoliko je ortodontska sila većeg iznosa od preporučenog, zbog toga što je konstantna, može uzrokovati stvaranje

hijalonskih zona koje kasnije vode k patološkoj pregradnji, što je neželjeni efekt.
Kao što je navedeno, u postojećoj literaturi su postavljene razne hipoteze koje pokušavaju opisati proces koštane pregradnje, ali sve imaju svoje limite jer pojednostavljuju PDL ili ga u potpunosti zanemaruju, ili pak pojednostavljuju geometriju.
Metode iz postojeće literature opisuju samo djelomično problem koji se događa prilikom procesa koštane pregradnje uvjetovane ortodontskom silom. Stoga je u doktorskom radu postavljena hipoteza koja ne narušava Wolffov zakon te se temelji na ideji da će do iniciranja koštane pregradnje doći zbog promjena u opterećenju, ali glavni temelj hipoteze leži u činjenici da zub „visi“ između mreže vlakana koja se nalazi u PDL-u i povezuje kost i zub, te kada se primijeni ortodontska sila, istezanje vlakana će voditi k većem opterećenju kosti na mjestu suprotno od smjera primijenjenog opterećenja (preopterećeni uvjeti), dok će se opterećenje na suprotnoj strani smanjiti (podopterećeni uvjeti). To dovodi do formiranja kosti na preopterećenoj strani, te resorpcije kosti na podopterećenoj strani, što zapravo znači da će se omogućiti pomak zuba u smjeru djelovanja sile (taj dio kosti je podopterećen te se resorbira), dok s druge strane kosti neće nastati mikrošupljine, već će se kost popuniti procesom formiranja. Također, u obzir je uzeto ne samo djelovanje ortodontske, već i djelovanje žvačne sile. Razlog tome je da mala poprečna sila, koja opisuje djelovanje ortodontske sile u kombinaciji sa žvačnom silom stvara moment koji vodi k promjenama u kosti, gdje dolazi do resorpcije kosti na tlačnoj strani PDL-a, te formiranja kosti na vlačnoj strani. Navedena hipoteza koja uključuje deformacije u PDL-u te kombinaciju djelovanja ortodontske i žvačne sile na mehaničko okruženje kosti potvrđuje dosadašnja saznanja o ponašanju kosti pod opterećenjem, gdje obuhvaća i Wolffov zakon te ranije dokazane eksperimente na životinjama [28, 29].
Prva faza istraživanja obuhvatila je izradu 2D modela koji se sastoji od kosti, njezinog kortikalnog i trabekularnog dijela, PDL-a i zuba, a zub se sastojao od cakline, dentina i cementa. Prva faza istraživanja imala je fokus na numeričkom opisu PDL-a, budući da je PDL meko tkivo, te samim time ima drugačije mehaničko ponašanje nego ostatak modela. PDL se sastojao od matrice i vlakana. Pod pojmom vlakna podrazumijevaju se kolagena vlakna postavljena horizontalno, te pod tri različita kuta u odnosu na referentnu ravninu, dok pojam matrica podrazumijeva ostatak supstanci u PDL-u. Cilj ove faze istraživanja bio je kvantificirati promjene opterećenja kosti zbog djelovanja ortodontske i žvačne sile.
U drugoj fazi istraživanja, definirana je trodimenzionalna geometrija zuba, PDL-a i kosti. Geometrija je dobivena iz CT snimaka snimljenih na cone beam CT-u (CBCT). Korištene snimke su snimke stvarnih pacijenata kojima je preporučena ortodontska terapija. Iz snimaka je dobivena geometrija pomoću programa Mimics. Mimics omogućava ne samo dobivanje željene geometrije, već i definiranje gustoće kosti koja je svojstvena za pojedinog

pacijenta, te je moguće personalizirati ortodontsku terapiju.
U trećoj fazi se, na temelju utvrđene geometrije jednokorijenskog zuba, generirala mreža konačnih elemenata. Mreža konačnih elemenata je definirana za svaki pojedini dio modela, te samim time i svojstva materijala. Budući da je debljina PDL-a puno manja od ostalih dijelova modela, bilo je potrebno riješiti kompatibilnost mreža konačnih elemenata na spoju zuba, PDL-a i kosti, te je mreža konačnih elemenata pojedinih modela međusobno povezana rubnim uvjetima kontakta. Na taj način je postignuto da se prilikom opterećenja, međusobno zasebne mreže ponašaju kao jedan model.
Za analizu 3D modela konačnim elementima koristio se softver Marc Mentat, MSC.Software grupe. Model je uveden s pripadajućom mrežom, svojstvima materijala te gustoćom koja je definirana za kost. Prilikom modeliranja PDL-a uzeta su u obzir realna svojstva vlakna i matrice. Vlakna su opisana spring elementima na način da povezuju čvorove kosti sa čvorovima zuba, te svaki od spring elementa predstavlja više stotina snopova vlakana. Vlakna su postavljena horizontalno i pod kutom da bi što vjernije opisala realnu situaciju. Izabran je ovaj način opisa vlakana jer u stvarnosti vlakna se nalaze djelomično u kosti, te djelomično u zubu i na taj način povezuju zub s kostima izvršavajući svoju osnovnu ulogu, amortizaciju opterećenja koja nastaje na zubima. Prilikom analize konačnim elementima u Marc Mentatu, zbog analize utjecaja opterećenja na model, primijenjene su tri kombinacije opterećenja: djelovanje samo žvačne sile, djelovanje samo ortodontske sile, te djelovanje obje sile zajedno.
Provedene su analize koje opisuju četiri različita tipa ortodontskog pokreta: nekontrolirano naginjanje (*uncontrolled tipping*), kontrolirano naginjanje (*controlled tipping*), pomak zuba translacijom (*bodily movement*) i rotacija zuba oko uzdužne osi (*rotation*). Prvo je provedena analiza sa žvačnom silom gdje je dobivena referentna vrijednost opterećenja u kosti, referentna vrijednost gustoće energije deformiranja, te nakon toga analiza koja uzima u obzir djelovanje žvačne i ortodontske sile zajedno. Ukoliko je u karakterističnim područjima opterećenje veće od referentnog, vladaju preopterećeni uvjeti i to vodi k formaciji kosti, a ukoliko je opterećenje manje od referentnog, vladaju podopterećeni uvjeti i to vodi k resorpciji kosti.
Zadnja faza istraživanja obuhvaćala je implementaciju algoritma za koštanu pregradnju. Algoritam je razvijen u programskom jeziku Fortran koji se pomoću specijalnih rutina povezuje s Marc Mentatom. Marc Mentat omogućava korisničko programiranje da bi se mogle izračunati željene vrijednosti i prikazati ih. Algoritam je pozvan pomoću tri glavne Marc Mentatove rutine, koje potom pozivaju ostale, korisnički definirane, rutine. Rutine omogućavaju računanje referentne vrijednosti gustoće energije deformiranja, tj. referentni stimulus. Zatim rutine omogućavaju računanje gustoće energije deformiranja u

svakoj integracijskoj točki uspoređujući izračunate vrijednosti s referentnom vrijednošću. Ukoliko je vrijednost dobivene gustoće energije deformiranja veća od referentne, događa se formiranje kosti, suprotno se događa resorpcija kosti. Također, algoritam omogućava izračun nove vrijednosti prividne gustoće.

Aktivnosti u okviru istraživanja provodile su se na Katedri za biomehaniku i ergonomiju Fakulteta strojarstva i brodogradnje Sveučilišta u Zagrebu i na Fakultetu za Biomedicinsko inženjerstvo Tehničkog sveučilišta u Eindhovenu, Nizozemska. CTCB snimke ustupila je Stomatološka poliklinika Apolonija, Zagreb.

Rezultati i zaključak

Dobiveni rezultati su uspoređivani s rezultatima iz dostupne literature. Rezultati dobiveni ovim istraživanjem prikazali su promjenu gustoće energije deformiranja prilikom iniciranja koštane pregradnje na način da prikazuju podopterećenu stranu kosti i preopterećenu stranu kosti inicirajući resorpciju na podopterećenoj strani te formiranje kosti na preopterećenoj strani kosti. Budući da je, prema teorijama koštane pregradnje, gustoća energije deformiranja povezana s promjenom gustoće kostiju, pomoću gustoće energije deformiranja pratila se pregradnja alveolne kosti. Također, uz pomoć algoritma za koštanu pregradnju, prikazana je i promjena gustoće koja nastaje uslijed djelovanja opterećenja. Algoritam je također omogućio prikaz stimulusa koji je pokazao područje formiranja kosti kao i područje resorpcije kosti. Nakon uspoređivanja s literaturom, vidljivo je da rezultati pokazuju područja formiranja kosti kao i područja resorpcije kosti kao što se mogu pronaći u literaturi te su ujedno potvrdili biološki proces koji se odvija u kosti [30, 14, 22, 17].
Znanstveni doprinos istraživanja provedenog u doktorskom radu predstavlja izrada numeričkog modela iniciranja koštane pregradnje koji je obuhvatio realniji opis parodontnog ligamenta nego što se može pronaći u dostupnoj literaturi [30, 14, 22], zahvaljujući CT snimkama točnu geometriju sustava kost-ligament-zub te djelovanje ortodontske i žvačne sile, a koji omogućuje u skladu s Wolffovim zakonom, na temelju promjena opterećenja koštanog tkiva, pouzdanije predviđanje ponašanja zuba i alveolne kosti nego što je moguće u dostupnoj literaturi [31, 15, 22, 16, 17].
Također, model je pridonio objašnjenju fizikalnih mehanizama kod iniciranja koštane pregradnje i boljem razumijevanju stvarne prirode ortodontskog pomaka zuba.
Korištena je individualna 3D geometrija koja omogućuje, uz definiranje fizikalnih svojstava alveolne kosti, individualni pristup pacijentu.

Ključne riječi: zubi, ortodontska terapija, koštana pregradnja, numerički model

1 Introduction

1.1 Motivation

Orthodontics, also known as dental-facial orthopedics, is a specialization of dental medicine that correct dental malposition and malformations of the jaws and improve chewing, respiration, speech and aesthetics. Orthodontic treatment uses fixed or removable appliances on the teeth that cause gradually imposed progressive and irreversible bone deformation, which leads to tooth movement in desired position [32].

Orthodontic treatments are limited to dental displacement, and dental movement is achieved through bone adaptation to external mechanical stimuli. During orthodontic treatment, fixed or removable appliances impact the teeth by using therapeutic forces called orthodontic forces. Orthodontic forces modify the physiological equilibrium and affect on the tooth,thus correcting its position. As a result, the tooth will gradually move through the surrounding bone and the treatment is continued until a satisfying result is obtained. The process of bone remodelling allows tooth movement in the way so that bone resorption happens in the direction of tooth movement, and on the other side, bone apposition takes place [32].

Many orthodontics treatment strategies are mostly based on models that implement data obtained from empirical studies [33]. In most cases the treatment follows a rather standardized schedule, even though there can be large differences between different cases. As result, frequent follow-up visits and corrections of the treatment are necessary. Whereas the final result thus might be satisfactory in most cases, it is quite possible that the efficacy of the treatment can be much improved, possibly leading to less frequent visits and shorter treatment periods.

The first approach towards a more efficient treatment would be to move from models based on standardized empirical rules to models that include patient-specific factors. Even though orthodontic tooth movement as a result of orthodontic force application is visible, the physiological reaction is different for every patient, so the treatment needs to be monitored and adjusted regularly [34]. A patient-specific model should be a simulation-based model which consists of exact patient geometry and a remodelling rule that numerically describes the process in the bone.

Geometry used for developing patient-specific model should consist of the exact geometry of the patient recommended for orthodontic treatment. To obtain the exact geometry, the best approach is to use CT-scans or MRI. These scans will provide the relevant geometry with high accuracy, which can be used for developing a numerical model. Also, another advantage of this approach is to obtain data about the patient's bone density which will be used as input data on bone remodelling description.

In orthodontic tooth movement three tissues have an important rule, the periodontal ligament (PDL) and the alveolar bone. Both tissues need to adjust in order to allow tooth movement. Adjustment implies the biological process of bone remodelling, and PDL stretching and transmitting force to the alveolar bone. As it is seen, orthodontic treatment couples biological and mechanical reactions into one biomechanical model. A mechanical description of bone remodelling was made by Wolff, 1892, in which he articulated Wolff's Law [3]. Wolff's Law is not a law in the traditional sense, but rather a qualitative observation of observed phenomena. Wolff's law states that bone will be formed on the side where bone loading is increased and removed on the side where bone loading is reduced. Whereas the bone remodelling theories based on Wolff's law have been successfully applied and tested extensively in the field of orthopedic research, they are not widely used in orthodontics. In that field, alternative theories have been introduced instead to explain tooth movement. These models [15, 16, 17] are usually based on empirical rules rather than on a fundamental load-adaptive bone remodelling theory. Many alternative theories have been put forward to describe bone remodelling induced by orthodontic force, but if they are viewed separately, their disadvantages are visible. One approach claims that bone remodelling induced by orthodontic force appears because of strains in the bone. This approach does not take into account the influence of PDL, which has a role in the orthodontic process. Another approach takes into account the influence of PDL, but PDL is usually described as continuum, and the approach does not take into account the influence of PDL fibres that play an important role in the whole process.

The reason for this lack of using Wolff's Law is that it is not obvious that it can describe bone remodelling induced by orthodontic force [34]. When the tooth in the bone is simply considered similar to a 'pole' in the 'soil', one would expect high compressive stress in the bone on the side to which it is pushed, but in fact bone resorption is visible here. One would also expect reduced stress on the other side, where in fact bone apposition takes place. This is obviously not in agreement with with Wolff's Law. Since it is unlikely that load bone remodelling in the alveolar bone would be opposite to load bone remodelling elsewhere in the body, a more likely explanation for this mismatch is that the simplified representation of a tooth as a 'pole in the soil' does not hold. A likely reason for this is that the PDL plays an important role in the load transfer from the tooth to the bone. By its structure the PDL is a soft tissue, and it consists of fibre bundles, cells that build the PDL, intercellular substance, blood and lymph vessels. Its complex structure makes it hard to describe the material properties of the PDL [35, 21].

In this research the focus was on the mechanical approach in describing bone remodelling. Phenomenological aspects of biology was taken into account as well. This leads to a numerical description of bone remodelling initiation in the alveolar bone induced by orthodontic force. The numerical model, which consists of patient-specific geometry of tooth, the periodontal ligament and bone, its cortical and trabecular part, are described with Finite Element Method (FEM). This allows for mechanical behavior prediction of biological tissue, which is hard to measure *in vivo* [31]. Also, the advantage of use of FEM is that it can deal with complex geometry, as it is used in this research, and also takes into account complex boundary and contact condition [19].

The motive behind this research are the disadvantages observed in literature. The literature review shows that there are still open questions in the field of biomechanical tooth movement [19, 22, 17]. In the last twenty years the field of orthodontics has improved a lot, new materials have been developed and orthodontic appliances have been optimized [16]. There are numerous studies that describe stress and strain distribution in the tooth, the PDL and the alveolar bone caused by different loading [16, 17, 36], but only a few studies offer analyses of bone remodelling induced by orthodontic tooth movement [31, 15, 22]. Most of these studies are limited because they simplify geometry, the PDL or even completely ignore the PDL. Also, the mechanism that describes tooth movement is still not understood enough. The proposed research should contribute to a better understanding of the real nature of tooth movement. The exact geometry of tooth-bone-PDL allows patient-specific approach of numerical simulation and is giving new paradigm of orthodontic treatment

and treatment planning.

1.2 Hypothesis

In the literature review it can be seen that load-adaptive bone remodelling theories that are based on Wolff's Law are successfully used in orthopedic biomechanics [12, 13, 8, 37], but are not widely used in orthodontics [31, 15, 22], alternative theories have been introduced to explain tooth movement [38]. These theories can be divided into two groups [38], one group uses the approach that the deformations of the periodontal ligament are the key the key stimulus for orthodontic tooth movement and orthodontic bone remodelling, and the other approach is that the deformations of the alveolar bone are the basis for orthodontic bone remodelling. These approaches are based on empirical rules, they simplify the geometry and the periodontal ligament, or also even completely ignore the periodontal ligament. The most important element here is that these approaches partially or wholly disagree with Wolff's Law, which leads to the conclusion that the bone remodelling process is different in the alveolar bone than in other bones in the human body, what is biologically inexplicable.

Methods found in existing literature only partially describe the problem that occurs during bone remodelling caused by orthodontic force. The hypothesis of this research does not violate Wolff's law. The hypothesis is based on the fact that teeth are "hanging" within the network of fibers that form the PDL and connect the tooth with the bone. When orthodontic force is applied, the stretching of the fibers will lead to higher bone loading on the side of the bone opposite to the loading direction (the tensile side where there is overloaded condition), whereas the loading on the compressive side, where there is underloaded condition, will actually be reduced. This leads to bone formation on the tensile side, and bone resorption on the compressive side, which means that tooth movement will occur in the direction of applied force [39]. Also, the research will not only consider consider orthodontic force, but also the influence of chewing force, which is considered to be a daily loading level. The hypothesis, which includes deformations in the PDL and PDL fibres and the combined action of of orthodontic and chewing forces on the mechanical environment, confirms today's knowledge of bone behavior under loading, including Wolff's Law and earlier experiments on animals [28].

The purpose of this research is to test if bone remodelling initiation resulting from orthodontic force application can be predicted by using load adaptive bone remodelling

theories developed in earlier studies when applied to the alveolar bone [12, 13, 8, 37]. The hypothesis investigated here is that the tooth is 'hanging' in the fibrous PDL when loaded by chewing forces, and that orthodontic forces would reduce the stresses in the fibres on the side which the tooth is pushed towards and increase the stresses in the fibres on the other side [40]. To test this, patient-specific 3D models of tooth and the alveolar bone are used.

The hypothesis of the proposed research is:
In accordance with Wolff's Law and taking into consideration a realistic description of the periodontal ligament, the exact geometry of the bone-ligament-tooth system and the action of the orthodontic and the chewing force, it is possible to numerically describe the bone remodelling initiation where bone resorption is initiated on the compressive side and bone formation on the tensile side. It is assumed that the suggested model will give a more accurate physical picture of the modelled behavior and allow for the prediction of the bone remodelling initiation and tooth movement.

1.3 Expected scientific contribution of proposed research

The scientific contributions of the proposed research are as follows. The first contribution is the development of a numerical model of the bone remodelling initiation, which includes a realistic description of the periodontal ligament, the exact geometry of the bone-ligament-tooth system and the action of the orthodontic and the chewing force, and which allows for a more reliable prediction of the tooth and the alveolar bone behaviour based on the changes in bone tissue loading then it can be found in todays literature. The next contribution is a description of the physical mechanism of the bone remodelling initiation and a better understanding of the real nature of the orthodontic tooth movement. The last contribution is the use of a personalized 3D geometry that would define the geometry and physical properties of the alveolar bone of a specific patient.

1.4 Outline of the thesis

This thesis is organized in six chapters. Following this introduction, Chapter 1 and Chapter 2 give a gives a brief overview of biology and orthodontics. The first part of Chapter

2 gives biological overview of bone, teeth and the periodontal ligament, and after that an insight into orthodontics is given, in which orthodontic tooth movement and types of orthodontic tooth movement are described. The last part of the second chapter is CT imaging overview, where CBCT is described. Chapter 3 gives literature overview. First it starts with a description of the mechanical properties of bone, followed by a mechanical description of bone remodelling. Afterwards, it gives insight into models developed in orthopedic biomechanics, and finally it describes models and approaches used in describing bone remodelling in orthodontics. Chapter 4 deals with the methodology of this research, in which the hypothesis is tested by developing 2D and 3D model. This chapter describes a numerical model of the physical mechanism of the bone remodelling initiation, including a realistic description of periodontal ligament, the exact geometry of the bone-ligament-tooth system which is loaded with orthodontic and chewing force. Chapter 4 also provides a description of a bone remodelling algorithm, which is used to describe the bone remodelling initiation. The algorithm is using SED as referent value, and then compares the newly calculated SED with referent value. In Chapter 5the results of the research are shown. 2D and 3D models are shown, which give a more reliable prediction of the tooth and alveolar bone behaviour based on the changes in the bone tissue loading by showing the underloading side of the bone and the overloaded side of the bone, initiating bone resorption on the underloading side and bone formation on the overloaded side of the bone, and confirming the proposed hypotheses. The algorithm provides data about the changes in densities that occur during the loading and also shows values of the mechanical stimulus. The concluding remarks are given in Chapter 6.

2 A biological and orthodontics overview

2.1 Biological description

The adult skeletal system consists of approximately 206 bones. Bones are associated with connective tissues, including cartilage, tendons and ligaments. The number of bones varies from person to person in accordance with age and genetic factors. Each bone is actually an organ that plays a part in the overall functioning of the skeletal system. The bones of the skeleton serve the mechanical function of supporting and protecting the body and permitting body movement. With regard to metabolic function, blood cells are produced and minerals are stored in the bones. All bones are formed through the process called ossification, the process of laying down new bone material. Ossification starts in prenatal development. Each bone has a characteristic shape and surface features that suggest its relationship to other bones, muscles and the body as whole. Bone tissue is composed of several types of bone cells embedded in a matrix of inorganic salts (calcium and phosphorus) and collagen fibers. Bone cells and ground substance give bone flexibility and strength, while the inorganic salts give it hardness [41]. Bone consists of trabecular and cortical bone. Trabecular bone is positioned on the inner side of bone, it is softer and weaker than cortical bone, and more flexible. Cortical bone covers the outside surface of the bone. Cortical bone is dense and it supports the weight of the body.
In this research the focus will be on the skull, or more precisely, the jaw. The skull consists of cranial and facial bones. The eight bones of the cranium form tight unions to enclose and protect the brain and the sensory organs. The cranial bones consist of one frontal bone, two parietal bones, two temporal bones, one occipital bone, one sphenoid bone, and one ethmoid bone. Bones of the skull are shown in Figure 2.1. The 14 facial bones shape the face, support the teeth, and provide attachment for the muscles that move the jaw and produce facial expression. With the exception of the vomer and the mandible, all facial bones are paired.

In order to describe body parts and positions correctly, a set of anatomical positions and directional terms has been developed. The anatomical reference point is a standard body position called the anatomical position. In the anatomical position, the body is erect, the palms of the hand face forward, the thumbs point away from the body, and the feet are slightly apart. To describe correctly the anatomical position of the human body, anatomical planes and orientation are used. An anatomical plane is a structure used to transect the human body, in order to describe the location of structures or the direction of movements. The anatomical position of the human body described by anatomical plane and orientation is shown in Figure 2.2. In human and animal anatomy, three basic planes are used:

- the *coronal* plane - (also known as frontal) plane is perpendicular to the ground, which (in humans) separates the anterior from the posterior, the front from the back, the ventral from the dorsal;
- the *sagittal* plane - (also known as lateral) plane is perpendicular to the ground, which separates left from right; the midsagittal plane is the specific sagittal plane that is exactly in the middle of the body;
- the *transverse* plane - (also known as axial or horizontal) plane is parallel to the ground, which (in humans) separates the superior from the inferior, or put another way, the head from the feet.

Orientation is defined according to directions relative to the body axis:

- *superior/inferior* - placement of a body structure along the long axis of the body, divides the body into upper and lower;
- *anterior/posterior* - the most anterior structures or surfaces are those that are most forward (face, chest, abdomen), posterior structures or surfaces are those toward the backside of the body;
- *medial/lateral* - toward the midline/away from the midline;
- *proximal/distal* - nearer the trunk or attachment end/farther from the trunk or point of attachment, used primarily to locate various areas of the body limbs.

In dentistry,the position of the specific tooth is also described by using three planes, but these planes are called frontal, medial and occlusal plane, as shown in Figure 2.3 (a). Also, there is a special set of terms, orientation points and areas, that explain completely the position of the tooth, (Figure 2.3 (b)), are:

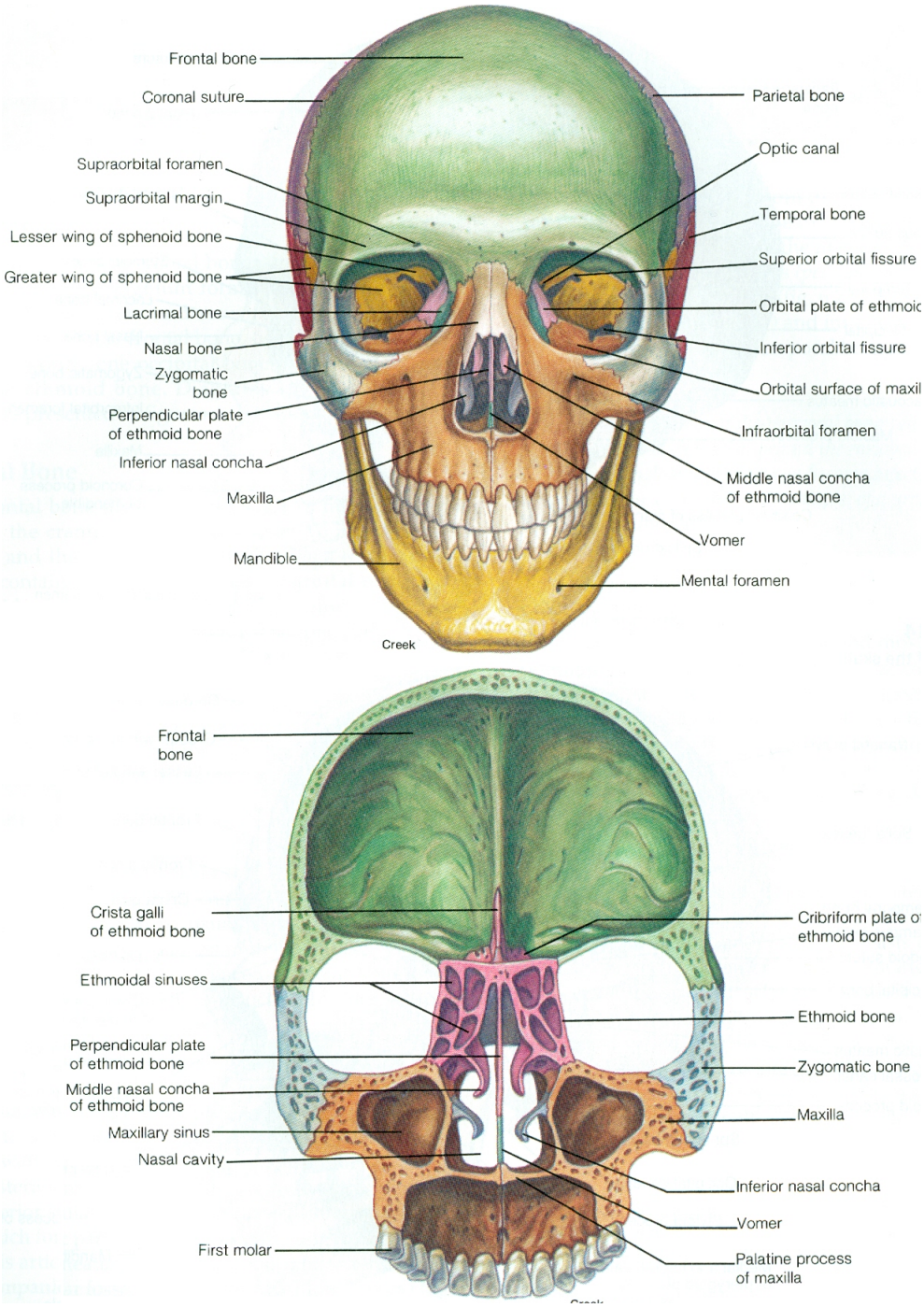

Slika 2.1: Bones of the skull [41]

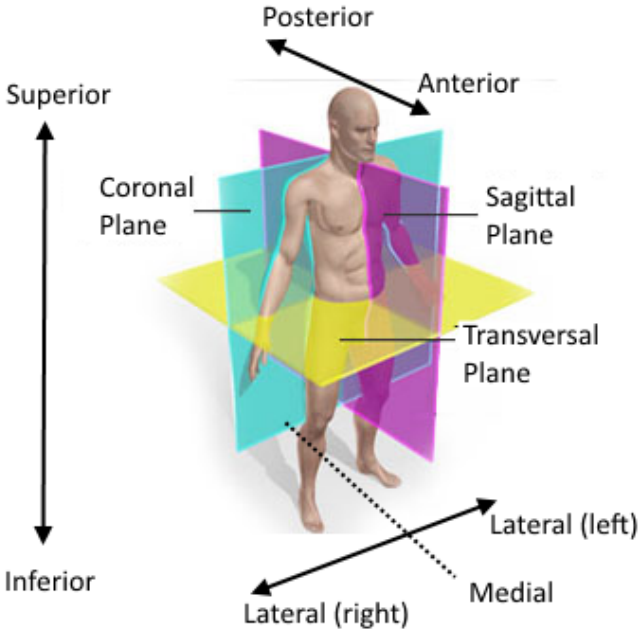

Slika 2.2: Anatomical planes and orientation[42]

- *lingual* - facing the tongue;
- *labial* - facing the lips;
- *apical* - towards the apex of a tooth;
- *coronal* - towards the crown of a tooth.

Teeth position in jaw and its shape are determined by genetics, the relationship between the cheek, the tongue and the joint, the equilibrium of facial forces, which includes the tongue and lips, chewing force and all other forces that have influence during growth and development.

Teeth are positioned in neutral position, where application of all forces is equal or almost zero. Muscle forces of the cheek and the tongue enable proper positioning in vestibulo-oral direction. During lifetime teeth tend to move or lean in mesial direction, and in normal conditions that will not influence the equilibrium in the mouth. However, if one or more teeth are lost, teeth can lean so much that the equilibrium and the whole chewing system can be seriously disturbed [43].

It can be seen that forces in the mouth can influence the equilibrium of the teeth when the jaw disturbs the unstable physiological equilibrium [43]. Representation of muscular and anatomical forces on the mandible in a physiological test is shown on the Figure 2.4 [44]. Figure 2.4 shows the arrangement of the muscles of mastication, the condyles,

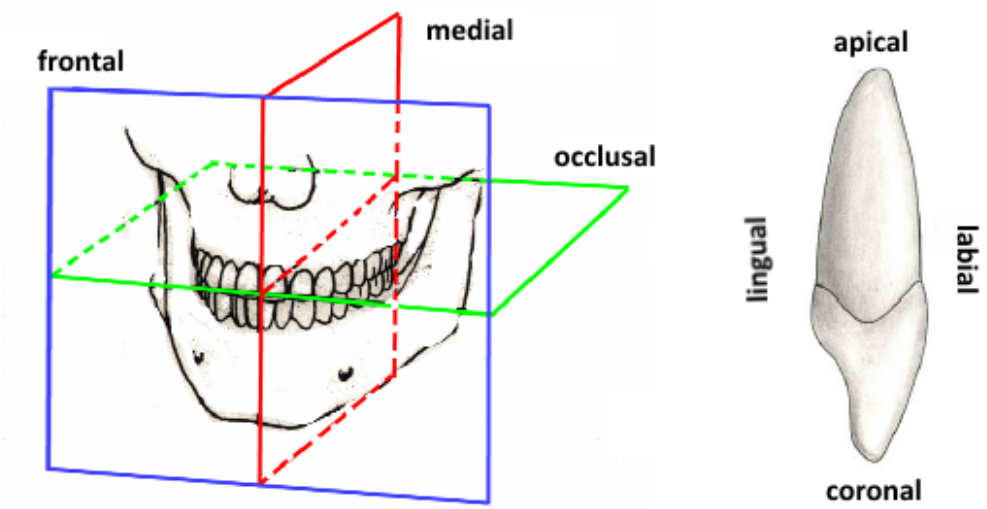

Slika 2.3: Dental planes (a) and orientation points and areas (b) [43]

and the tooth row described relative to a coordinate system. The x, y and z coordinates were determined for the centroids of the origins and insertions of the masseter (M_1, M_2), anterior temporalis (M_3, M_4), medial pterygoid (M_5, M_6), lateral pterygoid (M_7, M_8), and anterior digastric muscles (M_9, M_10). Arrows demonstrate the approximate direction of muscle pull. Positions of condylar forces ($F_{condyle,R}$, $F_{condyle,L}$) and mandibular teeth are also represented.

Every tooth is in specific relationship to its neighboring tooth in both jaws. The upper incisors are bigger than the incisors in the lower jaw, so the dental arch of the maxilla (upper jaw) is bigger than the dental arch of the mandible (lower jaw). Viewed from the horizontal plane the maxillary dental arch has the shape of an ellipse and the mandibular dental arch has the shape of a parabola [43]. Shapes of dental arches are shown on Figure 2.5.

Viewed on the sagittal plane, all teeth in the mandible and the maxilla are leaning in mesial direction, which means that dental axes are focused forward in regard to the occlusal plane. Leaning of dental axes is shown on Figure 2.6. This kind of position of teeth enables correct occlusion contact (relationship between the maxillary and mandibular teeth when they approach each other) between non-congruent arches.

As a consequence of this relationship, two curves which define the position of occlusion surface in three-dimensional view can be determined. These curves are *curve of Spee* and *curve of Wilson*, shown on Figure 2.7. *Curve of Spee* is defined as the curvature of the mandibular occlusal plane beginning at the tip of the lower cuspid and following the buccal cusps of the posterior teeth, continuing to the terminal molar. *The curve of Wilson* is a

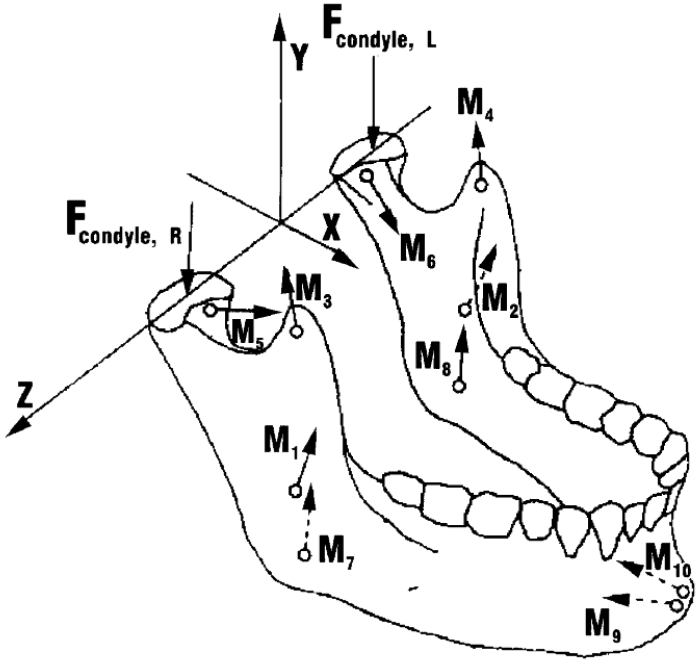

Slika 2.4: Forces of muscles [44]

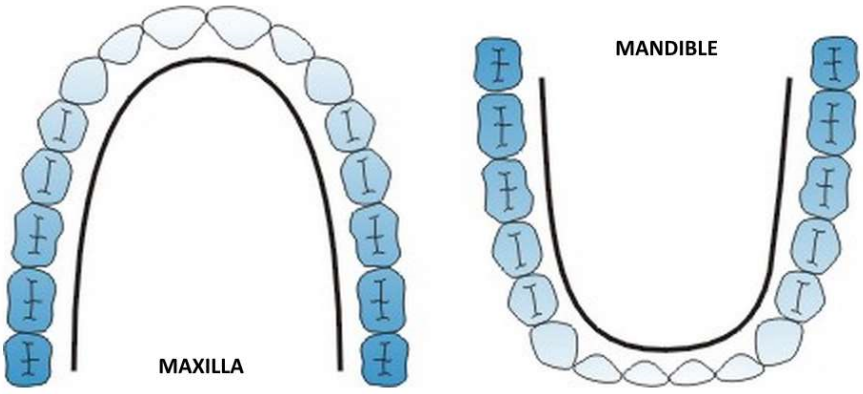

Slika 2.5: Dental shape [43]

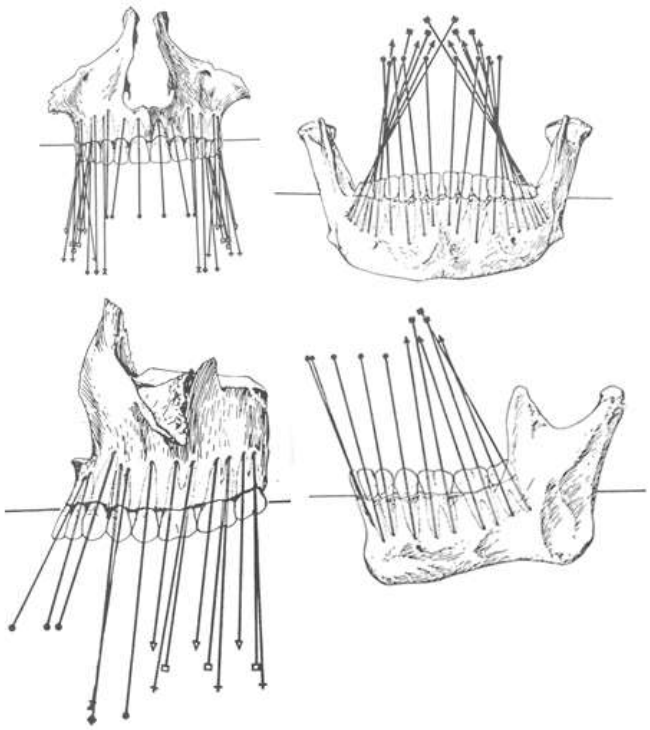

Slika 2.6: Dental axis [43]

curve, viewed from the front, that contacts the buccal and lingual cusps of the molars, being lower in the middle due to the lingual inclination of the long axes of the mandibular molars.

2.1.1 Teeth and environment

Teeth are small, calcified, hard, whitish structures, made of multiple tissues of varying density and hardness. The main function of the teeth is mechanical, where they chop up food into small pieces by cutting and crushing it in preparation for swallowing and digestion. They are named by their set, arch, class, type, and side.
Humans have two sets of teeth in their lifetime. The first set of teeth to be seen in the mouth is the primary or deciduous dentition, which begins to form prenatally at about 14 weeks *in utero* and is completed postnatally at about 3 years of age. In the absence of congenital disorders, dental disease, or trauma, the first teeth in this dentition begin to appear in the oral cavity at the mean age of 6, and the last emerge at a mean age of 28 $\pm$ 4 months. Among deciduous (primary) teeth, ten are found in the maxilla (upper jaw) and ten in the mandible (lower jaw), for a total of 20 [45]. At about 6 years of age, the first succedaneous or permanent teeth begin to emerge into the mouth. The emergence of

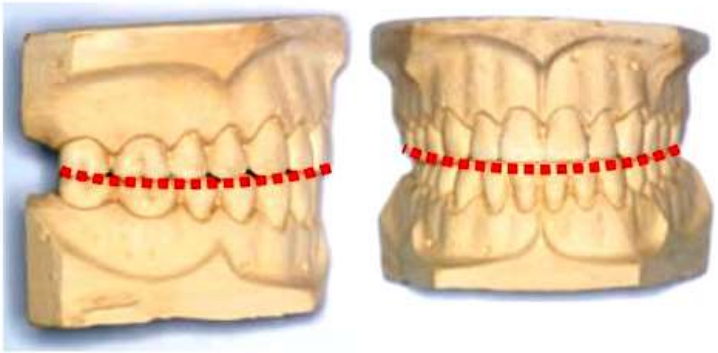

Slika 2.7: Curve of Spee (a) and curve of Wilson (b) [43]

these teeth marks the beginning of the the transition or mixed dentition period during which there is a mixture of deciduous and succedaneous teeth. Succedaneous teeth consist of 32 teeth, 16 in each jaw and they are the second set of teeth that humans have.
There are several different dental notation systems for associating information to a specific tooth. Depending on the country. Mediosagittal line is an imaginary vertical line which divides each arch as well as body into approximately equal halves, left one and right one. Also, jaws are divided into quadrants, four approximately equal portions of each arch divided by mediosagittal line.
Teeth can be single root or multi root teeth, and they are divided into 4 groups, as shown on Figure 2.8. They are incisors, canines, premolars and molars. Incisors and canines are mostly single root teeth and premolars and molars are mostly multi root teeth. The incisors are the two teeth of each quadrant which are closest to the midline, and there are 4 incisors in both jaws, which means 8 in total. Their functions in mastication are biting, cutting, incising and shearing. The canine is the third tooth from the midline in each quadrant. Its function in mastication is cutting, tearing, piercing and holding the food. There are two permanent canines per arch, and a total of four in the mouth. The premolars are the fourth and fifth teeth from the midline. They are termed first and second premolars. Their mastication role is tearing, holding, and grinding the food. For premolars it is characteristic that they do not exist in deciduous dentition, only in permanent dentition. As with the incisors, there are four per arch, and eight total premolars. The molars are the sixth, seventh, and eighth teeth from the midline. Their masticatory function is grinding. There are six permanent molars per arch, and twelve total permanent molars [45].

Around teeth there is soft tissue named periodontium. A tooth is divided into crown and root, clinical crown of the tooth is visible above the gingiva (gum) and the clinical root is the region of the tooth that is below the gingiva, Figure 2.9. The four tooth tissues are enamel, cementum, dentin, and pulp. The first three are known as hard tissues, the

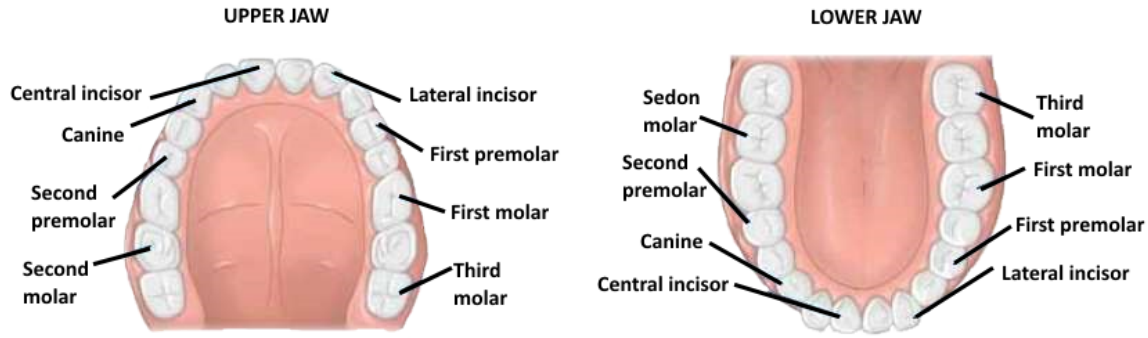

Slika 2.8: Types of teeth in both jaw [46]

last as soft tissue. The anatomical crown of each tooth has a coating of enamel, which protects the underlying dentine.

Enamel is the hardest substance in the human body, harder even than bone. It gains its hardness from tightly packed rows of calcium and phosphorus crystals within a protein matrix structure. Once the enamel has been formed during tooth development, there is little turnover of its minerals during life. Mature enamel is not considered to be a 'living' tissue.

The major component of the inside of the tooth is dentine. This substance is slightly softer than enamel, with a more of a bone-like structure. It is elastic and compressible in contrast to the brittle nature of enamel. Dentine is sensitive and it contains tiny tubules throughout its structure that connect with the central nerve of the tooth within the pulp. Dentine is a 'living' tissue.

In the tooth's root there is cementum, pulp and root canal. Cementum is a specialized calcified substance covering the root of a tooth. Cementum is slightly softer than dentin and consists of about 45% to 50% inorganic material by weight and 50% to 55% organic matter and water by weight. The organic portion is composed primarily of collagen and protein polysaccharides [45].

The pulp forms the central chamber of the tooth. The pulp is made of soft tissue and contains blood vessels to supply nutrients to the tooth, and nerves to enable the tooth to sense heat and cold. It also contains small lymph vessels which carry white blood cells to the tooth to help fight bacteria.

The extension of the pulp within the root of the tooth is called the root canal. The root canal connects with the surrounding tissue via the opening at the tip of the root. This is an opening in the cementum through which the tooth's nerve and blood supply enter the pulp from the surrounding tissue [45].

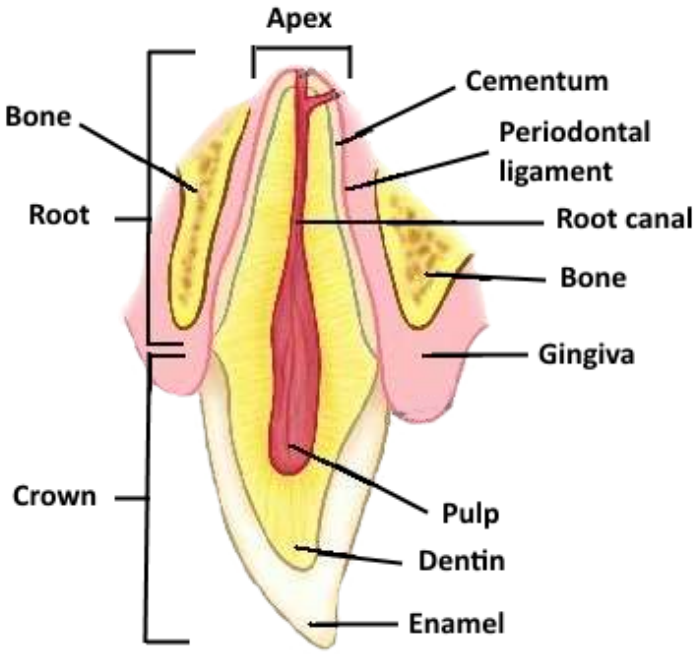

Slika 2.9: Tooth and surrounding tissues [47]

The periodontium is the term used to collectively describe the tissues involved in tooth support, and it is composed of the cementum on the tooth side, the alveolar bone on the jaw side, and by a layer in between these two hard tissues, the periodontal ligament, making the connections and allowing for relative displacements of the tooth with respect to the bone. The gum, the soft tissue which overlies the bone and forms a protective collar around the tooth, is also considered part of the periodontium. Compared with the soft tissue linings of the lips and cheeks, most of the gum are tightly bound to the underlying bone which helps resist the friction of food that passes over them. The periodontium supports the teeth during their function and it depends on the stimulation it receives from the function for preservation of its structure. Therefore, a constant state of balance always exists between the periodontal structures and the external forces [45].

2.1.2 Bone tissue

A bone is a rigid organ that constitutes part of the skeleton. Bones support and protect the various organs of the body, produce red and white blood cells, store minerals and also enable mobility. Bone tissue is a type of dense connective tissue and at submicroscopic

level, the bone matrix is mineralized fibrous tissue. The minerals in the matrix give bone compressive strength and the fibers give tensile strength. Bones come in a variety of shapes and sizes and have a complex internal and external structure. They are lightweight, yet strong and hard, and serve multiple functions. Bone tissue is the major structural and supportive connective tissue of the body. Bone tissue forms the rigid part of the bones that make up the skeleton. Bone is a self-repairing structural material, able to adapt its mass, shape, and properties to changes in mechanical requirements and endures voluntary physical activity for life without breaking or causing pain [48].
At the macroscopic level there are two major forms of bone tissue, called compact or cortical bone and cancellous or trabecular bone. Cortical or compact bone is a dense material and it forms most of the outer shell of a whole bone, a shell of variable thickness [48]. Cancellous bone fills the hollow interior and it is it consists of of trabeculae. The tissues are biologically identical; the difference is in how the microstructure is arranged. Generally, cortical bone is structurally predominant in the neighborhood of the joints and cancellous bone is structurally predominant in the central sections of the femur away from the joints [49].

Cancellous bone

Cancellous bone generally exists only within the confines of the cortical bone coverings. Cancellous bone is also called trabecular bone because it is composed of short struts of bone material called trabeculae, as shown on Figure 2.10. The connected trabeculae give cancellous bone a spongy appearance, and it is often called spongy bone. There are seldom blood vessels within the trabeculae, but there are vessels immediately adjacent to the tissue and they weave in and out of the large spaces between the individual trabeculae [48]. Cancellous bone accounts for the remaining 20% of total bone mass but has nearly ten times the surface area of compact bone and its porous nature makes it well adapted to supporting the complex loading applied to the bone near the joints.

Cortical bone

Cortical bone is a dense, solid mass, but looked microscopically it is not entirely solid, it is traversed by many channels, as shown on Figure 2.11. The hard outer layer gives bone its smooth, white, and solid appearance, and accounts for 80% of the total bone mass of an adult skeleton. It consists of microscopic cylindrical structures running lengthwise in the bone. These column-like structures are the osteons of the bone tissue, also called

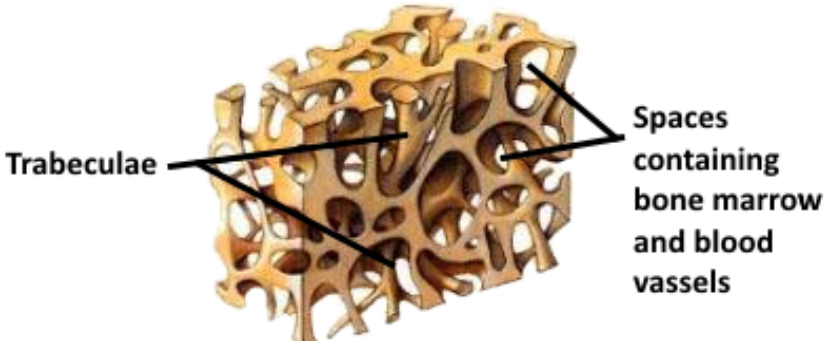

Slika 2.10: Cancellous bone [50]

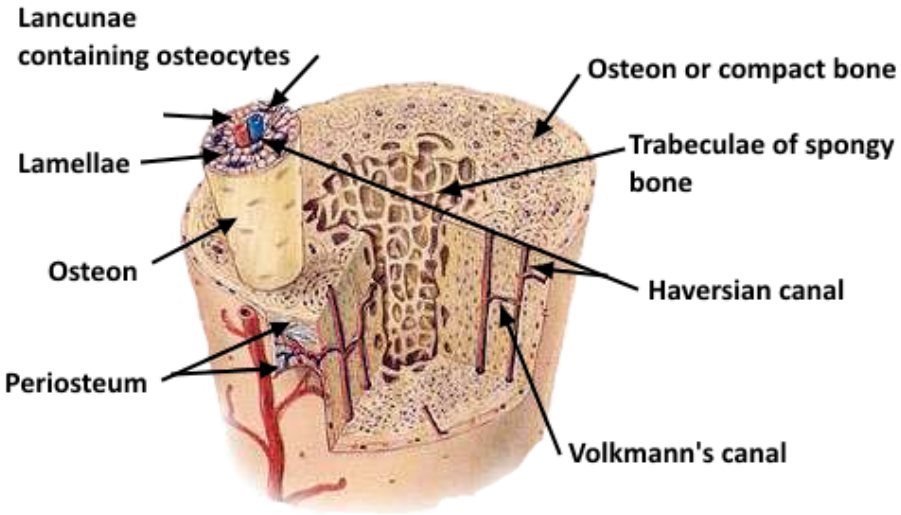

Slika 2.11: Compact bone [50]

Haversian systems. Osteon is the chief structure unit of cortical bone. The matrix of an osteon is laid down in concentric rings called lamellae. The lamellae surround a central canal that contains tiny vessels and a nerve. Individual bone cells, osteocytes within spaces called lacunae are regularly arranged between the lamellae. The lacunae are connected by canaliculi and Volkmann's canal penetrates compact bone, connecting osteons with blood vassels and nerves [41]. Osteons in compact bone, like trabeculae in cancellous bone, are aligned to the principal stress direction.

Alveolar bone

The alveolar bone is found in the mandible (lower jaw) as well as in the maxilla (upper jaw) [51]. The alveolar bone is the bone where teeth are anchored. Like any other bone in the human body, the alveolar bone grows and declines throughout life. The alveolar bone is especially thick and dense when compared to other types of bone so that it can provide adequate support for the teeth, along with attachment points for muscles in the jaw and for the gums. This bone is also known as the "alveolar process." It includes sockets (dental alveolus) which are designed to accommodate the roots and lower part of the teeth, with each socket separated from the next by an interdental septum. The gums attach to the alveolar process, and the bone has accommodations to allow blood vessels to enter for the purpose of supplying blood to the teeth. Damage to the alveolar bone can have serious consequences, including the risk of loss of teeth and septicemia if the damage is caused by an infection. The structure of the alveolar bone consists of cortical plate from the outside and cancellous bone and marrow from inside, as shown on Figure 2.12.
Main functions of the alveolar bone are: protection (it forms and protects the sockets for the teeth), attachment (it provides attachment for the periodontal ligament fibers), support (it supports the tooth root) and shock-absorber (it helps absorb the forces in mouth). The alveolar bone is dependent on the presence of teeth. Where there is no tooth present, the alveolar bone does not form, and this leads leads to bone loss.

Bone cells

There are three forms of bone cells, osteoblasts, osteocytes and osteoclasts. These cells respond to trauma, such the fracture, and to any another loading by starting the process of bone remodelling.
Osteoblasts are bone-forming cells that synthesize and secrete unmineralized ground substance and they are derived from mesenchymal stem cells. They are abundant in areas of high metabolism, so they produce the organic bone matrix and aid its mineralisation. Some of the osteoblasts are embedded in the unmineralized, organic portion of the bone matrix, osteoid, to become osteocytes. As the formation site develops, the osteoblasts on the surface change into bone lining cells or die by apoptosis. Bone lining cells are inactive osteoblasts that cover bone surface and bone lining cells is thought to have a specific role in coupling bone resorption to bone formation perhaps by physically defining bone remodelling compartments [1]. Osteocytes are mature bone cells derived from osteoblasts that deposit minerals around themselves.
Osteocytes maintain healthy bone tissue by secreting enzymes and influencing bone mineral

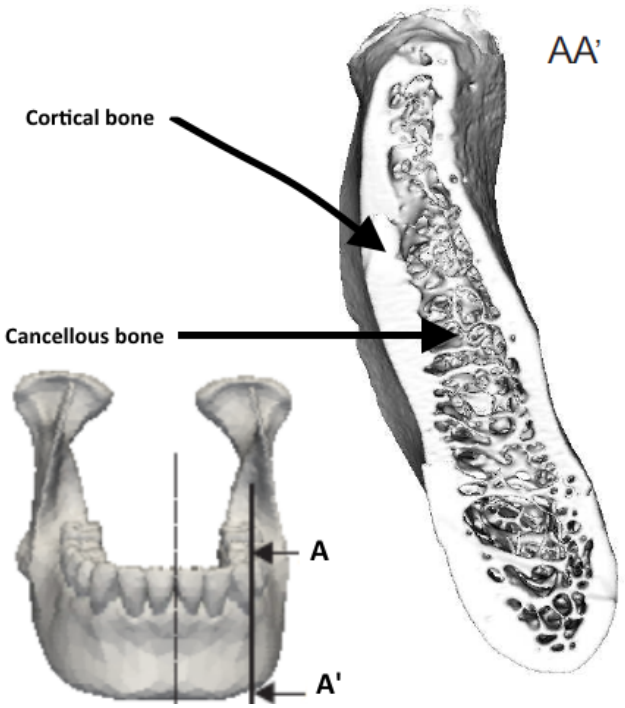

Slika 2.12: Alveolar bone of mandibular [30]

content. They also regulate the calcium release from bone tissue to blood. Osteocytes remain in contact with the cells on the bone surface and it is believed that they serve as mechanosensors because of their location in the lacuno-canalicular network and also, they show a metabolic response to bone strains [41].
Osteoclasts are large multinuclear cells, about 50-100 μm in diameter, that use enzymes to break down bone tissue. Osteoclasts are unique type of exocrine cell that dissolves bone mineral and enzymatically degrades extracellular matrix. They are derived from hematopoietic stem cells. These cells differentiate into mononuclear osteoclasts, which adhere tightly to bone, and fuse with each other into multinucleated osteoclasts [52]. These cells are important in bone growth, remodelling and healing, tunneling deep into the bone [41].

Growth, reinforcement and resorption

Living bone is continually undergoing processes of growth, reinforcement and resorption. These processes are termed collectively as ”remodelling”. Bone remodelling can only take place by the activity of certain cells, that are mentioned above, which are embedded within its matrix structure. Bone remodelling is the process of resorption of bone tissue material

and the subsequent formation of new bone tissue by bone cells, allowing the maintenance of the shape, quality, and size of the skeleton. During bone remodelling, bone formation is tightly coupled to bone resorption, and direct contacts between osteoclasts and osteoblasts have been proposed to maintain this relationship.
The main function of bone remodelling is to remove damaged bone, but since bone also act as a calcium reservoir, bone remodelling also has a function in preserving the equilibrium of calcium in the human body. This process is characterized by the coordinated actions of osteoclasts and osteoblasts, organized in bone multicellular units (BMU) that follow an activation-resorption-formation sequence of events [53]. To preserve a normal bone mass and microstructure, it is important that the processes of bone resorption and bone apposition are in equilibrium. The remodeling processes in living bone are the mechanisms by which the bone adapts its histological structure to changes in long term loading [49].

Bone remodelling has 5 phases: quiescent, activation, resorption, reversal, formation, and mineralization [54, 55]. Schematic view of bone remodelling phases are shown on Figure 2.13. *Quiescent phase* is the state/phase of the bone when it is at rest. The factors that initiate the remodelling process remain unknown. *Activation phase* is the first stage of bone remodelling which involves detection of an initiating remodelling signal. This signal can take several forms, e.g. direct mechanical strain on the bone that results in structural damage or hormone action on bone cells in response to more systemic changes in homeostasis. In *resorption phase* osteoblasts respond to signals generated by osteocytes and recruit osteoclast precursors to the remodeling site. The osteoclasts then begin to dissolve the mineral matrix and decompose the osteoid matrix. This process is completed by the macrophages (cells which stop formation of osteoclasts when resorption is finished). During the *reversal phase*, bone resorption transits to bone formation. Once osteoclasts have resorbed a cavity of bone, they detach from the bone surface and are replaced by cells osteoblast which start bone formation - *formation phase*. Last stage is *mineralization*, where mature osteoblasts undergo apoptosis, revert back to a bone lining phenotype or become embedded in the mineralized matrix, and differentiate into osteocytes. After this last phase, the resting bone surface environment is reestablished and maintained until the next wave of remodelling is initiated.

Mechanical force is a key regulator of bone remodelling and of bone architecture in general. It influences bone metabolism not only locally but also systemically. However, the precise mechanical stimulus that is sensed by bone cells in vivo and the signal produced as a result remain unclear [1].

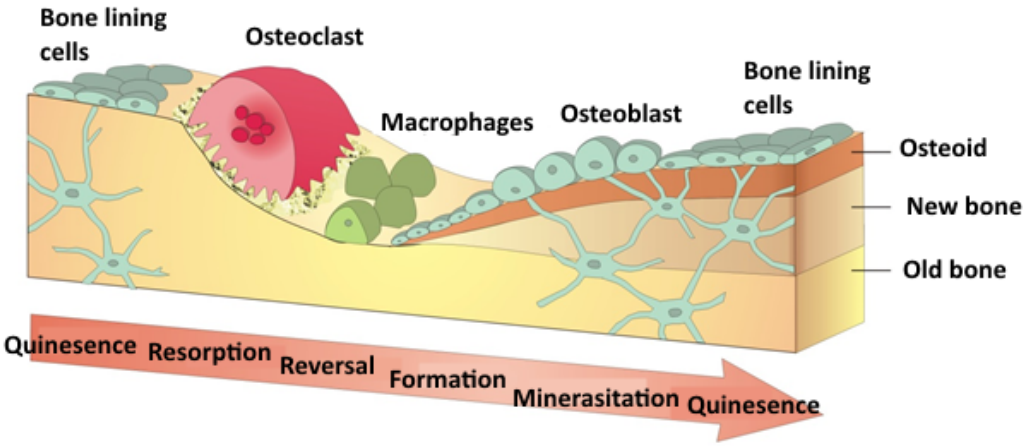

Slika 2.13: Schematic view of bone remodelling phases [56]

All bones in the human body are remodelled in the same way. This means the same rules refer to the alveolar bone as well. Whereas the overall formation and regulatory events in the alveolar bone are the same as on other anatomical sites, the alveolar bone is distinctive because it turns over very rapidly and it is lost in the case of tooth absence. This shows importance of the periodontal tissues and emphasizes that periodontal tissues function together as a unit.

As it is mentioned, remodelling process of the alveolar bone is similar to that of bone remodelling in general. All forces that are at play in the mouth on a daily basis influence the alveolar bone remodelling, but the focus of this research is the alveolar bone remodelling induced by orthodontic force.

During orthodontic tooth movement, the distribution of force is such that bone lost by resorption on one surface of the tooth socket is balanced by bone formation along the opposite surface. This bone balance together with the continued deposition of cementum throughout life acts in maintaining a more or less constant relationship between the root surface and that of the alveolar socket [57].

The final goal of the influence of orthodontic force on the alveolar bone remodelling is tooth movement. Orthodontic tooth movement is achieved by a delicate balance between bone resorption and formation which arise from a combined influence of physical, cellular, biochemical and molecular events taking place in the periodontal tissues surrounding the roots. The tooth moves in the periodontal space by generating a compression side and a tension side.

2.1.3 Periodontal ligament

The periodontal ligament, or shortened the PDL, is a dense fibrous connective tissue and it is part of the dental periodontium. The PDL is positioned between tooth and bone, occupying the periodontal space, and it connects tooth root, cementum, to the surrounding bone.

The periodontal space ranges in width from 0.2 to 1.5 mm, with its thinnest portion around the middle third of the root, showing a progressive decrease in thickness with age. The PDL substance has been estimated to be 70% water, which is thought to have a significant effect on the tooth's ability to withstand stress. The completeness and vitality of the PDL are essential for the functioning of the tooth [45, 51].

The PDL is a connective tissue particularly well adapted to its principal function, supporting the teeth in their sockets and at the same time permitting them to withstand the considerable forces of mastication. In addition, the periodontal ligament has the capacity to act as a sensory receptor necessary for the proper positioning of the jaws during mastication and, very importantly, it is a cell reservoir for tissue homeostasis and repair - regeneration [57]. Since the PDL consists of bone and cementum cells, it has an important role in bone and cementum remodelling. Therefore, it can be said that main PDL functions are supportive, sensory, nutritive, and remodelling.

Along with the cells mentioned above, the PDL also consists of intercellular substance and fibers.The PDL is provided with blood vessels and lymphatic vessels and with nerves as well. The cells that can be found in the PDL are fibroblasts, epithelial cells, undifferentiated mesenchymal cells, bone and cementum cells. These cells are responsible for bone and cementum formation and resorption. Cells and intercellular substance in this research will (be called) be called the PDL matrix.

The PDL fibers are 90% collagen fibers bundles that are embedded in intercellular substance, it can be said that collagen fibers dominate [58]. Individual fibrils have a relatively smaller average diameter, so they make bundles. The ends of collagen fiber bundles are embedded in cementum or bone, and that is referred to as *Sharpey's fibers*. The PDL collagen fibers are categorized according to their orientation and location along the tooth: alveolar crest, horizontal, oblique, apical and interradicular fibers. Groups of fibers are shown on Figure 2.14. All these fibers help the tooth withstand the naturally substantial compressive forces which occur during chewing and remain embedded in the bone [45, 51].

From mechanical point of view, the PDL has an important role [59] in bonding of the teeth to the surrounding alveolar bone, cushioning and distributing the shocks caused by physiological or pathological loadings to the contiguous alveolar bone and allowing dental

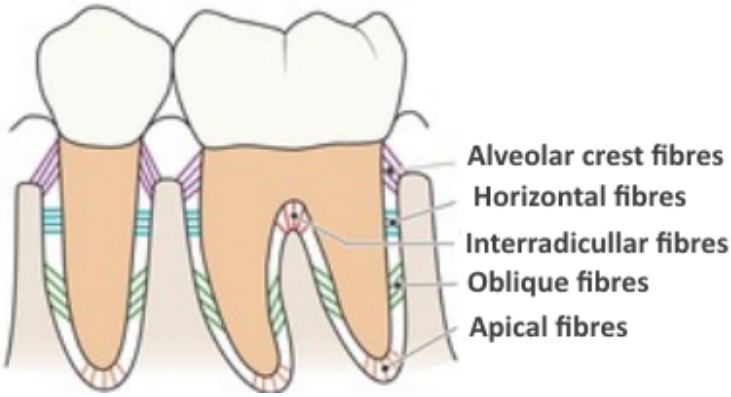

Slika 2.14: Group of PDL fibers along tooth [46]

mobility (the direction, frequency, duration and magnitude of the applied forces determine in part the extent and rapidity of bone remodelling). Teeth mobility, in particular, is a unique functionality of the PDL and, in fact, it has been verified that, when forces are applied to teeth or osteointegrated implants with no surrounding PDL, the rate and extent of bone remodelling is very limited.
Thus, the presence of the PDL, together with the application of some external forces, allows teeth to move within their bone support. The connections between these elements is still not well understood even today. Nevertheless, the biological structure of the PDL (rich in cells responsible for tissue generation) can provide some insights on the mechanisms behind teeth mobility [51].

2.2 Principles of orthodontics

Orthodontics is a field of stomatology that uses biomechanical principles to correct dental and skeletal malposition and malformations. The definition of orthodontics proposed by the American Board of Orthodontics (ABO) and later adopted by the American Association of Orthodontists states:
”Orthodontics is that specific area of the dental profession that has as its responsibility the study and supervision of the growth and development of the dentition and its related anatomical structures from birth to dental maturity, including all preventive and corrective procedures of dental irregularities requiring the repositioning of teeth by functional and mechanical means to establish normal occlusion and pleasing facial contours” [60].

The orthodontic treatment should satisfy the patient’s aesthetic desires but also it is important to satisfy certain functional and physiologic requirements. These aims can be

divided into three groups [60]:

- *functional efficiency* - the teeth along with their surrounding structures are required to perform certain important functions and orthodontic treatment should increase this efficiency;
- *structural balance* - the treatment should maintain a balance between the teeth and the surrounding tissue, and the correction of one should not be detrimental to the health of another;
- *aesthetic harmony* - the orthodontic treatment should increase the overall aesthetic appearance of the individual; this might just require the alignment of certain teeth or the forward movement of the complete jaw including its basal bone.

Proper position of teeth in the jaw and relation between upper and lower jaw allows a steady transfer of chewing and other forces that can be found in the mouth. These procedures lead to a normal anatomic and functional correlation between the teeth and their bone basis. Orthodontic treatment can be used at any age, but it is recommended to start with it at teenage years or earlier.

To obtain the proper position of teeth in the jaw, fixed or removable orthodontic appliances (devices) are used. Orthodontic appliances can be defined as devices, which create and/or transmit forces to individual teeth/a group of teeth and/or maxillofacial skeletal units so as to bring about changes within the bone with or/without tooth movement which will help to achieve the treatment goals of functional efficiency, structural balance and aesthetic harmony [60].

As mentioned above, orthodontic appliances can be divided into fixed and removable appliances, as shown is shown on Figure 2.15. *Fixed appliances* consist mainly of braces and/or bands which have horizontal slots or tubes on the inside of which wires of various materials and sizes are inserted, then ligated by means of metal or elastic ligatures. To this basic system, common to all techniques, springs or elastics can be added. *Removable appliances* are orthodontic appliances that can be inserted and removed from the oral cavity by the patient. In general, they basically consist of acrylic resin, designed according to the problem involved, to which various pieces like arches, clasps, springs or screws can be added or inserted. The choice of the best appliance for any single patient is a pure consequence of the diagnostic and treatment process. At present, both fixed and removable appliances are used on the basis of the scientific knowledge about their properties and their treatment potential [32].

Both appliances should fulfill these three requirements: biological requirements (its basic

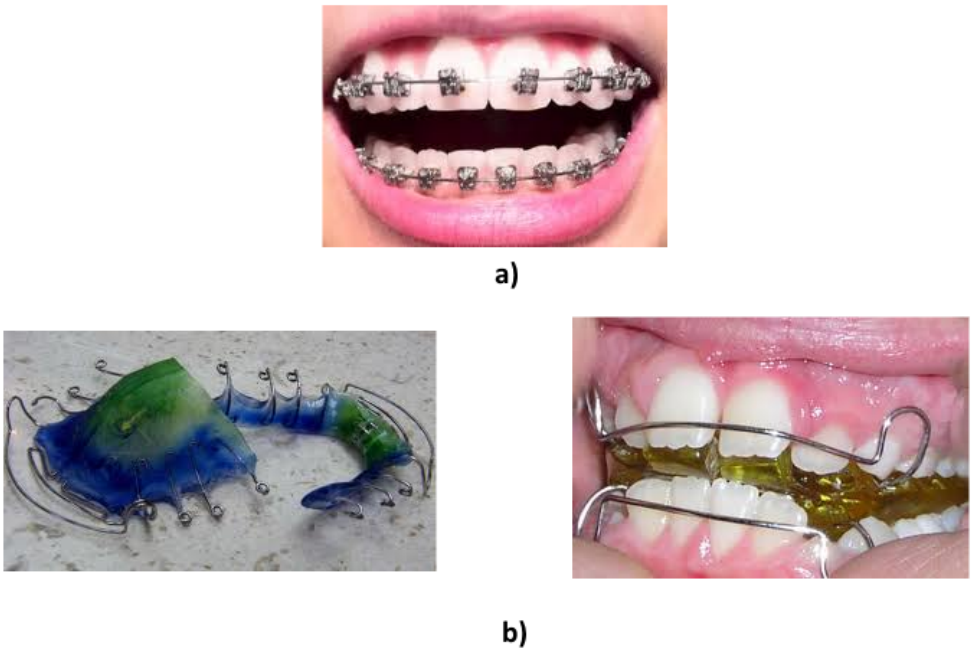

Slika 2.15: Orthodontic appliances: a) fixed, b) removable [61]

purpose of bringing the desired tooth movement and should not have a detrimental impact on the teeth, and/ or periodontium), mechanical requirements (it should be able to deliver continuous controlled forces of the desired intensity in the desired direction) and aesthetic requirements (it should be esthetically acceptable to the patient)[60].

2.2.1 Orthodontic tooth movement

Orthodontic tooth movement, shorten called OTM, results from the application of forces to the teeth. The selected orthodontic appliances, that are inserted and activated by the clinician, produce these forces. The teeth and their associated support structures respond to these forces with a complex biological reaction that ultimately results in the teeth moving through their supporting bone.

To allow orthodontic tooth movement in the direction of the force application, the alveolar bone needs to remodel, enabling tooth movement through the bone. As mentioned before, bone remodelling in the alveolar bone is same as bones in other parts of the body. This means that because of the application of orthodontic forces, in the direction of tooth movement, bone resorbs itself, and on the other side, forms new bone. This is based on the principle that a change in mechanical loading on a biological system results in strain, which subsequently leads to cellular responses aiming at adapting the system to

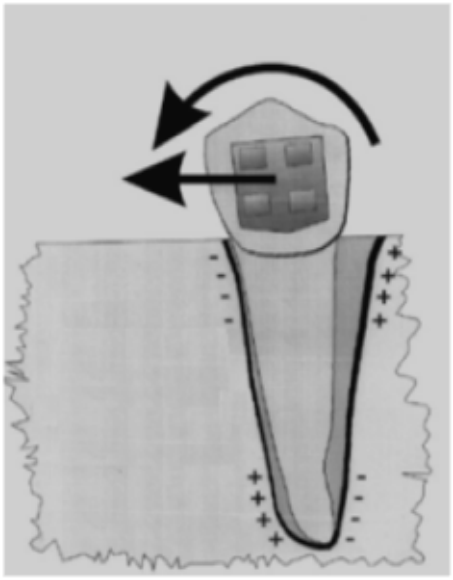

Slika 2.16: Stress distribution in the periodontal ligament and the alveolar bone [63]

the changed conditions [34]. The difference in bone remodelling here as opposed to bone remodelling in other parts of the body is the impact of the soft tissue between tooth and bone, the influence of the PDL. The PDL and the surrounding bone are both influenced during orthodontic tooth movement.

In orthodontics, two sides are important during tooth movement, the resorption and the apposition side [39]. In the direction of force application, tooth moves in the periodontal space causing the unloading of PDL fibres. The amount of movement depends on the biomechanical properties and the dimensions of the PDL [33]. It is important to realize that the PDL is loaded in tension sites and unloaded in compression sites [62].

The PDL contains many cells, and the most abundant cells are fibroblasts which cause collagen fibers remodelling [35]. Osteoclasts are also found in the PDL, which are triggered by strains on the resorption side. Osteoclasts resorb bone on the side where they are activated and allow tooth movement in the direction of force application. On the other side, the apposition side, PDL fibers are stretched, pulling the bone on that side, and causing micro-damages in the bone. Since the PDL also contains osteoblasts, and they are activated by PDL stretching, the bone formation starts on the apposition side of the bone. Resorption and apposition sides are shown on Figure 2.16 where minuses ($''-''$) correspond to the resorption side of the bone and pluses ($''+''$) correspond to the apposition side.

From a clinical perspective, orthodontic tooth movement has three distinct phases [62, 60]:

- *initial phase* - the initial phase of tooth movement is immediately seen following the application of a force on a tooth, the phase is characterized by a sudden displacement

of the tooth within its socket;

- *lag phase* - the lag phase is characterized by very little or no tooth movement, it is the phase where the cellular components around the area of interest get activated to cause tooth movement;

- *post-lag phase* - this phase is characterized by the removal of the hyalinized tissue (necrotic tissue full of PDL bundles) and tooth movement, the movement is mediated by osteoclasts and there is direct resorption of the bone surface facing the periodontal ligament.

All three phases are shown on diagram on Figure 2.17. The initial phase is usually very short and maximum displacement is never bigger than PDL space width. The duration of the lag phase is highly variable, and it depends on time needed to resorb hyaline zones that occur. Hyaline zones are composed solely of bundled collagen fibers. These zones appear at compression sites in the PDL and lead to a locally decreased cell quantity and loss of structure which leads to osteoblasts and osteoclasts no longer performing bone remodelling. If force increases, that can lead to pathological remodelling and bone loss. So, it can be seen that stress state in the PDL is the key factor on which desirable or undesirable tooth movement movement depends [64]. The lag phase is longer if heavier forces are applied, as the area of hyalinization created is large and the resorption is rearward. The phase is shorter if force are lighter. Post lag phase is the phase in which actual tooth movement happens and it can last up to 2 years.

Both fixed and removable appliances create a therapeutic force that is called orthodontic force. The type of force to be employed is also a parameter that should be planned. Optimum orthodontic movement is produced by light and continuous forces. Clinically speaking, optimal orthodontic force is considered as the force leading to maximal rate of movement without causing damage to the periodontal tissues or discomfort of patient. The force that delivers the highest rate of tooth movement with the minimal damage" has yet to be described [65]. The forces are to be neither too big nor too variable over time. It is particularly important that the light forces do not decrease rapidly, decaying away. Obviously, treatment planning, from a biomechanical point of view, must seriously consider the anatomy of each single patient [32].

A continuous force can be obtained by using wires with low load/deflection rate and high working range. In the leveling phase, where there is considerable variation in level between teeth, it is advantageous to use these wires to control anchorage and maintain longer intervals between orthodontic appointments. Continuous force decreases slowly, but it never diminishes to zero within two activation periods; thus, constant and controlled tooth

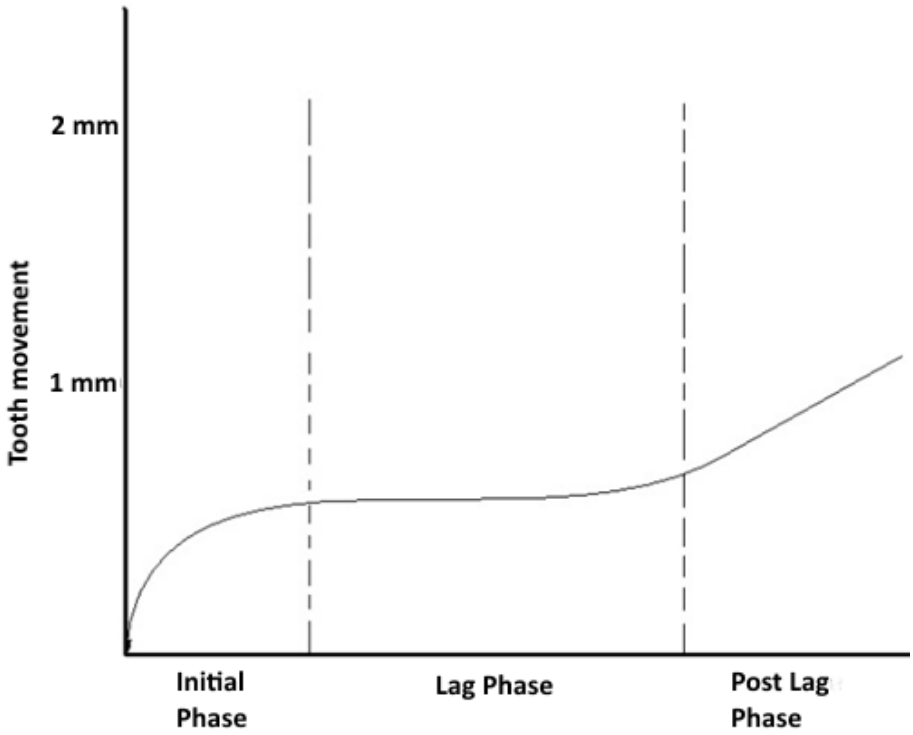

Slika 2.17: Phases in orthodontic tooth movement

movement results [66]. At the present there is no universal consensus nor scientific evidence regarding a threshold of force level that would "switch on" tooth movement [67, 68]. This is evident from the research performed on dogs and humans by the application of different force levels to second premolar teeth. The results of these studies indicated that the same rate of tooth movement occurs with the different levels of force applied. Both studies concluded that the variation in the rate of tooth displacement was mainly related to the individual and not to the force level [65]. Quinn and Yoshikawa [69] have described four alternative models for relationship between orthodontic force magnitude and the rate of tooth movement. The first model supposes an on/off switch that is switched on at a certain force level. All forces above this threshold will lead to the same rate of tooth movement. In the second model, a force threshold is also indicated. With forces above the threshold, a linear dose-response relationship is assumed. Several studies [70, 71] have shown that higher forces were generally more efficient in moving teeth, and they support this model. In the third model, forces above a certain threshold are necessary to induce movement. A dose-response relationship exists in a lower force range up to a certain level. The last model generally resembles the third, but it lacks the decreasing part. Values of optimal force on the crown recommended in the orthodontics and that could be found in literature are from 0,2 N to 5 N [24, 25, 18, 16].

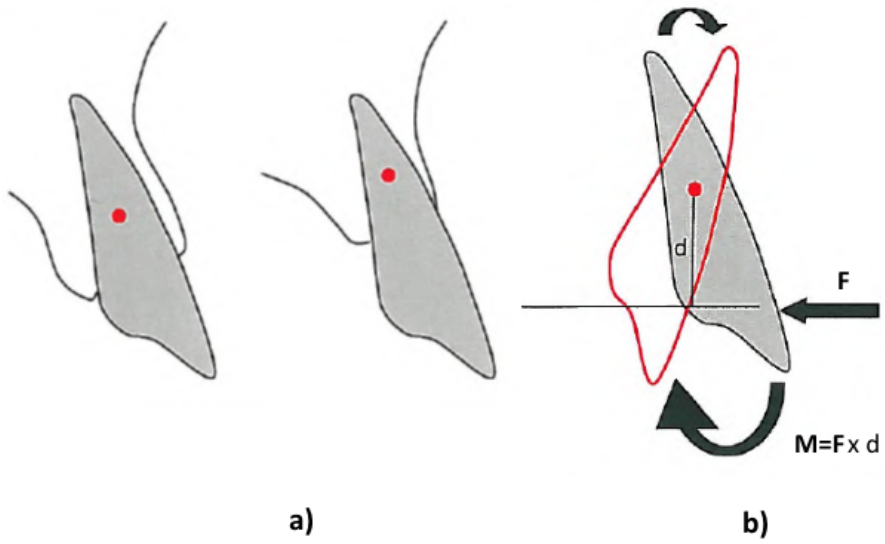

Slika 2.18: Position of centre of resistance (a) centre of rotation (b) [66]

2.2.2 Types of orthodontic tooth movement

During application of force on the crown of the tooth, the result is, as it was explained above, tooth movement. Depending on force vertex, there are four different tooth movements. Tooth movement can be described by two characteristic points, *centre of resistance* and *centre of rotation*.

Centre of resistance is a point where the line of action of the resultant force vector intersects the longitudal axis of the tooth, causing translation of the tooth. Position of centre of resistance is shown on Figure 2.18 left (a). Theoretically, the center of resistance of a tooth is located on its root, but the location has been extensively investigated. Studies show that the centre of resistance of single-rooted teeth is on the long axis of the root, approximately 24% to 35% of the distance from the alveolar crest. It is important to emphasize that the centre of resistance and the centre of mass are not the same point, and the center of resistance must be considered a balance point of restrained objects. The center of resistance is unique for every tooth; the location of this point depends on the number of roots, the level of the alveolar bone crest, and the length and morphology of the roots. Therefore, the center of resistance sometimes changes with root resorption or loss of alveolar support because of periodontal disease. For example, in the case of loss of alveolar support, this point moves apically [66, 38, 72, 24].

Centre of rotation is the point around which the tooth rotates. The location of this point is dependent on the force system applied to the tooth, that is, the moment-to-force (M/F)

ratio. Position of centre of resistance is shown on Figure 2.18 right (b). The higher the moment, the more the centre of rotation moves towards centre of resistance. When coupled forces are applied on the tooth, this point is superimposed on the center of resistance (i.e., the tooth rotates around its center of resistance). In translation, centre of rotation becomes infinite, meaning there is no rotation [66, 38, 72, 24]. In determining tooth movement, the crucial element is moment-to-force ratio, and depending on its magnitude, the tooth moves or rotates.

Types of tooth movements are tipping, bodily movement, rotation and intrusion/extrusion movement.

Tipping, in practice, is the easiest type of tooth movement. When a single force is applied to a bracket on a round wire, the tooth tips about its center of rotation, located in the middle of the root, close to its center of resistance. There are two types of tipping movement, controlled and uncontrolled tipping movement. Both movements are shown on Figure 2.19, where the upper figure is showing uncontrolled tipping movement and the lower one is showing controlled tipping movement. In the uncontrolled tipping movement this single force causes movements of the crown and apex in opposite directions. This type of movement is in the most clinical cases undesirable. If a light, counterclockwise moment is added to the system with a rectangular wire while the single distal force is still being applied, the tooth tips distally in what is called controlled tipping, which is clinically desirable. In this movement, the center of rotation moves apically, and the tooth tips around a circle of a greater radius.

Bodily movement is shown on Figure 2.20. Theoretically, bodily movement or translation of a body is the movement of any straight line on that body, without changing the angle with respect to a fixed reference frame. During translation, all the points on the body move the same distance, and they therefore have the same velocity. The center of rotation is effectively at an infinite distance away from the tooth because there is no rotation.

Rotation of a body is the movement of any straight line on that body by a change in the angle with respect to a fixed reference frame. If the tooth rotates about its longitudinal axis through the center of resistance, it is called pure rotation. This movement is shown on Figure 2.21. So, the centre of rotation is at the center of resistance.

Intrusion and extrusion involve movement along the longitudinal axis of the tooth. Recall from translation, the center of rotation is at infinity in this type of movement, shown on Figure 2.22. Intrusion movement can lead to hyaline zone appearance followed by pathological remodeling at the apex.

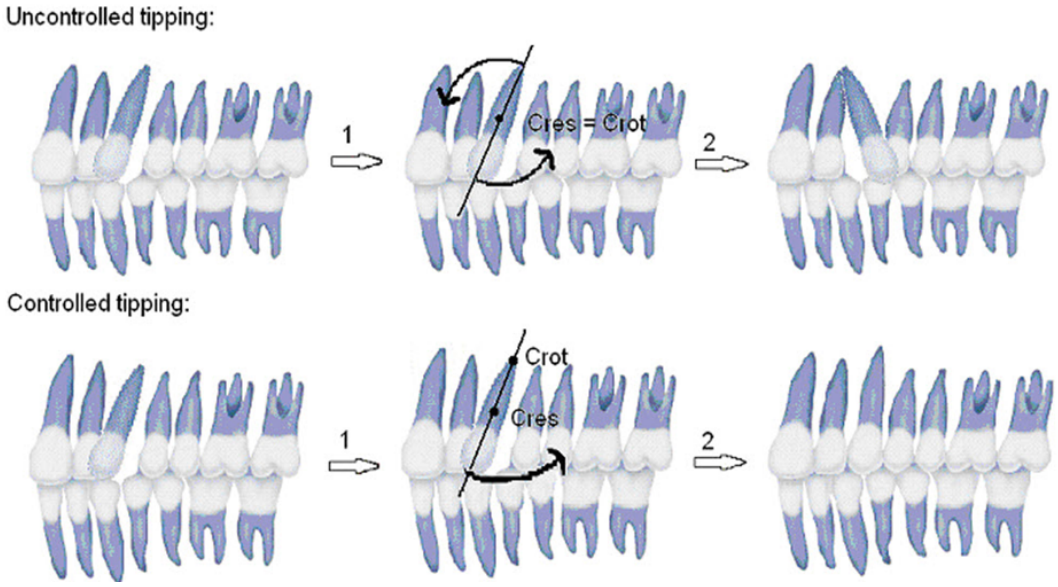

Slika 2.19: Tipping movement [73]

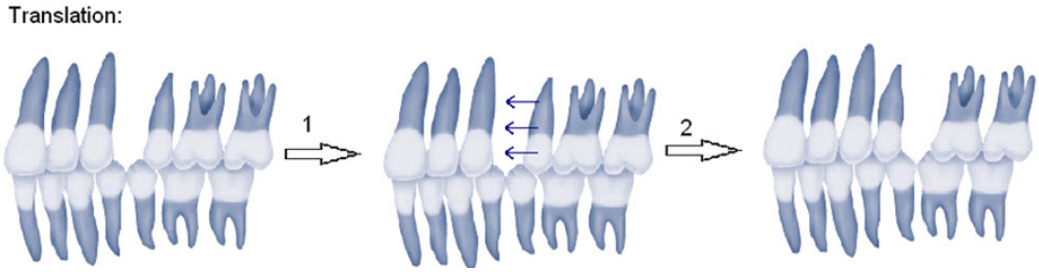

Slika 2.20: Bodily movement [73]

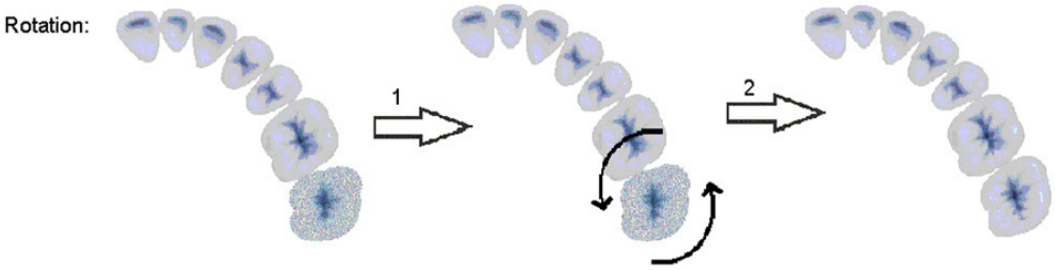

Slika 2.21: Rotation [73]

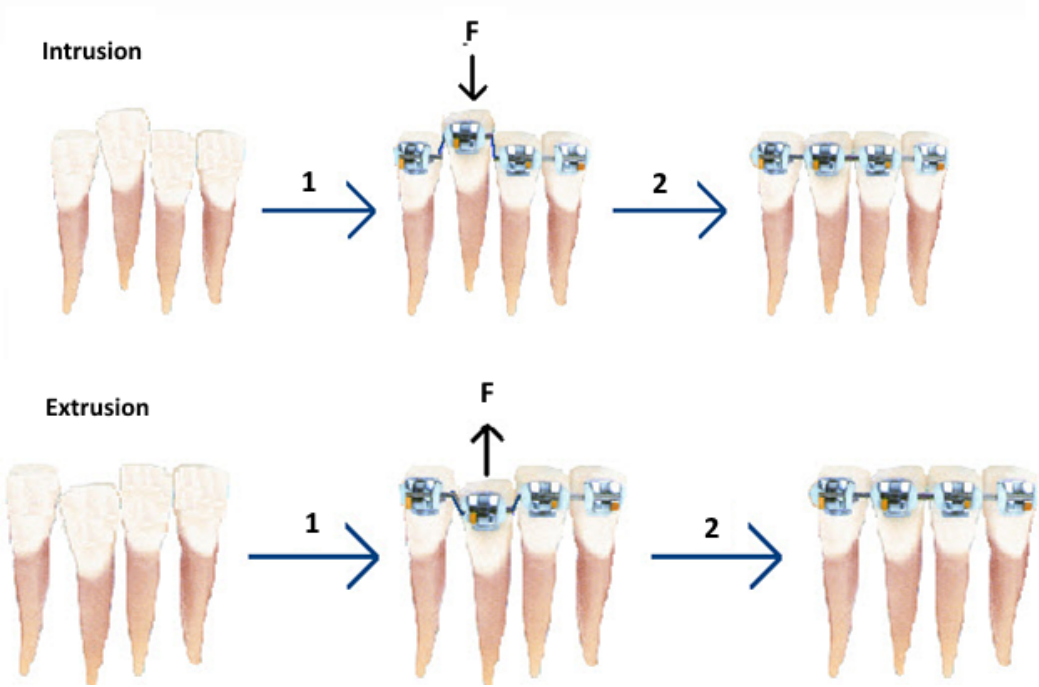

Slika 2.22: Intrusion and extrusion [73]

2.3 Computer Tomography imaging overview

In today's biomedical research Computed Tomography (CT) and Magnetic Resonance Imaging (MRI) have a big influence. These techniques visual representations of the interior of a body for clinical analysis and medical intervention. Medical imaging seeks to reveal internal structures hidden by the skin and bones, as well as to diagnose and treat disease. Therefore, the use of these techniques facilitate biomedical research without harming the patient. This approach allows three dimensional modelling of the observed part of the human body, which leads to patient-specific modelling [74, 75].

Computed Tomography refers to the cross-sectional imaging of an object from either transmission or reflection data collected by illuminating the object from many different directions. Fundamentally, tomographic imaging deals with reconstructing an image from its projections. The technique consists of irradiating a section of a sample from a number of position angles and then measuring the intensity of the transmitted or reflected radiation. These projections can represent, for example, the attenuation of X-rays through an object as in conventional X-ray tomography, the decay of radioactive nucleoids in the body as in emission tomography, or the refractive index variations as in ultrasonic tomography. This attenuation is caused by photons either being absorbed by the atoms of the material, or being scattered away from their original directions of travel. From the projections for

each angular position, one can reconstruct an image and differentiate the constituting materials considering the variation of the attenuation coefficient and the initial energy of the rays. The images obtained are 2D maps of the distribution of the attenuation coefficient of X-rays. By stacking the obtained 2D images, one can reconstruct 3D images [74].

2.3.1 Morphological analysis

Computed tomography reconstructs the image of an object by dividing it into contiguous parallel slices and it is based on the fundamental principle that the density of the tissue passed by the X-ray beam can be measured from the calculation of the *attenuation coefficient* (the difference between the energy that enters a body part and the energy that is not detected) [74, 75]. The data, which represent the physical properties of a material strip, are acquired by a set of linear sampling at different projection angles. The pixel value (picture element) of the two-dimensional cross-section or the voxel value (volume element) of the three-dimensional image provide information on the internal structure of the scanned object. It is important to note that the set of two-dimensional scans may be seen as a three-dimensional image, if all 2D scans are stack. Finally the voxels may be seen as a set of points in 3D with specific values, each point being the centre of the hexahedral voxel in the image [75].

Medical images (2D or 3D) are not suited for computational analysis and must be preprocessed. They contain too much information, and it is necessary to extract the surface or the volume needed to model. This means that the part of the body to be modelled has to be segmented from other parts by thresholding techniques. Segmentation is the process in image analysis in which the object of interest is isolated from the background. The ultimate goal of segmentation is to identify the part of the data array that makes up an object in the real world [76]. Threshold limit is set in the software that is used to obtain geometry, and pixel values that are in threshold boundaries represent 2D geometry. Threshold values depend on the gray value of images, and they are experimentally determined [77]. After that 3D geometry can be obtained.
In volumetric (3D) digital radiology, the radiographic density in each voxel of the volume of interest is expressed by a number called the *CT number*. *CT numbers* correlate to gray values, or gray shades, when the volumetric dataset is rendered into images, which are displayed on a monitor.

In the field of radiodensity the attenuation coefficient is measured in CT numbers which are expressed as *Hounsfield Units* (HU). The *Hounsfield Units* scale [78] is a linear

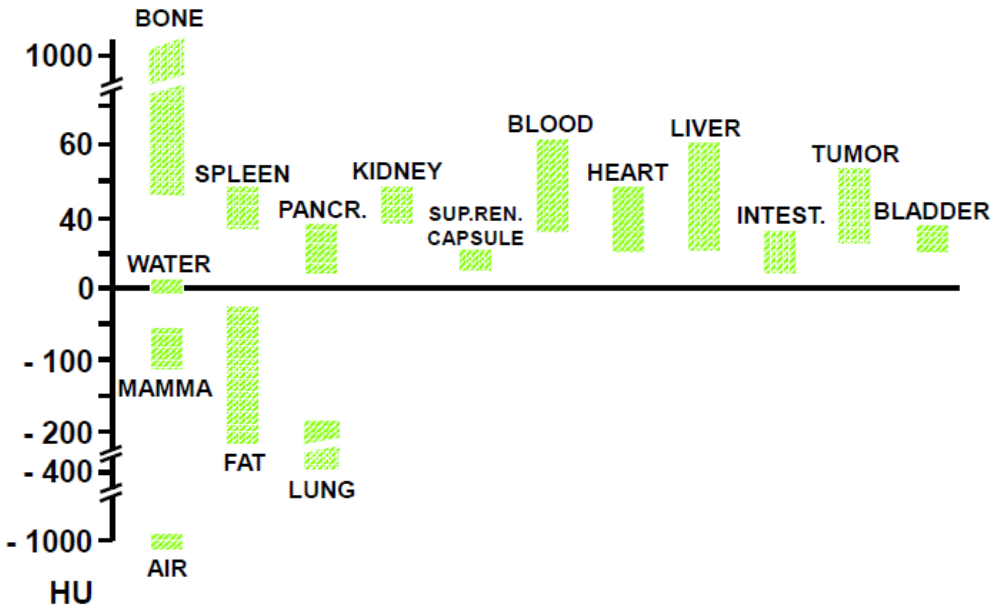

Slika 2.23: Hounsfield Units [77]

transformation of the linear attenuation coefficient measurement into one in which the radiodensity of distilled water (at standard pressure and temperature) is defined as zero HU, while the radiodensity of air at standard pressure and temperature is defined as -1000 HU. HU values of some materials are shown on Figure 2.23. For a material X with linear attenuation coefficient μ_X, the HU value is therefore given by expression 2.1.

$$\text{HU} = \frac{\mu_X - \mu_{water}}{\mu_{water} - \mu_{air}} \times 1000, \tag{2.1}$$

where μ_{water} and μ_{air} are the linear attenuation coefficients of water and air, respectively. The *Hounsfield Units* is not part of the SI (Système Internationale des Unitès de Mesure). In fact, it is neither a SI fundamental unit nor a derived unit It is a useful practical unit. But also, the HU is the standard scale for the measurement of conventional CT values. Without HU, it can be difficult to analyze bone quality and to process and scan through two-dimensional and three-dimensional images using various standard DICOM software products with default settings for conventional CT images [79]. Values of HU unit for some tissue are shown on table 2.1.

2.3.2 Cone Beam CT

Cone Beam Computed Tomography or CBCT, also referred to as C-arm CT, cone beam volume CT, or flat panel CT, is a medical imaging technique consisting of X-ray computed

Tablica 2.1: Values of HU for different types of tissues [80, 81]

Material	Hounsfield Units
Air	-1000
Lung	-500 to -200
Fat	-500 to -50
Water	0
Blood	25
Muscle	25 to 40
Cancellous bone	150 to 660
Cortical bone	660 to 2000
Tooth	1200 to 3070

tomography where the X-rays are divergent, forming a cone. Cone beam CT systems offer many advantages over medical CT for dental treatment and planning, including a lower radiation dose to the patient in most instances, shorter acquisition times for the resolution desired in dentistry, an affordable cost alternative to medical CT, better resolution and greater details and also allows simultaneous sampling of an entire volume without the patient having to move [82, 32].

CBCT usually uses one rotation around the patient similar to the panoramic radiography. The image is collected for either a complete dental/maxillofacial volume or limited regional areas of interest. The information obtained can be reformatted to produce images in the coronal, sagittal, or panoramic orientation which are not magnified nor distorted in size or shape. The scan time with CBCT is approximately 40 to 75 seconds for the complete volume and 17 seconds for specific areas [83]. Figure 2.24 shows simplified representation of image acquisition using CBCT.

Unlike conventional CT, CBCT uses a narrow cone-shaped beam to rotate 194 to 360 degrees around the patient. Traditional medical CT scanners use pixels, as it is explained above. The slice thickness is defined by gantry movement. The thickness is defined by the operator. CBCT devices gather the volume information directly using voxels or cubes with known dimensions (typically 0.15 to 0.6 mm). All CBCT slice thicknesses in the resulting image are much thinner than slices created by medical CT devices [84]. The use of CBCT technology in clinical practice provides a number of potential advantages for maxillofacial imaging compared with conventional CT [85]:

- *X-ray beam limitation* - Reducing the size of the irradiated area, by collimation of the primary x-ray beam to the area of interest minimizes the radiation dose.

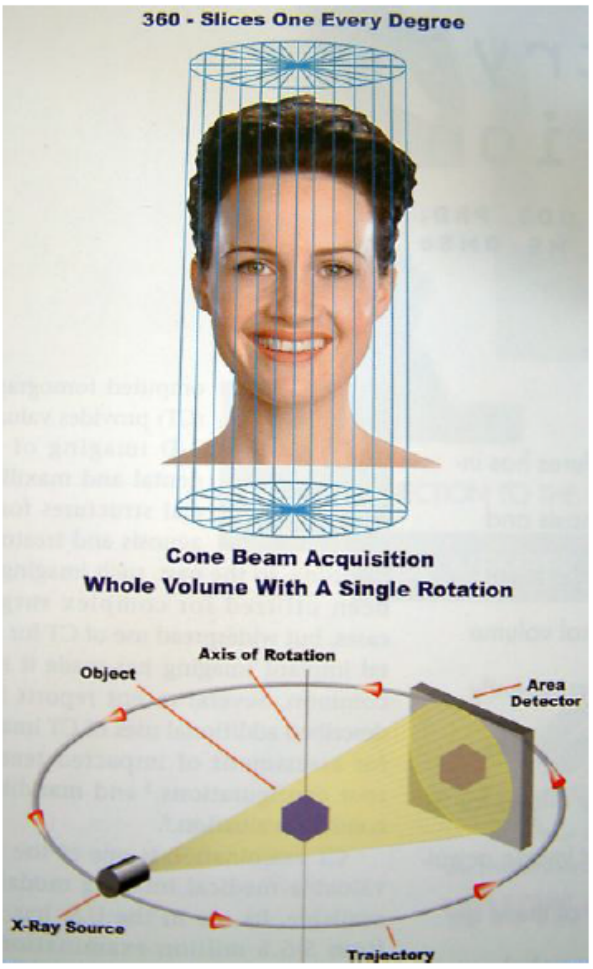

Slika 2.24: Image acquisition of the Cone Beam Computed Tomographer [83]

- *Image accuracy* - All CBCT units provide voxel resolutions that are isotropic. This produces sub-millimetre resolution (often exceeding the highest grade multi-slice CT).

- *Rapid scan time* - Because CBCT acquires all basis images in a single rotation, scan time is rapid (10–70 seconds) and comparable with that of medical spiral MDCT systems.

- *Dose reduction* - Published reports indicate that the effective dose of radiation is significantly reduced by up to 98% compared with "conventional" fan-beam CT systems.

- *Display modes unique to maxillofacial imaging* - Reconstruction of CBCT data is performed natively by a personal computer. In addition, software can be made available to the user, not just the radiologist, either via direct purchase or innovative "per use" licence from various vendors. This provides the clinician with the opportunity to use chair-side image display, real-time analysis and MPR modes that are task specific.

- *Reduced image artifact* - With manufacturers' artifact suppression algorithms and increasing number of projections, clinical experience has shown that CBCT images can result in a low level of metal artifact, particularly in secondary reconstructions designed for viewing the teeth and jaws.

The application of CBCT devices enables wider application of 3D diagnostics in dental medicine. Due to its significant advantages compared to two-dimensional radiological diagnostic methods, the application of 3D diagnostics is expanding in all fields of stomatology and also has great potential for future application in scientific research [86, 87].

3 Bone remodelling

Bone is a remarkable and extremely complex connective tissue. Owing to its interesting properties, it has always captured the attention of scientists to investigate its characteristics. Mass of the bone is related to its function, and the shape of each bone and its inner structure are adjusted to its function as well. As a structural material, bone has an ideal combination of properties: high stiffness, strength, fracture toughness, and light weight [88].

The stiffness of bone is the key to understanding why it differs so greatly from other tissues. Bone differs from the other connective tissues because of its greater stiffness and strength. These properties stem from being a composite material formed by the deposition of a mineral, apatite or hydroxyapatite, in a frame of collagen. Bone is unique in that, while other connective tissues grow interstitially, bone grows only by the addition of tissue on a cell-laden surface. Bone does not retain its scar tissue like other tissues do, and long bones have a very complicated mechanism for growing longer [89].

3.1 Mechanical properties of bone

Great mechanical properties of bone are prescribed by its complex hierarchical structure from nano-structure to the whole bone. Bone structure and its mechanical properties can vary depending on hierarchical level and, also, on its density and mineral composition. Therefore, bone structure is complex, multiphase, heterogeneous and anisotropic. Also, it is important to mention that mechanical properties of bone are not constant, they are changing under different mechanical loading, age, diet, medicines etc.

Curry [90] discusses five mechanical properties on which natural selection can have influence. The first one is *stiffness* which refers to elastic behavior of bone. The second one is *resilience* - this is the ability to absorb energy before reaching the yield stress. Within

this range the bone will not break, but damage will accumulate in the bone. The third one is *quasi-static strength* which can be tested with standard tensile and compressive experiments. The fourth one is *toughness*. This is the ability to prevent dangerous cracks forming and, if they do form, to make it difficult for them to spread. The fifth one is *fatigue resistance*. This property is important since bones are constantly exposed to cyclic loading.
To the mechanical properties of bones, many approaches are used. They can be divided into numerical approaches and experimental approaches. Both types of approaches can be used to define mechanical properties of cortical and trabecular bone at any level. Both types of approaches have their advantages and disadvantages.

Trabecular bone is porous in nature and the cavities in the porous structure are filled with bone marrow. The porous structure of trabecular bone enables adaptation to loading to which it is exposed daily. Moreover, trabecular bone absorbs that loading and distributes it to the rest of the bone. Furthermore, trabecular bone is light and does not have much influence on total bone weight. Trabecular bone is a complex material presenting at the continuum level large heterogeneities based on variations due to location of anatomical sites, age and gender. This in turn affects its mechanical properties, resulting in stiffness and strength variations. Trabecular bone's mechanical behavior at large compressive strain resembles an elastoplastic cellular solid. Under compressive load, trabecular bone shows a decrease of the apparent tangent stiffness before reaching a maximal force.
Many approaches have been used to describe the mechanical behavior of trabecular bone, and depending on the model, trabecular bone can be seen as isotropic, orthotropic or anisotropic, and also as linear elastic, viscoelastic or viscoplastic. In compression, the mechanical behavior of compact and trabecular bone presents distinctly different characteristics. Compact bone is quasi-brittle, while the mechanical behavior of trabecular bone is typical of an elastoplastic cellular material. For both types of bone under compressive monotonic loading, the tangent stiffness decreases already before the maximum force is reached. For trabecular bone, a smooth and gradual reduction of the stress (softening) occurs until a local minimum is reached, followed by slight rehardening. In their study, Hazrati Marangalou *et al.* [91] explored a different approach to derive patient-specific fabric information by using a database of high-resolution bone models. By combining the density information measured from a patient's CT scan with fabric information from the database, patient-specific anisotropic properties were defined. The goal of their study therefore was to investigate if models with fabric derived from a database can produce more accurate results than isotropic models. To investigate this, they have compared the

stress and damage distribution as well as the whole bone stiffness and strength for FE models with fabric derived from the actual bone with those of model with fabric mapped from the database or isotropic mechanical properties. Newitt *et al.* [92, 93] determined the effects of trabecular bone microarchitecture on bone mechanical properties using a combination of magnetic resonance (MR) imaging and micro-finite element analysis (mFE) in the distal radius. They have related these measures to BMD at the distal radius, lumbar spine and proximal femur, as well as to the systemic rate of bone turnover. They have also determined whether the inclusion of structure measures improves the prediction of bone mechanical properties as assessed using μFE analysis.
In his research Zysset [94] put fabric tensor to describe microstructural architecture of trabecule. Fabric tensor is quantitative stereological measure of the microstructural architecture, a positive-definite second order tensor that establishes the principal values and directions of bone mass distribution [95]. He has compared theoretical models relating morphology to the elastic properties of human trabecular bone using experimental and numerical data sets available in literature. Later, Wolfram *et al.* [96] used Zysset's orthotropic model to confirm their experiments. Results of nanoindentation of wet and dry bone are used as input data for theoretical Zysset's model. Hosseini [97] in his work extended the phenomenological model of trabecular bone limited to infinitesimal strains to model that includes large compressive strains by including post-yield softening and densification. His model was able to predict the damage localization and densification of trabecular bone. Charlebois *et. al.* [98] proposed a model which aims at describing the mechanical behavior of trabecular bone in the range of small to moderate compressive strains and thus considers simultaneous accumulation of plastic deformation and damage that eventually leads to softening.

In cortical bone the mechanical properties are influenced greatly by the porosity, the mineralization level and the organization of the solid matrix [99]. Cortical bone is both stronger and stiffer when loaded longitudinally along the diaphyseal axis compared with the radial or circumferential "transverse" directions. Cortical bone is also stronger in compression than in tension. It is also important to note that the microstructure of compact bone varies markedly between different species of animals and even different bones of the same animal, and different sites of the same bone that in turn leads to variability in properties. Previous studies showed that the mechanical properties of bones are significantly affected by its microstructural characteristics.
In his research Schneider [100] found the relationship between density and components of modulus of elasticity assuming cortical bone as orthotropic. The density was read from CT scans in HU units. An approach to determine mechanical properties of cortical bone by

multiscale method was adopted by Hamed [88, 101]. He proposed a step-by-step modeling of effective elastic properties of cortical bone at four different structural scales, from the nanostructural level (level I) up to the mesostructural level (level IV). Focus of Abdel *et. al.* [102] in their research was on quantification of elasto–plastic behaviour of cortical bone using specimens cut along different directions with regard to the bone axis—longitudinal (axial) and transverse. Due to pronounced nonlinearity of the elastic–plastic behaviour of the tissue, they performed cyclic loading–unloading uniaxial tension tests to obtain the magnitudes of elastic moduli not only from the initial loading part of the cycle but also from its unloading part. The second part of their study covered creep and relaxation properties of cortical bone for two directions and four different anatomical positions to study the variability of bones properties. In order to obtain subject-specific bone mechanical properties, Duchemin *et. al.* [103] presented a study which aims at finding a relationship between the bone density measured by CT and the longitudinal elastic modulus as well as the ultimate strength. A large number of specimens of femoral cortical bone were considered. In their study Novitskaya *et. al.* [104] investigated the mechanical properties of fully demineralized, fully deproteinized and untreated cortical bovine femur bone by compression testing in three anatomical directions (longitudinal, radial and transverse). They observed anisotropic mechanical properties: the radial direction was found to be the strongest for untreated bone, while the longitudinal one was found to be the strongest for deproteinized and demineralized bones. The aim of Szabó and Thurner's [105] study was to compare the accumulated microdamage prior to failure and the local strains at microdamage initiation as well as at failure in three different anatomical orientations: longitudinal, tangential (or circumferential) and radial. The bone whitening effect was used for detecting microdamage.

Some of the researchers were investigating mechanical properties of bone as a whole, where the research was usually made on the femur and the vertebra. The approaches were the same as for the research on cortical and trabecular bone. In many published studies, elastic properties of bone are correlated to bone density, in order to derive an empirical elasticity–density relationship. Helgason *et al.* [106] did a literature review, in which they included elasticity–density relationships derived only from similarly controlled experiments and properly normalized results. The resulting relationships were grouped according to the most important methodological differences: type of end support during testing, specimen geometry, and anatomical sampling location. They made recommendations for the application of elasticity–density relationships to subject-specific finite element studies. The importance of defining a standardized mechanical testing methodology for bone specimens is stressed,so they proposed some guidelines that emerged from the literature. In their

research Boutroy *et. al.* [107] compared in vivo measurements of BMD, microarchitecture, and bone mechanical parameters assessed by μFE analysis in women with and without prior history of wrist fracture. They analyzed the correlations between density, microarchitecture, and μFE-predicted parameters and to establish which parameters or combinations of parameters were most relevant. Dall'Ara *et. al.* [108, 109] evaluated the ability of voxel FE models in predicting femoral stiffness, strength and failure location for a large number of pairs of human femora tested in two different loading scenarios. Pahr *et. al.* [110] compared compressive strength measurements obtained from in vitro tests with the ones from two different simulation models: clinical quantitative computer tomography (QCT) based homogenized finite element (hFE) models and preclinical high-resolution peripheral QCT-based (HR-pQCT) hFE models. They concluded that HR-pQCT-based hFE models increased the predictability considerably and did not need any tuning of input parameters. In contrast, QCT-based hFE models usually need some tuning but are clinically the only possible choice at the moment.

3.2 Mechanical description of bone remodelling

During the course of a person's life, both the cortical and the trabecular bone are constantly renewed by the process of bone remodelling. The process of bone remodelling was explained from a biological point of view in Chapter 2.1.2. But, the question remains what causes bone remodelling and how it can be described from a biomechanical point of view.

It is well known that mechanical loading plays an important role in bone remodelling in both the cortical and the trabecular bone since its effect on bone morphology is obvious. It was Wolff (Wolff, 1892) who first observed the relationship between bone structure and applied loads. He stated [6]:
"Every change in the form and function of bone or their function alone is followed by certain definite changes in their internal architecture, and equally definite alteration in their external conformation, in accordance with mathematical laws."
This statement says that bone will be formed on the sides where bone loading is increased and removed on the sides where bone loading is reduced, and today that statement is known as Wolff's law. It is important to emphasize that Wolff's law is not a law in the traditional sense, but a qualitative observation. The current concept is that bone architecture is controlled by a local regulatory mechanism. This idea originates from Roux (1881), who proposed that bone remodelling is a self-organizing process [6].

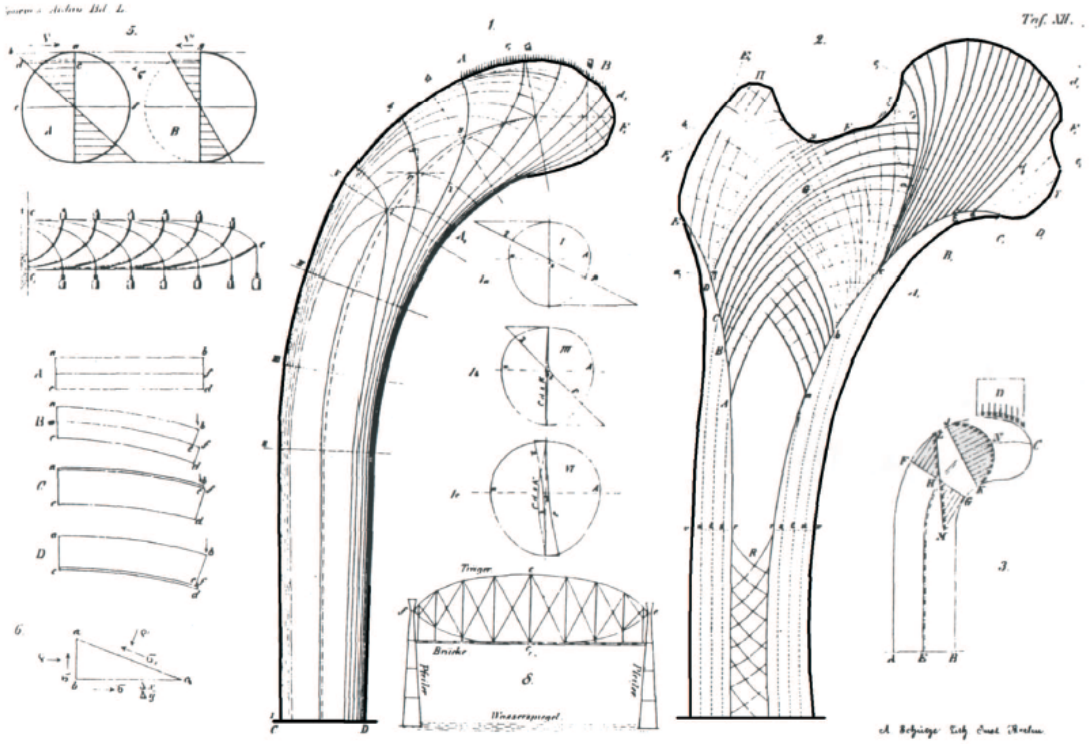

Slika 3.1: Culmann's crane and von Meyer's trabecular architecture [89]

In the same period von Meyer and Culmann made a correlation between cancellous bone structure and the mechanical loads, which is a historical root of study of tissue adaptation [89]. In Figure 3.1 on the left, Culmann's graphical statics of stress trajectories in a crane can be seen. On the right, von Meyer's sketch of the trabecular architecture in a section through the proximal end of the human femur is shown. This sketch is often cited as the first parallel drawn between biology and mechanics, leading to the start or initiation of the field of biomechanics. The mechanical stress patterns in a curved column structure that Culmann had been analyzing (known as a Fairbairn crane) were remarkably similar to the patterns of internal trabecular patterns documented by von Meyer [89].

Frost [3, 4, 5, 111], in 1960's, captured both these statements and provided more quantitative description in his 'mechanostat' theory, in which he assumes that local strains regulate bone mass. Frost proposed a mathematical description of bone remodelling assuming two thresholds on the stress level. He proposed that local stress regulates bone mass in a way that new bone is formed when the stress exceeds the upper stress threshold level and is removed if the stress is below the lower stress threshold level. He also differentiated between internal and external remodelling. Internal remodelling refers to the change in

the distribution of the material properties and external remodelling analyses changes in the external geometry.
After Frost's mathematical and mechanical formulation of bone remodelling, Cowin, in 1970's, provided the first complete mathematical model of bone remodelling (theory of adaptive elasticity). In his approach bone is modelled as a poroelastic medium with a solid phase surrounded and perfused by a fluid component. Bone remodelling considered to be a considered as a strain-controlled transfer of mass between the fluid phase and the solid phase [49].

Whereas the bone remodelling theories based on Wolff's law have been successfully applied and tested extensively in the field of orthopaedic research, they are not widely used in orthodontics. In that field, alternative theories have been introduced instead, to explain tooth movement. These models are usually based on empirical rules rather than on a fundamental load-adaptive bone remodelling theory.
Orthodontic tooth movement has been defined as the result of a biologic response to interference in the physiological equilibrium of the dentofacial complex by an externally applied force [38]. To explain the biological response, two theories have been developed, *pressure-tension theory* and *bone bending theory*. These theories are used as approaches to to biomechanical explanation of explain bone remodelling induced by orthodontic tooth movement.

Pressure-tension theory is based on the assumption that the deformation in the periodontal ligament is a stimulus that induces bone remodelling and thus enables tooth movement. The tooth moves in the periodontal space by generating a "compression side" and a "tension side." This hypothesis proposes that, on the compression side, the PDL displays disorganization and diminution of fiber production. Here, cell replication decreases seemingly due to vascular constriction. On the tension side, stimulation produced by stretching of PDL fiber bundles results in an increase in cell replication. This enhanced proliferative activity leads eventually to an increase in fiber production [38].
Bone bending theory is based on the assumption that deformation in the alveolar bone is the major cause of bone remodelling, so the pressure state (positive or negative) of the bone matrix is the key stimulus to differentiate apposition and resorption in overloaded conditions. When an orthodontic appliance is activated, forces delivered to the tooth are transmitted to all tissues near the force application. These forces load the bone, tooth, and the solid structures of the PDL. Bone was found to be more elastic than the other tissues and to bend far more readily in response to force application. The active biological

processes that follow bone loading involve bone turnover and renewal of cellular and inorganic fractions. These processes are accelerated while the bone is held in the deformed position [38].

3.3 Models in orthopedic biomechanics

Models in orthopedic biomechanics describing bone remodelling are widely used and developed. From the beginning these models have experienced quite a revolution. Initial models were observed bone from a macroscopic view and today's models explain bone remodelling on cell level. But all of them are based on the assumptions and research of Wolff and Frost. The evolution of models used in orthopedic biomechanics can be divided into three stages, first generation models, second generation models and third generation models.

First generation models are phenomenological models and linear elastic models. They based their theory on the existence of a mechanical stimulus, where stimulus is a scalar representation of the applied mechanical load. Mechanical stimulus produces bone apposition or resorption in a way that the stimulus tends to reach homeostatic level in the long term (homeostasis) following Frost's mechanostat theory explained in the section above. These models relate Young's modulus to bone density and they compute the change of bone apparent density (and therefore stiffness) as a function of a given mechanical stimulus. Apparent density is ratio of bone without marrow and fat (mineralized bone mass) and whole bone volume (bulk volume) [112].
There are two important groups that made notable contributions in this field that can be placed in first generation models. These are the group from Stanford University, USA, and the group fromthe University of Nijemegen, The Netherlands.
Stanford model [7, 9, 10] presented an isotropic remodelling model, in which the mechanical stimulus was identified with the so-called daily tissue stress level, ψ_t, a scalar quantity, and it included several load cases. They also established a relation between the stress at the continuum level σ and the one at the tissue level σ_t, following a standard homogenization procedure and supported by experimental data. Bone resorption and apposition occur on internal surfaces, so the mechanical stimulus is directly related the surface remodelling rate, $\dot{r}$, which quantifies the bone volume formed or eliminated over the available surface per time unit. They also put forward a criterion for formation and resorption. It is graphically shown on Figure 3.2 (a) [7]. This diagram shows remodelling rate as a function of the tissue-level stimulus, ψ_t. The first section shows underloaded conditions in which

resorption takes place,the second section shows a lazy zone, in which no remodelling takes place, and the last section shows overloaded conditions where formation takes place. In the middle boundaries of a lazy zone can be seen ($\psi_t^* \pm \omega$), and 2ω is the length of the lazy zone. They defined stimulus by the relation 3.1

$$\psi_t = C\frac{\sqrt{\sigma : \varepsilon}}{\rho^{2-\frac{\beta}{2}}}, \tag{3.1}$$

where C and β stands for experimental data, σ and ε are stress and strain and ρ apparent density. $C{=}N^{1/m}\rho_0^2\sqrt{B}$ where N is the number of different load cases for m load cases, ρ_0 is the density of the fully calcified bone. B and β are experimental data used to determinate elasticity modulus and the Poisson ratio of bone by relation $E = B(\rho)\rho^{\beta\rho}$ The Stanford's model is used in an explicit scheme at the end of each time step of a finite element analysis, the density is updated according to its evolution rate and then the mechanical parameters are updated at each element for the next time step.

The group from University of Nijemegen, Huiskes *et al.* [11, 113, 12, 13, 114] chose the strain energy density (SED) per unit of bone volume as the remodelling stimulus. The reason for choosing this variable is that SED can be directly calculated from the stresses and the strains in each point of the bone. The remodelling signal is based on the assumption that bone strives to normalize the average elastic energy per unit of mass for a particular loading history. Also, this group follows the similar diagram of bone remodelling as the group from Stanford. Diagram on Figure 3.2 shows remodelling velocity as a function of stimulus, in this case SED. Boundaries of the lazy zone are $(1\text{-}s)\,U_n \leq U \leq (1{+}s)\,U_n$, whereby s is threshold level and $2s$ the length of the lazy zone. Huiskes *et al.* calculated internal and external bone remodelling. They defined remodelling signal S as:

$$S = \frac{1}{n}\sum_{i=1}^{n}\frac{U_i}{\rho}. \tag{3.2}$$

where U_i is SED in the bone for loading case i, ρ is apparent density and n is is the number of loading cases considered.

Jacobs [115, 116] made energy based anisotropic extension of Stanford's model. He assumed that bone remodelling was an optimal process in some energetic sense. The goal of the adaptation is thus considered as obtaining a globally efficient mechanical structure. The efficiency is computed as the difference between the power associated with external loads and rate-of-change of the total internal energy.

Stress-induced changes in bone microstructure not only result in changes in the apparent bone density, but also lead to trabecular reorientation, which is reflected at the macro-level in the non-isotropic character of the stiffness tensor $\mathbf{C}$. So, Jacobs [115, 116] provided an

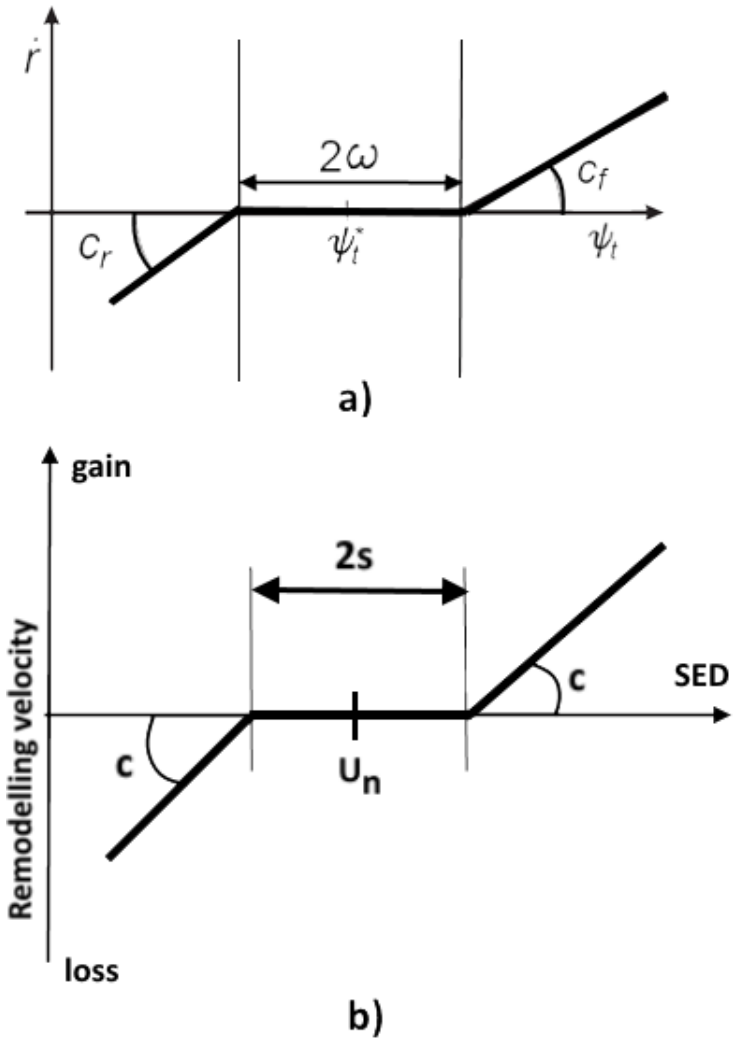

Slika 3.2: Remodelling rate as a function of stimulus Stanford model: (a) [7], Huiskes *et al.* (b) [11]

expression for anisotropic adaptation of stiffness as

$$\dot{\mathbf{C}} = \frac{\beta\dot{\rho}}{\rho}\frac{\sigma \otimes \sigma}{\sigma : \varepsilon}, \tag{3.3}$$

where $\dot{\mathbf{C}}$ is stress-induced anisotropy, i.e. rate-of-change of the stiffness tensor, $\dot{\rho}$ accounts for the development of stress-induced density inhomogeneity, i.e. rate-of-change of density, σ is stress and ε is deformation. Relation 3.3 includes the rate-of-change of density and the rate-of-change of the stiffness tensor which is coupled to density; however, it can no longer be directly computed from density as in the isotropic case. Furthermore, any features of the isotropic density formulation such as a dead zone, linear surface apposition rates, or the effect of available specific surface area are automatically accounted for in the rate-of-change of the stiffness tensor. In this way, when density changes are prohibited due to physical limitations on the porosity the changes in the stiffness tensor likewise cease [116].

Second generation models are phenomenological models based on first generation models and the characteristic of these models is that they coupled two laws into one trying to describe bone remodelling. Doblaré and García [95, 37] have upgraded Stanford model with general damage-repair theory following the principles of Continuum Damage Mechanics. They defined a damage-repair remodelling tensor, $\mathbf{H}$, in terms of apparent density and Cowin's fabric tensor, respectively associated with porosity and directionality of the trabeculae. With all this in mind, they defined stimulus $\mathbf{Y}$ as

$$\mathbf{Y} = \Big[2\hat{G}sym[(\mathbf{H}\varepsilon\mathbf{H})(\mathbf{H}\varepsilon)] + \hat{\lambda}tr(\mathbf{H}^2\varepsilon)sym(\mathbf{H}\varepsilon))\Big], \tag{3.4}$$

where $\hat{G}$ and $\hat{\lambda}$ are Lamé parameters of the ideal compact bone with null porosity.
One other model should also be mentioned here, the model by Prendergast *et al* [117]. They developed damage-adaptive remodelling laws and a remodelling law to predict the time course of bone adaptation. It is shown that this is an integral remodelling law which accounts naturally for the stress history to which the tissue has been exposed since formation. They hypothesize that damage exists in the form of inter-constituent microcracks present within the bone, even at remodelling equilibrium. The stimulus for remodelling is the change in damage from this equilibrium amount, so the stimulus for bone adaptation is not determined by the strains as such but rather by the effectiveness of the strain in creating damage of the microstructure. They defined stimulus as

$$\Delta\omega = \omega - \omega_{RE} \tag{3.5}$$

where ω denotes the actual damage in the microstructure, and index RE refers to remodelling equilibrium.

Later, McNamara and Prendergast [118] updated Prendergast's model [117]. They tested the hypothesis that bone remodelling may be regulated by signals caused by both strain and microdamage and studied four mechano-regulation algorithms, in which the stimulus is strain, damage, combined strain-damage, and either strain or damage with damage-adaptive remodelling prioritized when damage is above a critical level. Each algorithm is implemented with both bone lining cell (surface) sensors and osteocyte cell (internal) sensors. Each algorithm is applied to prediction of a bone multicellular unit (BMU) remodelling on the surface of a bone trabecula. It is predicted that a regulatory system capable of responding to changes in either strain or microdamage but which prioritizes removal of damaged bone when damage is above a critical level, is the only one that provides a plausible prediction of BMU behaviour. As the basis of their approach, they used Huiskes *et al.* theory [11, 113, 12, 13]. They stated the strain-related bone remodelling stimulus at a site as S^j_{strain}:

$$S^j_{strain} = U^j - U_{ref}, \tag{3.6}$$

where j refers to location, and U_{ref} is the reference stimulus calculated from values of E and ρ from bone at homeostatic equilibrium.

Fernardez *et al.* [119, 120] studied from a numerical point of view a strain-adaptive bone remodelling that coulped the displacements and apparent density (the porosity) of the bone. The rate of this density at a particular location is described as an objective function, which depends on a particular stimulus at that location. The variational problem is written as a coupled system of a nonlinear variational equation for the displacement field and a nonlinear parabolic variational inequality for the apparent density. They have predicted a reasonably accurate density distribution with a intramedullary canal. The evolution of the apparent density function is obtained from the following first-order ordinary differential equation

$$\dot{\rho} = B\left(\frac{U(\sigma(\mathbf{u}), \epsilon(\mathbf{u}))}{\rho} - S_r\right), \tag{3.7}$$

where B and S are experimental constants and $U(\sigma(\mathbf{u}),\epsilon(\mathbf{u}))$ is mechanical stimulus defined by strain energy density.

Idhammad *et al.* [121, 122] developed a new law of bone remodelling in the context of damaged elastic by applying the thermodynamic approach in the case of small perturbations. The model is solved numerically by a finite difference method in the one-dimensional bone structure of a n-unit elements model. The new law of bone remodelling may be written as

$$R\Big(\phi, D\Big) = -\frac{\sigma^2 f_d}{2c} \cdot \frac{D}{(1-D)^3} \cdot \frac{1}{\phi^\alpha \phi}, \tag{3.8}$$

where R is remodelling variable, D is damage variable, ϕ is bone density, and c and α are

a constant characteristic for bone experimentally obtained in research made by Curry [123].

The third generation models used in orthopeadic biomechanics are different types of models that can be grouped into mechanobiological models, μFE models, nonlinear models and multiscale models.

Mechanobiological models take into account detailed biological activity and predict the evolution of the microstructure and biological constitution. Pivonka *et al.* [124, 125] used a mechanobiological model and developed an extended bone–cell population model describing functional behaviour of basic multicellular units. They also focused on the mechanism of bone cells, which involves the morphology of the microstructure of bone. They developed a sophisticated mathematical model of bone cell interactions that takes into account biochemical, biomechanical and geometrical regulations. Then, they investigated numerically the influence of bone surface availability in bone remodelling within a representative bone tissue sample. They defined bone remodeling as a change of bone volume over time as

$$\frac{dBV}{dt} = AF \cdot (-V_{res} + V_{form}), \tag{3.9}$$

where BV denotes the total bone mass and AF (in [1/t]) is the activation frequency of BMU corresponding to the number of BMU being formed in a unit volume per unit time, and V_{res} and V_{form} are the volume of resorption cavity and the deposited volume of completed osteon.

Mechanobiological models were also used by Adachi. Adachi *et al.* [126] proposed a theoretical framework of trabecular bone remodelling that interconnects the microscopic cellular activities to the macroscopic morphological changes through the mechanical hierarchy by constructing a mathematical model of this complex adaptation mechanism. Their model can predict bone functional adaptation by remodelling. By integrating the fluid-induced shear stress on the cell processes, they defined the mechanical stimulus $S_{oc}(\mathbf{x})$ sensed by the osteocytes per unit of volume as

$$S_{oc}(\mathbf{x}) = \int_0^{2\pi} \mathrm{d}\varphi \int_0^{2/\pi} \frac{2r_p}{r_p^2} \rho_c(\mathbf{n}) \overline{|\tau_P \mathbf{n}|} \mathrm{d}\theta, \tag{3.10}$$

where θ is angle between x_3 in the Cartesian coordinate system and vector $\mathbf{n}$, φ is angle between x_1 axis and the projection of $\mathbf{n}$ onto the x_1x_2-plane, measured anticlockwise, $\mathbf{n}$ is vector and ρ_c canalicular volume fraction, τ_P is shear stress acting on the osteocyte processes that align in direction $\mathbf{n}$, r_p is radius of osteocyte processes. Modelling framework of trabecular remodelling made by Adachi *et al.* is shown on figure 3.3 where it can be seen position of vector $\mathbf{n}$ and angle φ.

The FE models for bone tissue are often built on image data provided from CT, and

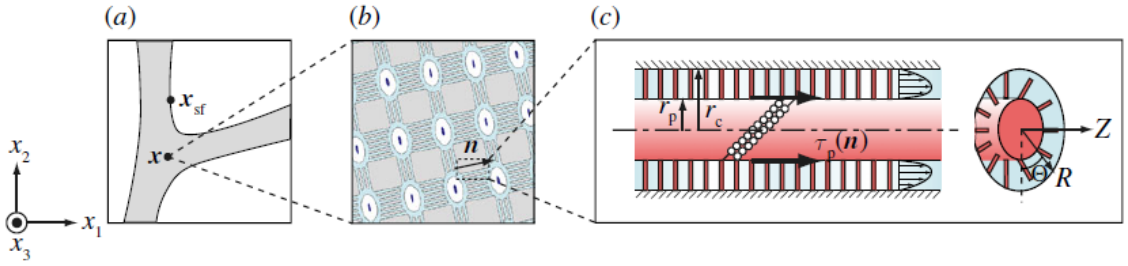

Slika 3.3: Modelling framework of trabecular remodelling made by Adachi *et al.* [126]

μFE models are based on images obtained from μCT. Ruimerman *et al.* [127, 128, 129] did a research in which they revealed how mechanical forces are sensed in the bone, and how these mechanical forces are translated to structural adaptation of the internal tissue architecture. They developed an μFE model in which they applied (re)modelling theory in order to search for pathways by which estrogen deficiency might affect the remodeling process and cause the phenomena that are typical for postmenopausal osteoporosis. They defined stimulus R on trabecular surface location x, depending on its mechanosensitivity μ_i as

$$R(x,t) = \sum_{i=1}^{N} f(x,x_i)\mu_i R(x_i,t), \tag{3.11}$$

where R is signal that osteocytes sense and $f(x,x_i)$ describes the decay in signal.
Verhulp *et al.* [130, 131, 132] aimed to quantify the effects of assumed isotropy, by comparing continuum-level voxel models of a healthy and a severely osteoporotic proximal femur with recently analyzed μFE models of the same bones. They used high-resolution cross-sectional images and converted to FE models incorporating the micro-architecture of trabecular bone in detail.
Mengoni and Ponthot [19] proposed a pressure dependent nonlinear model for trabecular bone remodelling accounting both for density change and anisotropy, coupled with an elastoviscoplastic bone matrix. This model was written within the framework of anisotropic continuum damage mechanics in finite strains. They defined mechanical stimulus Y as

$$Y = \frac{1}{2G} sHs + \frac{\eta p^2}{3K(1-\eta D_h)^2} H^{-3}, \tag{3.12}$$

where H is remodelling tensor, s and p are the stress deviator and the pressure (nominal stress $\sigma = s + p\mathbf{I}$), D_h=1/3 tr(D), D is damage tensor.
Multiscale modeling is the determination of material properties or behavior on one level using information or models from different levels, so this is one of the approaches to describe bone remodelling. This approach was used by Scheiner *et al.* They [133] developed a mathematical framework describing this process at the (macroscopic) level of cortical

bone, by combining, for the first time, bone cell population kinetics with multiscale bone mechanics. Key variables are concentrations of biological cells and biochemical factors, as well as mechanical strains, both at the ("macroscopic") level of cortical bone and at the ("microscopic") level of the extravascular bone matrix.

3.4 Models in orthodontics

As mentioned above, bone remodelling theories that are based on Wolff's Law are not widely used in orthodontics. High compressive stress could be expected in the bone on the side to which tooth is pushed, but in fact it is bone resorption that occurs here, low stresses could be expected on the other side, where in fact bone apposition takes place. This is not in accordance with with Wolff's Law. Models used in orthodontics are based on empirical rules rather than on a fundamental load-adaptive bone remodelling theory and they simplify geometry and the periodontal ligament, or also even completely ignore periodontal ligament. Also, two approaches are used to explain this phenomenon. One approach states that deformations of the periodontal ligament are the key stimulus to start orthodontic tooth movement and orthodontic bone remodelling while the other approach states says that deformations of the alveolar bone are the basis of orthodontic bone remodelling.

Bourauel *et al.* [15, 14] are pioneers in this field and they have carried out many numerical and experimental studies. In their research they have used both approaches and have come to the conclusion that the approach focused on the deformation of the PDL as the key stimulus is the approach that better explains the problem. They have used linear elastic models. Field *et al.* [16] also used the approach with the deformation of the PDL as the key stimulus and in their study they aimed to provide a better understanding of the stress-strain patterns in the initial stage of OTM. They assumed that the structures responded to tipping load linearly, and all materials in this analysis were modelled as isotropic and elastic.
The approach that deformations of the periodontal ligament are the key stimulus to start orthodontic tooth movement was also used by Penedo and van Schepdeal. Penedo *et al.* [17] developed and validated a three-dimensional numerical model of a maxillary central incisor to simulate tooth movement using the Finite Element Method, and they performed a simulation of different tooth movements and the establishment of centres of rotation and resistance. Van Schepdeal *et al.* [35, 21] developed a mechanobiological model using partial differential equations to describe cell densities, growth factor concentrations, and

matrix densities occurring during orthodontic tooth movement. They hypothesized that such a model can predict tooth movement based on the mechanobiological activity of cells in the PDL. Tominaga *et al.* [20] clarified the effect of the play between the bracket and the archwire on anterior tooth movement subjected to the retraction force from various lengths of power arms in sliding mechanics.

The approach that deformations of the alveolar bone are the basis of orthodontic bone remodelling was used by Mengoni and Ammar. The goal of Mengoni *et al.* [30, 31] was to provide a constitutive phenomenological model able to simulate this bone adaptation to external loading, taking into account the particular pressure effect macroscopically observed on alveolar bone. She proposed a pressure dependent model for trabecular bone remodelling accounting both for density change and anisotropy, coupled to an elastoviscoplastic bone matrix. Ammar *et al.* [18] determined stresses in bone which occur due to implants and orthodontic wires that cause orthodontic tooth movement.

4 Materials and methods

In the proposed research, the bone remodelling initiation caused by wearing a fixed orthodontic appliance is numerically described. Also, the goal is to develop a numerical model that is patient specific, which would result in personalized orthodontic treatments. In the research, a single root tooth, incisor, is used, which will be loaded with the vertical force that describes chewing force, as well as with the transversal force that describes the influence of orthodontic force.
The goal is to test whether tooth movement resulting from orthodontic force applied to the alveolar bone can be predicted by using load adaptive bone remodelling theories developed in earlier studies. This was tested by using patient-specific 3D models of tooth and the alveolar bone.

4.1 Approach

Literature review has shown that there are still open questions in the field of biomechanical description of tooth movement. It can be seen that over the last twenty years the field of orthodontics has improved significantly. New materials have been developed and orthodontic appliances have been optimized. Literature shows most research focuses on describing stress and strain distribution in tooth, PDL and alveolar bone caused by different loading. However, few studies focus on the analysis of bone remodelling induced by orthodontic tooth movement. Furthermore, the analyses are limited because they use simplified geometry, simplified or not modelled PDL. Furthermore, it has been noticed that the mechanism which describes tooth movement is still not understood enough. The research presented here should improve the understanding of tooth movement and in that way contribute to the development in the development of orthodontic treatment and planning.

In Chapter 3 two approaches were explained that are used to clarify bone remodelling induced by the orthodontic force. They are called, from the point of view of medicine and dental medicine, bone bending theory and compression-tension theory.
From a biomechanical point of view, differences between these theories are the use of stimulus for triggering bone remodelling and allowing for tooth movement in the direction of the applied force. Bone bending theory focuses on the deformations of the alveolar bone as stimulus, where it is assumed that the pressure state (positive or negative) of the bone matrix is the key stimulus to differentiate between apposition and resorption in overloaded conditions. Compression-tension theory focuses on the deformations of the periodontal ligament as the key stimulus to start orthodontic tooth movement and orthodontic bone remodelling. On the compression side, the PDL displays disorganization and reduction a of fibre production resulting in resorption and a decrease of cell replication. On the tension side, stimulation produced by stretching of PDL fibre bundles results in an increase in cell replication and bone formation. These theories explain bone remodelling and tooth movement only partially for the reason explained next.

The approach that uses the deformations of the alveolar bone as stimulus does not take into account the influence of the PDL. Therefore, two hard tissues are in contact and when force is applied to the tooth, the tooth starts to move in the direction of applied force. In the direction of tooth movement, bone compression starts on that side. Wolff's Law states that this results in adding the bone onto the so-called compression side and removing the bone on the tension side. This results in disabling tooth movement in the direction of the applied force. This approach is shown on Figure 4.1 (a)in which $''+''$ refers to bone formation and $''-''$ refers to bone resorption. This schematic figure,4.1 (a)shows bone bending theory which is, by theory, taking into account Wolff's Law. It can be seen that it does not fully explain bone remodelling caused by orthodontic force application. Even traditional orthodontics relates compression to resorption, and tension to apposition. This is in contrary to Wolff's Law and opposite to orthopeadic research that has been done in great detail. In orthopeadic bone remodelling research, remodelling is linked with the magnitude of loading and not with the sign of loading. Melsen [33, 34], an orthodontist, tried to test both theories, and came to the conclusion that bone bending theory does not explain tooth movement.

The other approach, compression-tension theory, uses deformations of the periodontal ligament as the key stimulus for bone remodelling. This theory is taking into account the influence of the PDL. The compressive-tension theory is schematically shown on Figure 4.1 (b). As explained above, the compressed side leads to bone resorption, because of PDL

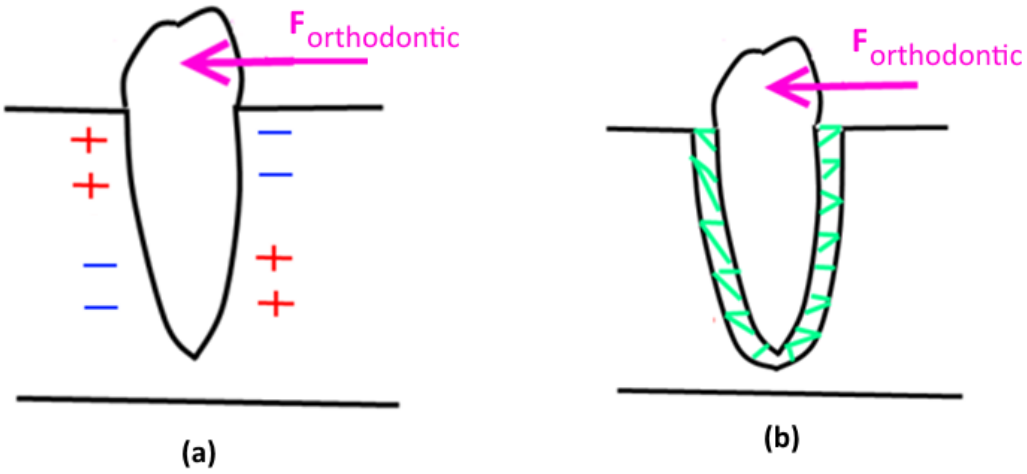

Slika 4.1: Bone bending theory (a), compression-tension theory (b)

compression. The other side leads to bone formation, because of PDL tension. This theory does not violate Wolff's Law. However, it does not follow the bone adaptation theories that have been developed [7, 8, 9, 11, 12, 13].
In load adaptive bone remodelling theories the mechanical stimulus plays a crucial role. As mentioned in Chapter 3, the mechanical stimulus is defined as daily tissue stress level. Thus, the influence of daily tissue stress is quantified, where in Stanford model is defined as effective stress at the tissue level, and in Dutch model strain energy density is remodelling stimulus. Even compression-tension theory is not contrary to Wolff's Law, it does not take into account the influence of mechanical stimulus. Therefore, compression-tension theory does not completely describe bone remodelling due to orthodontic force.

The research presented in this thesis uses an alternative theory which does not violate Wolff's law and also takes into account the influence of mechanical stimulus. The hypothesis used in this research is based on the assumption that teeth are supported by a network of fibres. These fibres form the PDL and connect the tooth to the bone. The fibres are stretched when an orthodontic force is applied and this stretching results in a higher loading of the bone, opposite to the loading direction. Thus, an overloaded condition leads to bone formation on the overloaded side, and bone resorption on the underloaded side. Therefore, tooth movement in the direction of the applied force will be established.
Furthermore, the research should not only consider orthodontic force, but the influence of chewing force as well. This is because small transversal forces will slightly tilt the tooth. As a result of this tilting, large chewing force is offset from its normal working line,

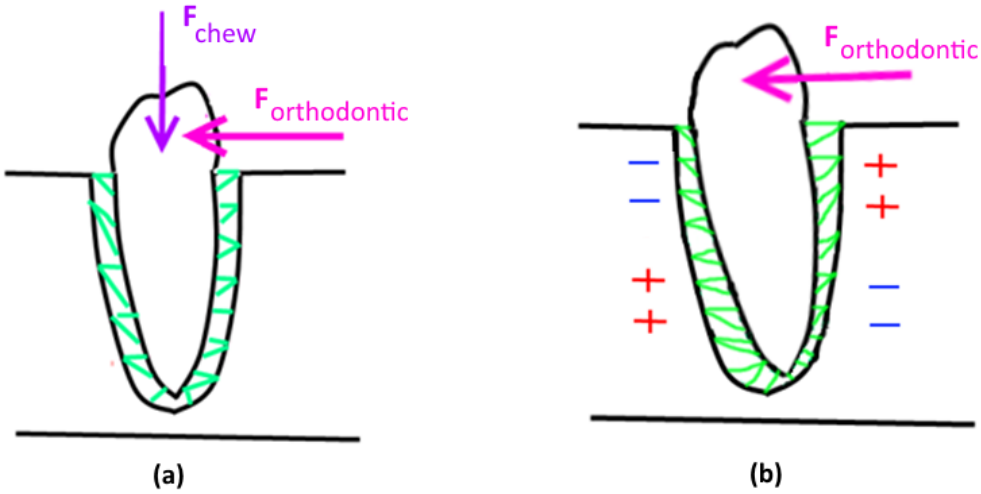

Slika 4.2: Hypothesis explaining bone remodelling initiation

and generates a large moment, leading to much larger changes in the bone loading than one would expect from orthodontic forces alone [134, 135, 36, 39]. Literature shows that chewing force, in combination with other forces in the mouth, plays an important role in bone remodelling in the alveolar bone. So, chewing force can be see as referent loading on the alveolar bone, because it constantly influences the alveolar bone. The hypothesis, which includes deformations in the PDL and PDL fibres and the combined action of orthodontic and chewing force on the mechanical environment, takes into account today's knowledge of bone behavior under loading, including Wolff's law and earlier experiments. The hypothesis is schematically shown on the Figure 4.2. On the left in Figure 4.2 (a) the position of both forces on the tooth is shown and on the right Figure 4.2 (b) stretching of the fibres is shown, where bone formation ($''+''$ in the figure) and bone resorption ($''-''$ on the figure) are marked.

Chewing force observed separately has a big influence on the alveolar bone. Bone remodelling is dependent on the maximum load experienced throughout its load history [7]. However, remodelling in alveolar bone is also characterised by the number of daily cycles that are consistent with mastication [10, 116]. Reina *et al.* [136] observed the influence of daily mastication force on the mandible. They assume that mastication is a pseudostatic process and that the maximum values of chewing force can be obtained by solving a static problem in which the forces developed by the masticatory muscles are applied on the teeth. Field *et al.* [134] studied how chew force influence the alveolar bone. They used the chew force as a static force in their analysis. These works concluded that the chew force has influence on alveolar bone by causing bone remodelling [10, 115, 136, 137].

Also, it is known via animal research [28, 29] that only a dynamic force can cause bone remodelling. Thus, orthodontic force which is, naturally a static force, will not cause bone remodelling by itself. Chewing force is dynamic force. In this research, chewing force is seen as a trigger for bone remodelling but it also represents daily loading, i.e. chewing force can be seen as a trigger and a stimulus for bone remodelling. Following the remodelling literature on the mandible, even though chewing force is a dynamic force in reality, it is going to be modelled as a static force, giving a referent value of the mechanical stimulus.

The role of PDL in the mouth is very important. PDL does not only feed and connect the tooth and the bone, but it also amortizes and absorbs all the forces that act on the tooth. For these reasons, PDL was extensively studied experimentally and numerically. Literature shows several different approaches to numerically and experimentally explaining the mechanical behavior of the periodontal ligament. Some research focused only on PDL, while others explain the properties of PDL by observing it as a part of tooth periodontum. Natali *et al.* [138], Pietrzak *et al.* [139] and Limbert *et al.* [140] considered the PDL as a hyperelastic material. Su *et al.* [141], Aversa *et al.* [142] and Toms *et al.* [143**?**] proposed models accounting for a time dependency through the use of viscoelastic models using up to four time constants. Furthermore, Provatidis [26, 27], Qian *et al.* [144] and Melsen [33, 34] modulated PDL as fibres. Borák *et al.* [23] proposed a bilinear model defined with three parameters, i.e., two different Young's modulus and the Poisson ratio. Cattaneo *et al.* [24, 25] introduced a multi-linear model with a different behaviour in tension and in compression.
As PDL is difficult to describe numerically, it is typically modulated as an isotropic linear elastic using two parameters, i.e. Young's modulus and Poisson ratio. In all studies, PDL is modulated as almost incompressible with a Poisson ratio, ν, usually 0.45 or 0.49. However, values of Young's modulus are found in a wide range, from 0.1 to 10 MPa. Some authors use experimental data found in literature. However, they do not take into account the limitations of the experiments. Material properties of PDL found in literature are sometimes unrealistic. Also, some values appear as a result of averaging properties of PDL fibres and PDL matrix which gives higher values of material properties of PDL.
As shown in literature review, analyses were performed that explain orthodontic bone remodelling or orthodontic tooth movement, where PDL is part of whole system, PDL is usually defined as continuum or as fibres. Models that take into account both, PDL matrix and PDL fibres could not be found. Also, geometry of PDL in most of the models is quite inquiring. Usually, even if it is said that geometry is obtained from CT scans, the geometry is so correct and thickness is so uniform that it resembles more to cone than to real PDL.

In this research, PDL is divided into fibres and matrix. The matrix contains all substances of PDL that are not fibres, i.e. like blood and lymph vessels and cells. The term fibres refers to collagen fibres that are put horizontally and under different angles. In 2D model, fibres were put under angles of 30°and 45°[144], and in 3D model fibres were put randomly, mimicking their real position in in jaw. Each modulated fibre represents thousands of fibres in the ligament. This position of fibres is referring to anisotropic behavior of PDL. The aim of this research is to show the initiation of bone remodelling induced by the orthodontic force. Thus, isotropic material properties of PDL will satisfy the analysis since PDL is part of the system tooth-ligament-bone, and it is not observed by itself.

To confirm the hypothesis, 2D and 3D models are developed which are loaded with a vertical force, i.e. chewing force, and a transversal force, orthodontic force. For both models, three types of analyses were done, 1) chewing force only; 2) orthodontic force only; 3) combination of both forces.
Since the strain energy density, SED, is associated with bone density changes, according to the bone remodelling theories [127], the remodelling of the alveolar bone is monitored by the strain energy density. The magnitude of chewing force and orthodontic force are different in literature [24, 25, 18, 16, 22]. Here, chosen values are 100 N for chew force, 5 N for orthodontic force and 10 N for orthodontic moment. Strain energy density is adopted as a biomechanical signal that controls the remodelling of the trabecular and cortical bone, and values of strain energy density in MPa will be observed in all analyses according to:

$$U = \frac{1}{2}\sigma_{ij}\varepsilon_{ij}, \tag{4.1}$$

The relationship between remodelling rate and strain energy density as mechanical stimuli [12] is shown on Figure 3.2 (b), where the relation between remodelling rate and strain energy density can be seen, in which U_n is a homeostatic value and s is the threshold level that marks the borders of the lazy zone [12].

A 2D model is developed to analyze uncontrolled tipping, and a 3D model is developed to analyze uncontrolled tipping, controlled tipping, bodily movement and rotation. Also, bone remodelling algorithm has been implemented in numerical analysis with 3D model to confirm the analysis. All numerical analyses are done in Marc Mentat, finite element software from MSC Software group (MSC Software Corporation, USA) [145]. Bone remodelling algorithm was developed in Fortran and by special subroutines implemented in Marc Mentat.

Tablica 4.1: Material properties of 2D model [26, 36]

Body name	E, MPa	ν	Elements
Cortical bone	13800	0,26	72
Trabecular bone	345	0,38	510
Dentine	20000	0,3	72
Enamel	80000	0,3	33
Cement	20000	0,3	244
PDL matrix	0,68	0,49	71
PDL horizontal fibres	10	0,49	58
PDL angular fibres	30	0,38	162

4.2 2D model

The aim of developing a 2D model is to quantify changes in bone loading caused by orthodontic and chewing force and in that way to confirm the hypothesis that was proposed at the beginning of the research.

Proposed 2D model consists of tooth, bone and PDL. Tooth is composed of dentin, enamel and cementum, and bone includes cortical and trabecular bone. PDL is divided to matrix and fibres, where fibres were put horizontally and under three different angles with respect to a reference plane. It is important to emphasize that 2D model is 2D drawing in Marc Mentat made according to dimensions from literature [144]. The model represents the upper right canine.

All material properties that are used are linear elastic, and isotropic [26, 36]. Material properties are put on Table 4.1. As shown in the table, tooth has the highest modulus of elasticity, which means it has the highest stiffness in this model, so strains and stresses will not be observed in the tooth. This also follows the biological process, since the tooth is not remodelling during the application of orthodontic or chewing force, and if it happens, the reasons are of pathological nature.

As mentioned in Chapter 2, there is a difference between stiffness of trabecular and cortical bone where stiffness of cortical bone is much higher than stiffness of trabecular, and the reason for that is the difference between bone structure. As it is expected, PDL, as soft tissue, has the lowest Young's modulus in this model, where Poisson ratio is the highest, acting almost as incompressible material. Material properties of 2D model are shown on Figure 4.3 where each color refers to different material properties.

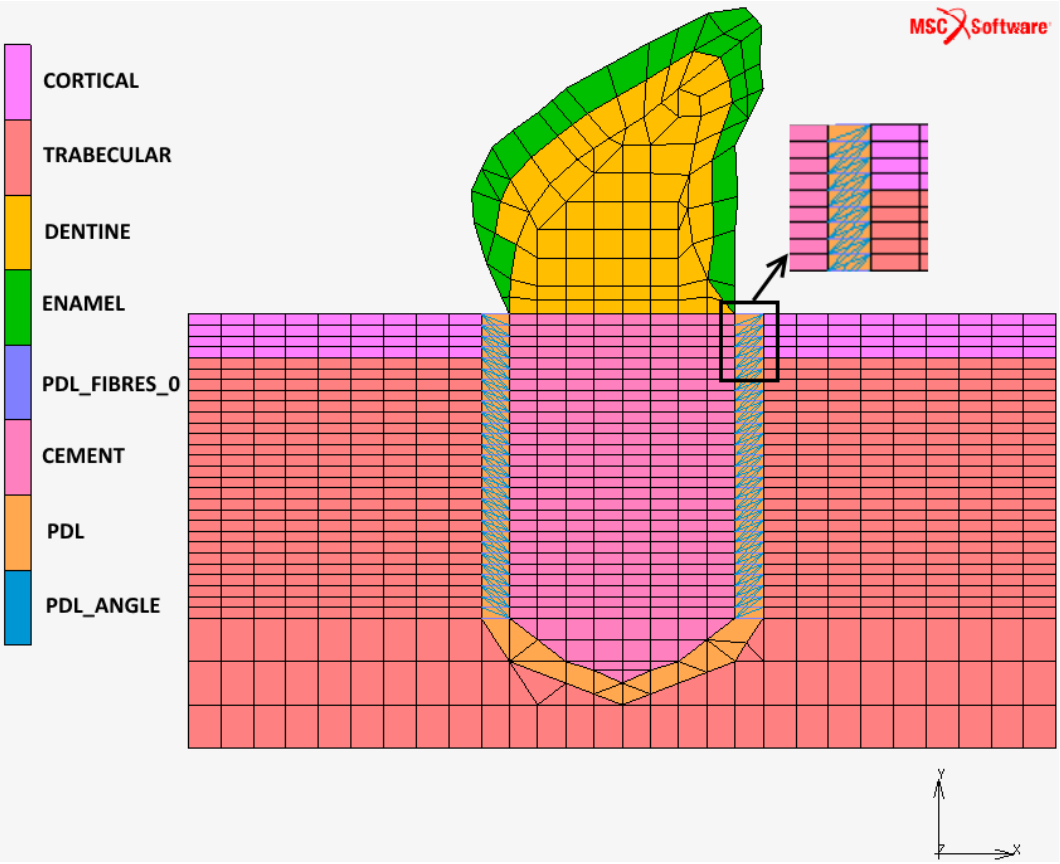

Slika 4.3: Material properties of 2D model

At the beginning of this stage of research, the main focus was on connecting bone and tooth with PDL, which means connecting soft tissue and hard tissue. Because of the large difference in material properties between hard and soft tissues, it is not easy to numerically describe it. First,a suggestion from literature, to describe the PDL as a continuum, was used. Preliminary results showed that the description of the PDL as a continuum would not provide realistic results, so another approach needed to be chosen. The PDL consists of fibres and matrix, so fibres were also included into the model. The most important and most common fibres in the PDL are collagen fibres. 60% of all fibres in PDL are collagen fibres [58].

Finite element mesh consists of quadrilateral finite element, triangular element and truss element. The quadrilateral finite element used in this research is class 4, type 3. Element 3 is a four-node, isoparametric, arbitrary quadrilateral written for plane stress applications, this element uses bilinear interpolation functions, and strains tend to be constant throughout the element [145]. This type of element is used to describe most of the mesh of the whole model. The second finite element used here is the triangular element, class 3, type 201. This element is a three-node, isoparametric, triangular element written for plane stress applications and it uses bilinear interpolation functions. This element is used in describing small parts of tooth, bone and PDL, where geometry is more complex. Truss elements are class 2, type 9. The truss element is a simple linear straight truss with constant cross section. Truss elements are used to describe fibres [145]. The whole model consists of 1222 elements, 1046 nodes.
As already mentioned, collagen fibres constitute 60% of PDL, so the total volume of fibres can be calculated. This is necessary because each truss element represents thousands of fibres, and to prescribe property of a truss element it is necessary to know the cross section of a truss element. In the model there are 220 truss element and with simple calculation, cross section was calculated. The value value of cross section is 0,082 mm^2.
The proposed model is part of the jaw. Boundary condition put on the other side is fixed displacement, and so this means that there is no displacement in x, y and z directions. Loading was chewing force, vertical loading, and orthodontic force, transversal loading. Boundary conditions are shown on figure 4.4.

However, as mentioned before, one of the challenges was how to connect PDL with tooth and bone, i.e. hard and soft tissue. In 2D model it was solved by putting the tying constraint, connecting nodes from bone with PDL and nodes from tooth with PDL. A tying constraint involves one tied node and one or more retained nodes, and a tying (constraint) condition between the tied and retained nodes. The degrees of freedom, like

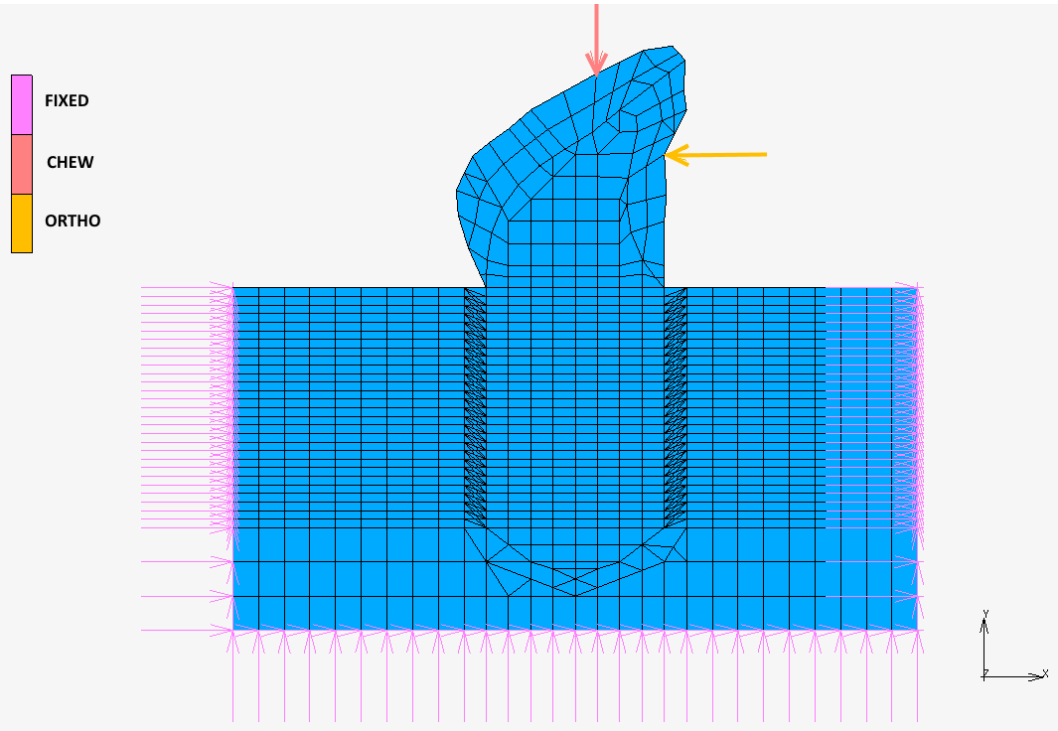

Slika 4.4: Boundary conditions of 2D model

displacements, of the tied node are dependent on the degrees of freedom of the retained nodes through the tying condition.

4.3 3D model

After hypothesis is confirmed on a 2D model, the next step was to make a 3D model. The 3D model is patient-specific model of the upper right incisor. The 3D model, as 2D, consists of tooth, PDL and bone. Loading applied on the 3D model is also chewing force and orthodontic force.

Geometry for the 3D model is obtained from CT images from a patient to whom orthodontic treatment was recommended, before the treatment started. CT scanning was made on CBCT in Apolonija Dental Clinic, Zagreb. Resolution of CT images was 200 microns. The CT images consisted of 375 transversal sections with a slice thickness of 0.200 mm and a pixel width of 0.200 mm. The resolution and amount of scans was enough to reconstruct tooth, bone and PDL.

To reconstruct 3D geometry from CT scans, the software Mimics 14.0 from the company Materialise (Leuven, Belgium) was used [80]. Mimics (**M**aterialise's **I**nteractive **M**edical

Image **C**ontrol **S**ystem) is a software for processing medical images and creating 3D models. Mimics uses 2D cross-sectional medical images such as from computed tomography (CT) and magnetic resonance imaging (MRI) to construct 3D models. A stack of images are loaded into the software, and this consists of images in the xy plain (axial images), and then Mimics calculates and creates images in the xz (coronal) and yz (sagittal) direction. This enables a more comprehensive 3D feel of the 2D data.

The key to converting anatomical data from images to 3D models is a process called segmentation. During segmentation, the structure of interest in the sliced image data should be indicated. This information is then used to recreate a 3D model from the segmented structures. To describe the outer surface of the 3D model, Mimics uses the STL format. The STL format allows describing the most complex geometries accurately. This is necessary, since anatomical data is in general very intricate. Accurate segmentation is important in order to extract meaningful information from images. An STL file is a triangulated surface mesh file. The file contains the three nodes of each triangle and defines the normal direction of the triangle. This file format is ideal for anatomical geometry because of its simple file structure and flexibility to match any contour desired. It is not controlled by parametric constraints such as true CAD files and IGES files.

The medical images coming from CT or MRI scanners consist of grayscale information. Mimics allows to create models based on the grayvalues (Hounsfield units, HU, in CT images) within these images. A grayvalue is a number associated with an image pixel defining the shade (white, gray, or black) of the pixel. There is a direct association between material density of the scanned object and the grayvalue assigned to each pixel in the image data. Because of this, Mimics has the flexibility to create models from any geometry distinguishable within the scanned data. By grouping together similar grayvalues, the image data can be segmented, and models created. This type of segmentation is called thresholding and yields accurate models. Using the segmentation and known information on the pixel size and the distance between the image slices, Mimics can calculate a 3D model. The accuracy in a Mimics model matches the accuracy of an object captured within the scan [80].

Hence, after the region of interest was chosen, the incisor with a piece of the surrounding bone, threshold level was set according to HU values for bone and tooth, a 2D mask from all three planes are obtained. Automatic segmentation operations were performed on morphology to reduce noise. Threshold levels for bone, tooth and PDL were set. For cortical bone the value was between 662 to 1988 HU, for trabecular bone it was between 148 and 661 HU, for tooth 1200 to 3071 HU and for soft tissue -70 to 225 HU. After obtaining the geometry of hard tissue, which is easier to see on CT images, the step

Tablica 4.2: Material properties of 3D model [26, 36]

Body name	E, MPa	ν	Elements
Cortical bone	13800	0,26	6278
Trabecular bone	345	0,38	3002
Tooth	20000	0,15	3963
PDL matrix	0,68	0,49	12761
PDL fibres	30	0,35	452

was to obtain the geometry of PDL, soft tissue which has lower values of HU. PDL is not easy to recognize on CT images, but the paradontal space is recognizable on images. Thickness of the periodontal space is at the most 1,5 mm [58], so on the images that periodontal space was between 1 and 4 pixels. Even 1 pixel is small value, and it is not easy to obtain geometry from it, but still the 3D geometry of PDL was made. Geometry of PDL completely follows the geometry of the bone from one side and tooth from the other side describing the real shape of PDL. Because the geometry of bone and tooth is not completely straight, the PDL does not have uniform thickness. PDL geometry obtained in this way refers to PDL matrix. Fibres are added later in the software Marc Mentat.
On the Figure 4.5 there are CT images of the upper jaw with teeth put in the Mimics interface in all three planes, and mask obtained by the procedure explained above. Figure 4.6 is showing 3D geometry of the whole model (a) and each part of the model separately (b), from the left bone, PDL and tooth.

After the geometry was obtained, the next step is to get a finite element mesh and to assign material properties. For obtaining a finite element mesh, 3-matic 5.1 from the same company, Materialise, is used. 3-matic software for mesh optimization enables modifying surface meshes quickly and easily, conforming them to the conditions required by FEA software. First, the surface mesh is built (following geometry from Mimics) for each part of the model and then 3-matic allows to create volume mesh using tetrahedron finite elements.
The next step is to assign material properties for each part of the model, and that is conducted in Mimics. As mentioned before, Mimics can differentiate parts on images by putting the threshold boundaries and therefore, by these boundaries material properties can be defined. Material properties for each part of the model are in Table 4.2. It can be seen that now tooth is not divided into its parts, but it is observed as a whole.

Since the material properties, as well as density, were assigned for the bone, it was assigned in Mimics, which calculated density according to HU values read from CT scans. Density

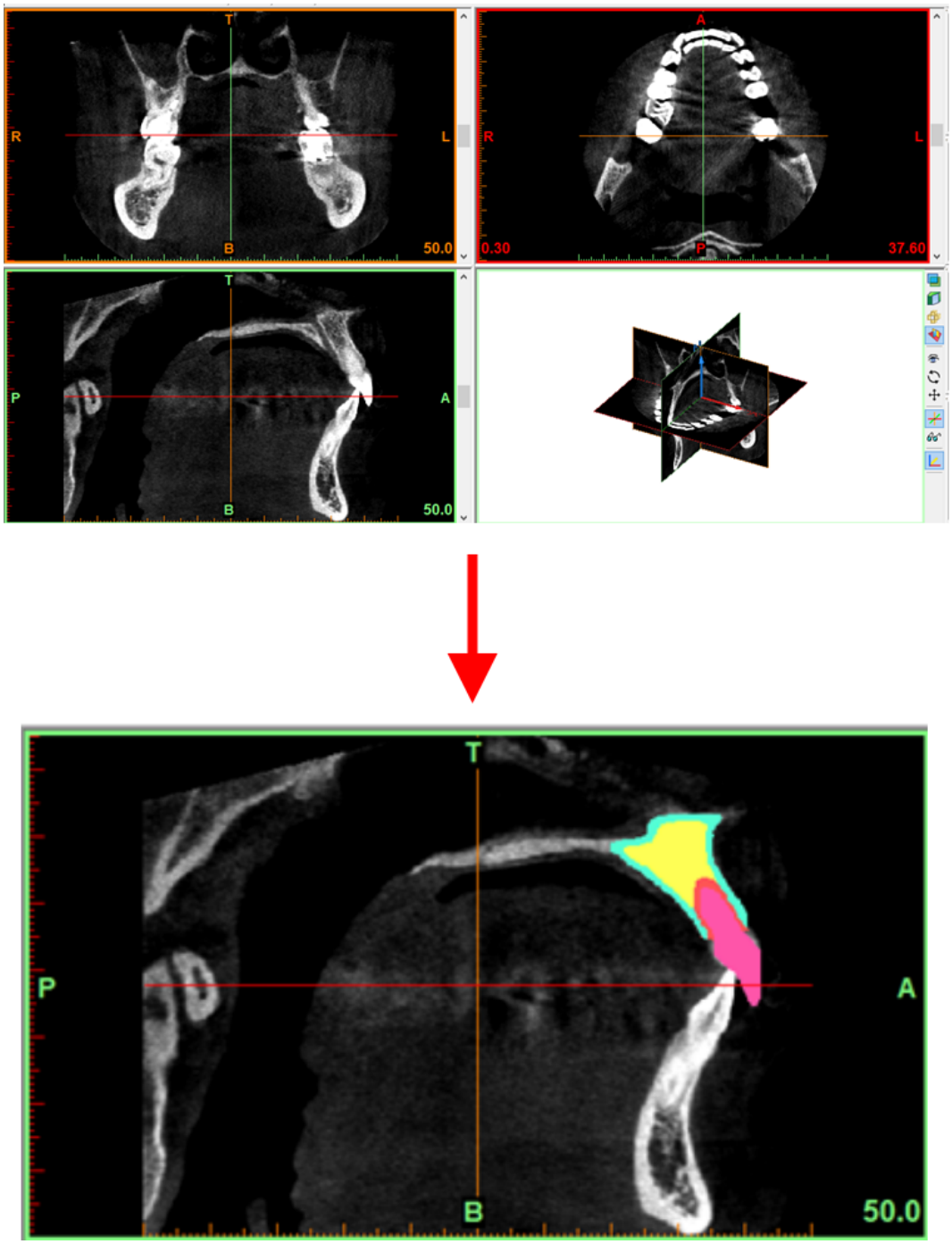

Slika 4.5: CT scans of upper jaw with teeth in Mimics

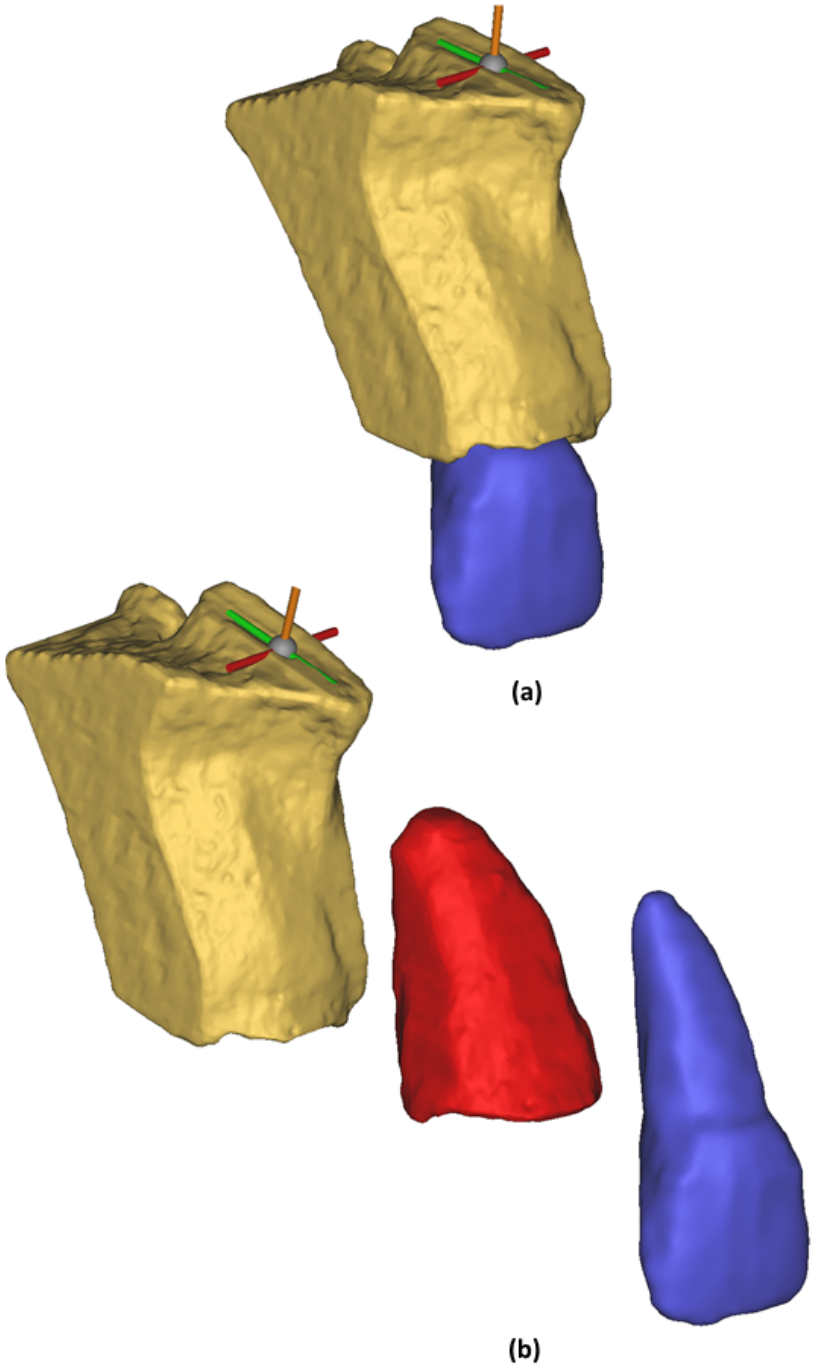

Slika 4.6: Geometry of 3D model in Mimics, whole model (a) and separate bone, PDL and tooth (b)

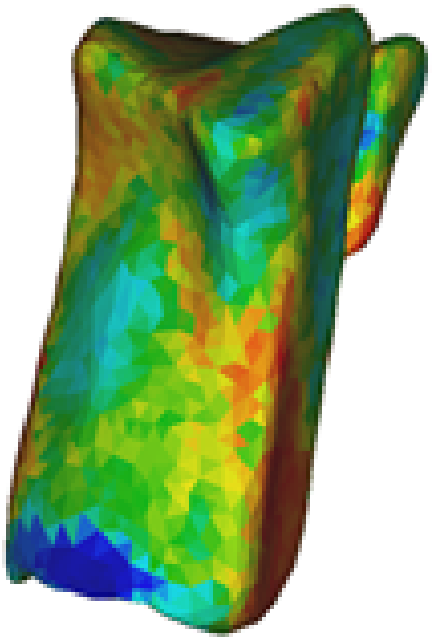

Slika 4.7: Density distribution of bone

was only prescribed for bone, because bone is the area of interest in this research. The distribution of density for the alveolar bone is shown on Figure 4.7. The density was calculated by equation (4.2), and material properties with finite element mesh are shown on figure 4.8.

$$\rho = 1.067 \times HU + 139 \tag{4.2}$$

As explained above, each component comprised in the whole model is discretized into finite elements describing the geometry of the bone, the tooth, and the PDL. Bone, tooth and PDL matrix is made by isoparametric three-dimensional tetrahedron finite element, class 18, type 134. Fibres are defined as spring elements, type 195, connecting nodes from tooth and nodes from bone and they are put horizontally and under different angles. Spring element is a generalized 3D spring-and-damper structural element that may exhibit nonlinear or frequency dependent behavior. Fibres are put by a mathematical algorithm made in Matlab R2013b (MathWork, USA) and then by Procedures function in Marc Mentat. How fibres are implemented in the model is described in Appendix B.
Spring elements are linking two nodes by a stiffness. The force generated in spring is related to the spring elongation, δl, through a stiffness parameter, k, following Hooke's law: $F = -k\delta l$. Stiffness parameter can be related to Young's modulus of a material as $K = EA/L$ where A is the cross-section area of the spring and L is the spring natural

length.

In this research linear springs were used to describe fibres. To specify spring properties, local coordinate system was used. In 3D, the local y-z axes are located by using an extra node or an orientation vector. If both are specified, the extra node takes precedence. The local y axis is first estimated by using the orientation vector or using the vector from the first bushing node to the extra node. The local z axis is then formed by taking the cross product of the local x and estimated local y axis. The final local y axis is obtained by taking the cross product of the local z and local x axes. Each part of the model has its own mesh and they are not connected. Contact boundary condition needs to be applied. A glue condition suppresses all relative motions between bodies through tying or boundary conditions applying them to all displacement degrees of freedom of the nodes in contact. Nodes in contact via the glue option are not allowed to separate. Contact was made between the outer side of tooth with the inner side of PDL (sides that are touching) and between the outer side of PDL and the inner side of bone (also the sides that are touching). All bodies that are in contact are put to be deformable. This type of contact, deformable-deformable contact, works in a way when a node contacts a deformable body, a tying relation is formed between the contacting nodes and the nodes of the contacted segment on the other body. This constraint relationship uses information regarding the normal vector to the segment and the closest point projection of the contacting node on the contacted segment. When the glue option is used between two deformable bodies, a simpler tying relationship is formed, such that no relative motion occurs. This type of contact is selected is as it describes the best real biological environment because it is preventing slippage or separation [30, 31, 19, 18]. Contactis described in detail in Appendix A.

The whole mesh and material properties are defined in Mimics, and after that, the whole model is imported in Marc Mentat, in which the rest of the analyses are carried out. In this research, four different orthodontic loading conditions are taken to reproduce the uncontrolled tipping, controlled tipping, bodily movement and rotation. First it is analyzed with chewing force, to obtain daily loading level, then follow the analyses mimicking four different movements and then follow the analyses mimicking tooth movement in combination with chewing force. In all analyses displacements in x, y and z direction were disabled on mesial and distal side of bone. The reason for this is that displacements in bone are considered to be non-existent, and the other reason is that only part of the bone is taken into account in the model. Boundary conditions for 3D model are shown on Figure 4.9, where they show the position of chewing force and disabled displacement of bone, and also the anatomical position of the tooth and the surrounding bone.

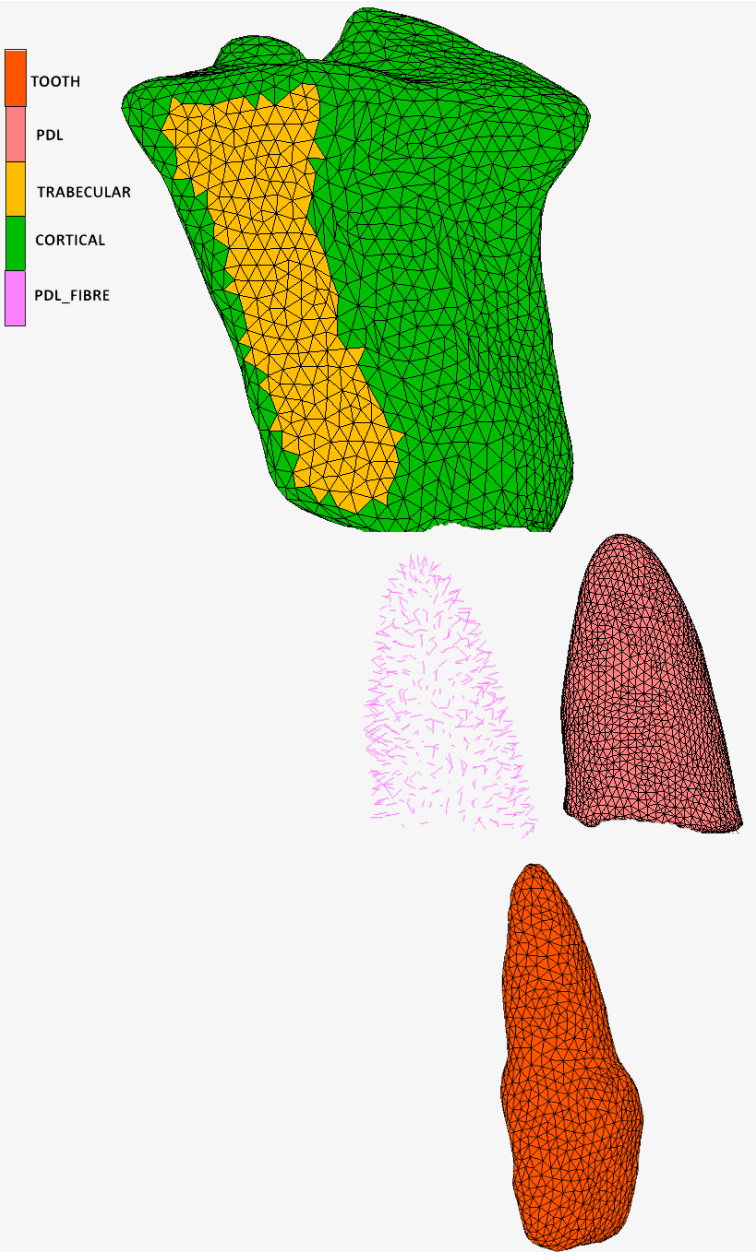

Slika 4.8: Material properties of 3D model

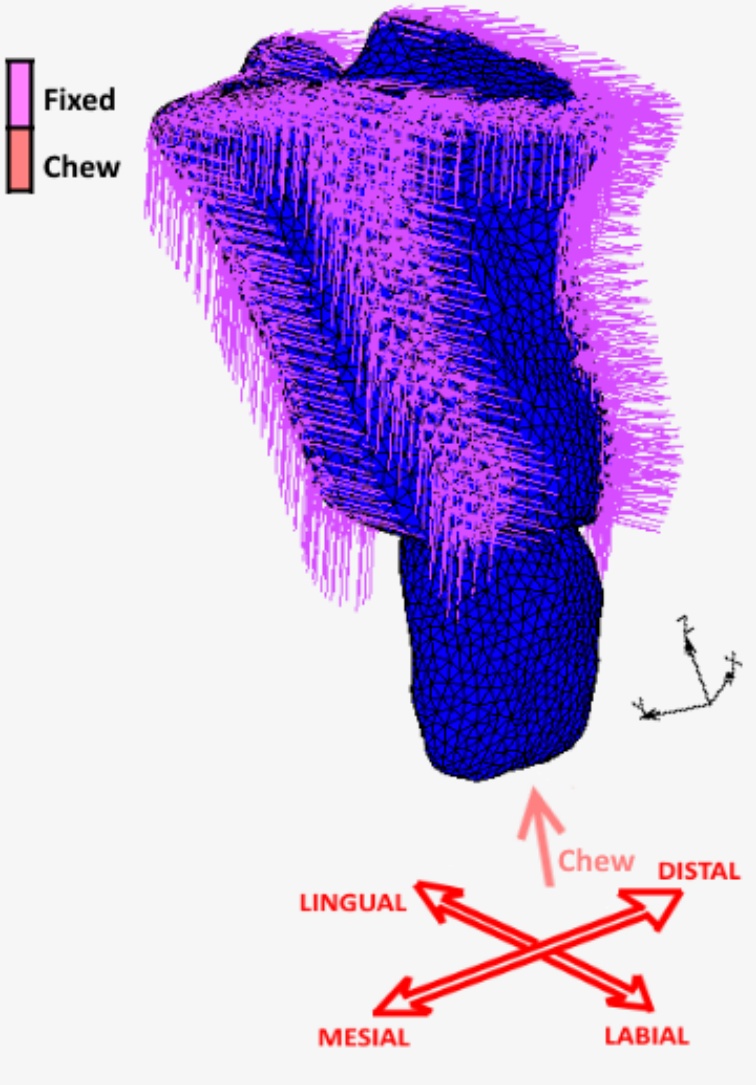

Slika 4.9: Boundary conditions of 3D model

As explained in Chapter 2, uncontrolled tipping the tipping of the tooth that occurs when orthodontic force is applied on the crown of the tooth and with this type of movement, the crown goes in one direction, the direction of applied force, and the apex moves in the opposite direction. Here, the centre of rotation is almost at the same place where the centre of resistance is. Direction of orthodontic force is lingual, so, tipping is lingual. Magnitude of orthodontic force is 5 N. Controlled tipping is a type of movement in which the tooth rotates around the centre of rotation which is positioned in the root apex, so here only crown rotates, around centre of rotation. Here, this movement was achieved by applying orthodontic force and orthodontic moment, and tooth moves lingually. Bodily movement is pure translation movement in which the whole whole tooth translates parallel from the initial position to the final position. This type of movement is in orthodontic practice

achieved by placing moment and force, but numerically it is achieved by putting transversal forces along the longitudinal axis of tooth [31]. Tooth is moved lingually. Rotation is a type of movement in which the tooth rotates around the long axis of the tooth. Here the centre of rotation is at the same position as the centre of resistance. Movement is achieved by placing moment around the long axis of tooth. Figure 4.10 graphically illustrates force system on the tooth of four different orthodontic loading, where (a) refers to uncontrolled tipping, (b) controlled tipping, (c) bodily movement and (d) rotation. Furthermore, it is assumed that applied forces remain constant during orthodontic treatment, mimicking intelligent retention wires that adapt themselves with tooth movement.

4.4 Bone remodelling algorithm

Schematic, hypothetical chain of events governing load-adaptive bone remodelling according to Wolff's law is shown on Figure 4.11, in which it can be seen that bone is loaded with external forces causing internal loads and deformations, which are represented by stress and strain in the bone material. It is assumed that these stresses or strains can be considered as local mechanical stimuli, which can be sensed by bone. If the stimulus becomes abnormal, due to changed loading, and since bone has the ability to form optimal structure for load resistance and adapt its structure to alternative loads, the mechanical stimuli is transduced to a biochemical one and subsequently integrated with several other factors, to cause remodelling potential. This potential will affect the turnover rate of the bone by activating osteoblasts or osteoclasts. This will result in the adaptation of density. As a result of osteoclast and osteoblast activation, the stress and strain in bone will change and therefore affect the remodelling potential again. This process will continue until the mechanical signal is normalized to the physiologic strain values (homeostasis), whereby bone density and shape are again optimally adapted to the loads [12].
In order to predict adaptive modelling and remodelling behaviour, mathematical description can be used to link the input (a mechanical signal) to the output (the amount of net bone loss or gain). Such description, or rule, can be characterized by a remodelling objective, which describes, in mathematical description, the assumed equilibrium relationship between the signal and bone mass.
Huiskes *et al.* [11, 12, 13, 114, 113] have developed a theory to predict adaptive-bone resorption phenomena using the local strain energy density (SED) as the remodelling signal, instead of strain tensor. In their model, they also took into account a lazy zone in the remodelling response, assuming that full SED normalization does not occur,

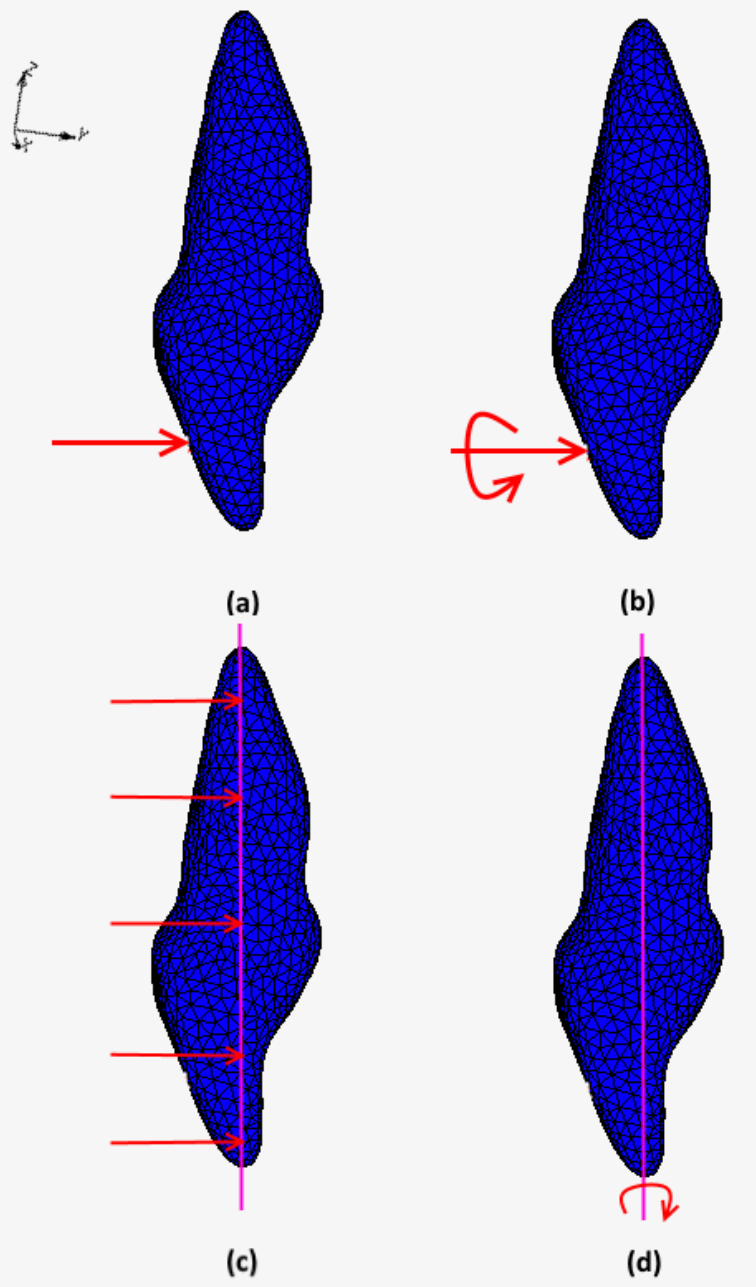

Slika 4.10: Orthodontic loading: uncontrolled tipping (a), controlled tipping (b), bodily movement (c) and rotation (d)

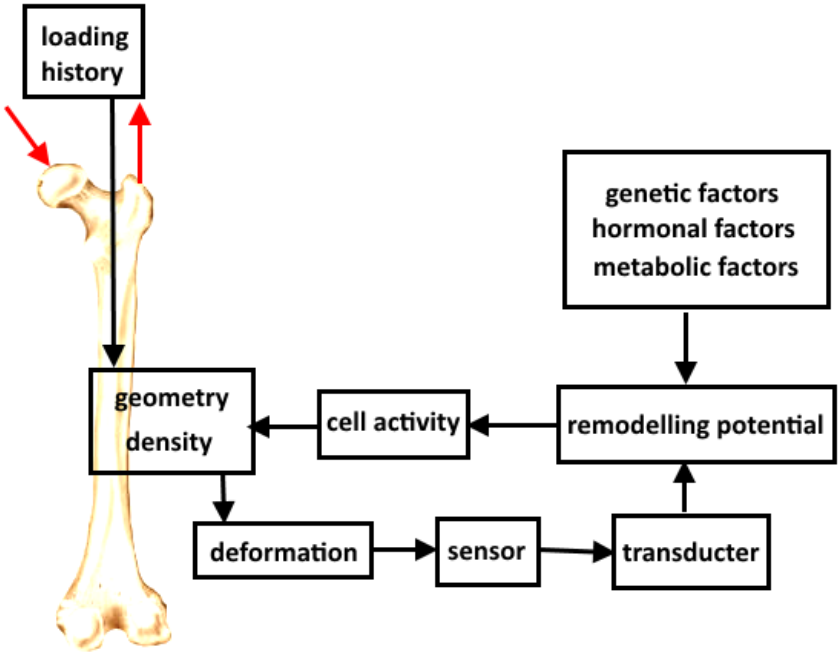

Slika 4.11: Schematic, hypothetical chain of events governing load-adaptive bone remodelling [11]

and that a certain threshold level in the SED-abnormality must be overcome before net modelling or remodelling starts, an assumption based on Frost mechanostat theory [3, 4, 5].

4.4.1 Remodelling model incorporated in code

The remodelling theory should be incorporated in finite element method computer codes to predict morphology and stimulate changes in morphology in actual bone structures. This is done iteratively whereby the FEM code determines the remodelling signal (strain energy density) per element in each iteration, and the adaptive remodelling rule determines the successive changes in density [11, 12, 13, 114, 113].

As explained in Chapter 4.1, the hypothesis used in this research does not violate Wolff's Law and is taking into account the influence of influences of PDL stresses and strains. As shown on Figure 4.12 the remodelling rule that was used to explain bone remodelling in long bones can be seen, and it can be used to explain bone remodelling in the alveolar bone. Bone remodelling algorithm developed by Huiskes *et al.*, and adjusted to the model proposed in this research, was used to explain bone remodelling initiation in the alveolar bone.

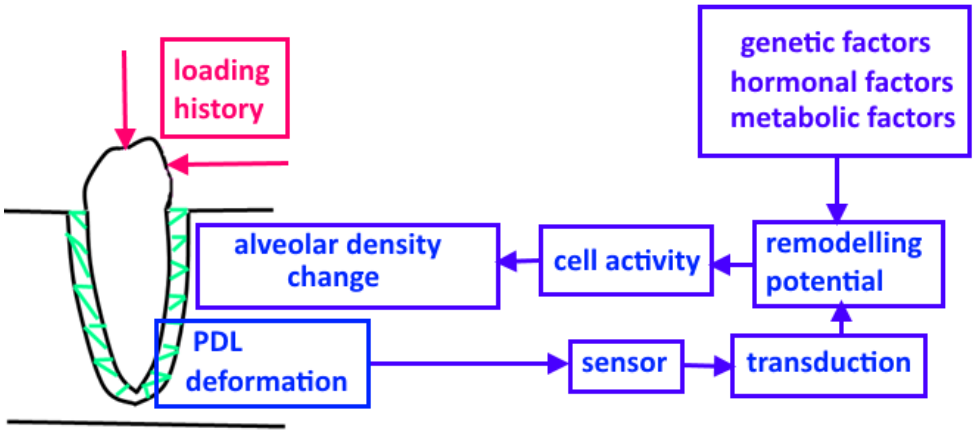

Slika 4.12: Schematic, hypothetical chain of events governing load-adaptive bone remodelling

Relationship between Young's modulus and apparent density is given by

$$E_i = c\rho_i^n \tag{4.3}$$

where c and n are constants, E_i local elasticity modulus and ρ_i is local density value.
Two options are available for local remodelling signal S. The signal can be described as strain energy density U, expression 4.1, or as strain energy density per unit of bone mass, expression 4.5. In the latter case the signal can be determined in a continuum model from strain energy density U over the apparent density ρ.
During loading cycle, several different load cases will attribute to the remodelling signal at different moments. The contribution of n different load cases to the remodelling signal S can be averaged:

$$S = \frac{1}{n}\sum_{i=1}^{n} U_i \tag{4.4}$$

or

$$S = \frac{1}{n}\sum_{i=1}^{n} \frac{U_i}{\rho_i} \tag{4.5}$$

The strain energy density U in the model is expressed in MPa, the apparent density ρ is expressed in g/cm^3, hence the U/ρ is expressed in J/g.

The remodelling objective can be "site specific" or "non site specific". A site specific approach assumes that the bone in the "disturbed" configuration strives to equalize the actual local remodelling signal S to the value in the original situation, S_{ref}. Hence, the inhibitory signal for bone resorption or formation is given by the difference between S and

S_{ref}. A reference model of the "undisturbed" bone should be used to provide the value for S_{ref}. If non site specific approach is chosen, S_{ref} is a constant.

In the remodelling model the existence of a threshold for the inhibitory signal can be accounted for. When the actual signal S is the remodelling signal in a particular location of the disturbed situation, and S_{ref} the signal in the same location of the natural situation, or the constant in the non site specific approach, the objective of the adaptive remodeling process can then be described by:

$$(1-s)S_{ref} \leq S \leq (1+s)S_{ref} \tag{4.6}$$

where s is the threshold value. The interval between $(1-s)S_{ref}$ and $(1+s)S_{ref}$ represents the dead zone, as it is shown on Figure 3.2. It is assumed that bone is unresponsive within these boundaries and no net bone apposition or resorption occurs. The remodelling rate beyond the boundaries can be chosen linear dependent on the stimulus value, or according to a power function:

$$\begin{aligned} &\frac{(S-(1-s)S_{ref})^{\lambda_u}}{((1-s)S_{ref})^{\lambda_u-1}} \qquad \text{if} \qquad S < (1-s)S_{ref} \\ &\frac{(S-(1+s)S_{ref})^{\lambda_l}}{((1-s)S_{ref})^{\lambda_l-1}} \qquad \text{if} \qquad S > (1+s)S_{ref} \end{aligned} \tag{4.7}$$

where λ_u represents the upper index, and λ_l the lower index in the stimulus-remodelling rate relation. Upper and lower index refer to type of curve that describes remodelling rate as a function of stimulus, where it refers to area of formation and resorption. If indexes are put as one, then curve is linear, and if they are put as higher then one, then curve is nonlinear.

The bone remodelling rate can be chosen to be dependent on the free-surface available in the bone. It is assumed that bone apposition and resorption can only occur on free bone surface, i.e. at the pore surface during internal remodelling. To determine the pore surfaces from the apparent density, the theory by Martin [146] is used. Using his assumptions, the internal free surface area per unit volume of whole bone $a(\rho) = A(\rho)/V$ can theoretically be estimated by Figure 4.13.

For ρ=ρ_{max}=1.73 g/cm^3 it is assumed that $a(\rho)$=0, hence no remodelling takes place. Martin [146] also determined an empirical formula to describe free surface density as a function of apparent density:

$$\begin{aligned} &A(\rho) = 32.2\upsilon - 93.9\upsilon^2 + 134\upsilon^3 - 101\upsilon^4 + 28.8\upsilon^5 \\ &\text{where} \qquad \upsilon = \frac{\rho}{\rho_{max}} \end{aligned} \tag{4.8}$$

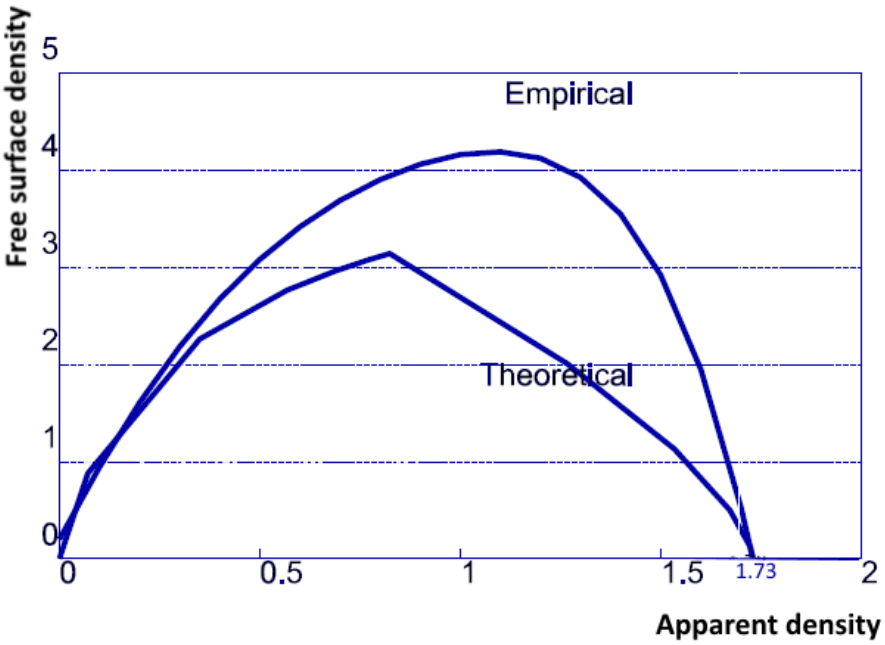

Slika 4.13: Free-surface density as a function of apparent density of the bone [146]

The adaptive process in the bone, using linear stimulus-remodelling rate relation (λ_u=1 and λ_l=1) can be expressed as a rate of change of bone mass:

$$\begin{aligned} \frac{dM}{dt} &= \tau A(\rho)(S-(1-s)S_{ref}) \qquad \text{if} \qquad S<(1-s)S_{ref} \\ \frac{dM}{dt} &= 0 \qquad \text{if} \qquad (1-s)S_{ref} \leq S \leq (1+s)S_{ref} \\ \frac{dM}{dt} &= \tau A(\rho)(S-(1+s)S_{ref}) \qquad \text{if} \qquad S>(1+s)S_{ref} \end{aligned} \tag{4.9}$$

The parameter τ is a time constant given in g/(mm^2(J/g)month), $A(\rho)$ is the free surface on the bone structure, and s represents the dead zone. If a site specific remodelling approach is used, S_{ref} is determined in each integration point and nodal point in the finite element model of the undisturbed natural situation. For a non site specific approach S_{ref} is a constant.

In the computer program, the integration is carried out in steps of $\tau\Delta t$, which represents the proceeding of the remodelling processes at an arbitrary scale, which can be considered as the simulation of a time scale. The time step in the integration process can be chosen constant or variable. If a variable time step is chosen, the time step is determined in each iterative step such that the maximal density change in the integration point where the maximal rate of density change occurs will not exceed $(\Delta\rho)_{max}$(g/cm^3). This is accomplished by calculating the time step Δt after each iterative step taking the maximal possible value for the expression $\{a(\rho)(S-(1\pm s)S_{ref})\}$ from all integration points. Hence, for $\tau\Delta t$ follows:

$$\tau\Delta t = \frac{(\Delta\rho)_{max}}{\{a(\rho)(S-(1\pm s)S_{ref})\}_{max}}. \tag{4.10}$$

The scheme on Figure 4.14 demonstrates the iterative computer simulation program for site specific remodelling. The model of the intact natural bone provides the reference stimulus S_{ref}, which is compared in each integration point with the actual stimulus S in the corresponding point in the model of the disturbed situation. The differences between S and S_{ref} determine the amounts of modelling and remodelling, which occur concurrently. After each iteration a new S is determined. In order to reach convergence, the process must be continued until no more density changes occur. This means that all points fulfill equation 4.6, or have reached the maximal or minimal values for the apparent density tolerated ($\rho = \rho_{max}$ or $\rho = \rho_{min}$). To monitor the convergence rate, object functions were defined according to

$$F = \frac{1}{n}\sum_{i=1}^{n} |S_i - (1\pm s)S_{ref,i}| \tag{4.11}$$

with the positive sign if $S \geq (1+s)S_{ref}$ and the negative sign if $S \leq (1-s)S_{ref}$. The summation takes place over n number of (sensor) points, which are represented in the iterative remodeling process by the integration points. Internal points with a maximal or minimal value for the apparent density, or points having a stimulus within the dead zone, take no part in the summation of equation 4.11. After each iteration it is tested to which extent the objective is met, in order to check the convergence.

In this research site specific remodelling objective objective is used, and Martin's empirical formula is used to calculate free surface density, which states ρ_{max}=1.73 g/cm^3. To calculate remodelling stimulus equation 4.4 it is used. Time step is chosen to be variable. As mentioned above, the remodelling rate is linear, so upper, λ_u, and under power, λ_l, index are set to be 1. Poisson ratio is set to be 0.3, and modulus of elasticity is calculated for each element depending on its density. Apparent density is defined at each integration point. The remodelling parameters are shown in Table 4.3. The flow chart of iterative process is shown on Figure 4.14. It can be seen from Table 4.3 that one load case is used for reference run, and that is chew loading. Reference run is used to obtain referent value of stimulus, S_{ref} from chew loading. After that a combination of chew and orthodontic loading is used for a remodelling run.

Bone remodelling algorithm was written in the programming language Fortran and linked with Marc Mentat with special user subroutines that can be flagged in Marc Mentat. Marc Mentat's subroutines called HOOKLW, ELEVAR and IMPD are used here. HOOKLW is a subroutine in which elastic stress-strain law is supplied by the user. This subroutine is

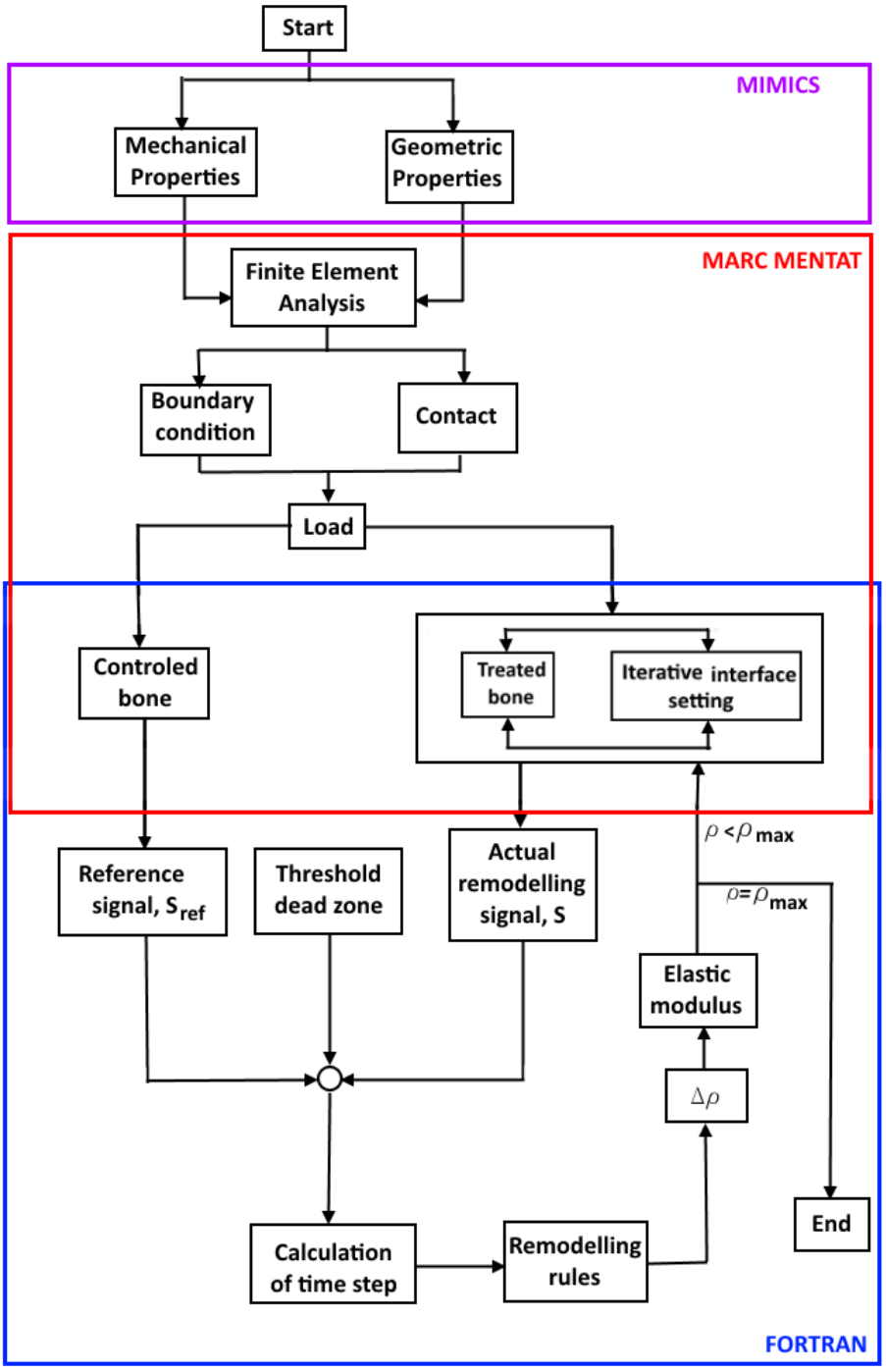

Slika 4.14: Schematic characterization of the iterative FEM-integrated computer simulation model of load-adaptive bone remodelling

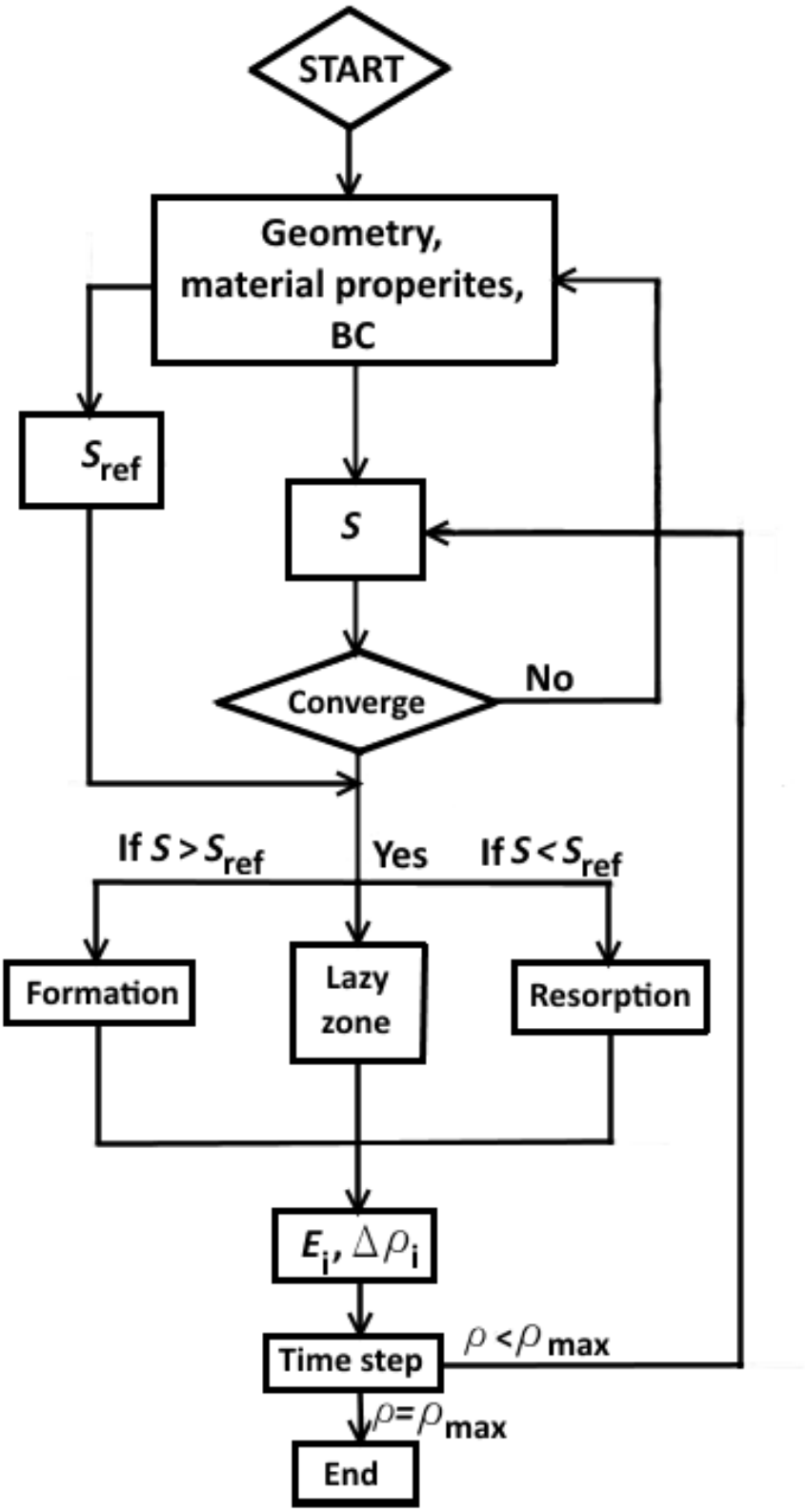

Slika 4.15: Flow chart of the iterative computer simulation model

Tablica 4.3: Remodelling parameters [11, 12, 13, 114, 113, 146]

Remodelling parameters	
Stimulus	$S{=}U$, equation (4.4)
Number of load cases	n=1 (reference run)
	n=2 (remodelling run)
Time step	$\tau\Delta$t, equation (4.10)
Time constant	τ
Threshold value	$s = \frac{1}{2} \cdot 35\%$
Upper index	λ_u=1
Lower index	λ_l=1
Constant modulus density	c = 3790 MPa/(g/cm^3)^3, equation (4.3)
Power in modulus density	n = 3, equation (4.3)
Maximal apparent density	ρ_{max}=1.73 g/cm^3
Material properties	isotropic
Poisson ratio	ν = 0.3
Free surface option	Martin, theoretical (4.8)

calculated for each integration point and it calculates the compliance matrix. This subroutine calls for subroutines that are reading input files, in which remodelling parameters and densities for each element involved in remodelling are defined.
ELEVAR user subroutine makes element (integration point) quantities available at the end of each increment. This subroutine calculates SED. This subroutine also calls for other user defined subroutines which calculate stress and strain components and writes them in output files in special blocks.
IMPD user subroutine makes the displacements, coordinates, reaction forces, velocities, and accelerations available at the end of each increment. It calls for other subroutines that calculate new apparent density and objective function of remodelling.

5 Results

For both models, 2D and 3D, three analyses were done. The first analysis was conducted with application of chewing force only, the second was conducted with orthodontic force application and the third one was conducted with a combination of these forces. As explained in Chapter 4, the first analysis was performed with chewing force to calculate strain energy density. This calculated strain energy density is referent value for daily loading on the bone.
After that analysis, the analyses with orthodontic force and with combined chewing and orthodontic force were performed. Obtained strain energy density from the analysis with orthodontic force and from the combination of these two force together was seen as a percentage of referent value.
Orthodontic force is a force of small magnitude, therefore, strain energy density calculated when orthodontic force is applied is of small value as well, hence the percentage of orthodontic loading also has a small value.
The proposed new approach takes into consideration that the value of strain energy density, when orthodontic and chew forces are applied, is higher than referent value, and it is assumed that overloading condition is on that side of bone. Overloading condition is shown as positive percentage due to referent value. Underloading condition is assumed when the value of strain energy density is lower than referent value and it is shown as negative percentage due to reference value.
The results are shown for the 2D model and for the 3D model.

5.1 2D model

As explained in Chapter 4, the 2D model consists of tooth, bone and PDL. The main focus of the analysis with the 2D model was how to connect PDL with the surrounding tissue

and how to numerically describe PDL so that its description represents real biological condition. It has been concluded that only if PDL is divided into matrix and fibres it gives realistic results.
The position of orthodontic force on the tooth produces tipping movement, in which tooth tips distally. This type of movement was chosen because it shows the best areas of bone remodelling initiation. In the analyses root resorption was not taken into account. All analyses were done as large strain, taking into account geometrical nonlinearities.
Figures 5.1, 5.2 and 5.3 are showing distribution of SED in model loaded by chew force, orthodontic force and combination of these forces together. All figures are in deformable view. As it is expected, values for SED are the highest when chew force is applied, and tooth is translated vertically in the direction of force application. Figure 5.1 shows deformed PDL. Figure 5.2 is showing SED distribution when orthodontic force is applied. The tilting of the tooth in the direction of force application can be seen, as well as the four regions in which values of SED are higher than in the rest of the model. Combination of both forces is shown on the Figure 5.3. In the Figure, four areas in which values of SED are higher than in the rest of the body can be seen as well, but now these values are higher than when only orthodontic force is applied.

The values of strain energy density for all three analyses were observed in four characteristic areas. Areas 1 and 3 are on the cervical side, where 1 is on the labial side and 3 is on the lingual side. Areas 2 and 4 are in the apical area, where 2 is on the labial side and 4 on the lingual side. These areas were chosen because in these areas bone remodelling initiation can be seen, according to [63]. As explained above, values for SED when chew force is applied are seen as referent values, and other loads are seen as percentage of referent value. Results are shown on Figure 5.19. The values for orthodontic loading are shown in blue boxes, and the values for the combination of orthodontic and chewing force are shown in red boxes.
As expected, the values are low when orthodontic force is applied only a small percentage of referent value, while the values for application of both forces are higher. Negative values refer to underloading condition and positive values refer to overloading condition.

5.2 3D model

The new proposed approach was used for 3D model as well. For the 3D model model four different types of movement were made, but they all consisted of of individual action of chewing force, orthodontic loading, and simultaneous action of chewing and orthodontic

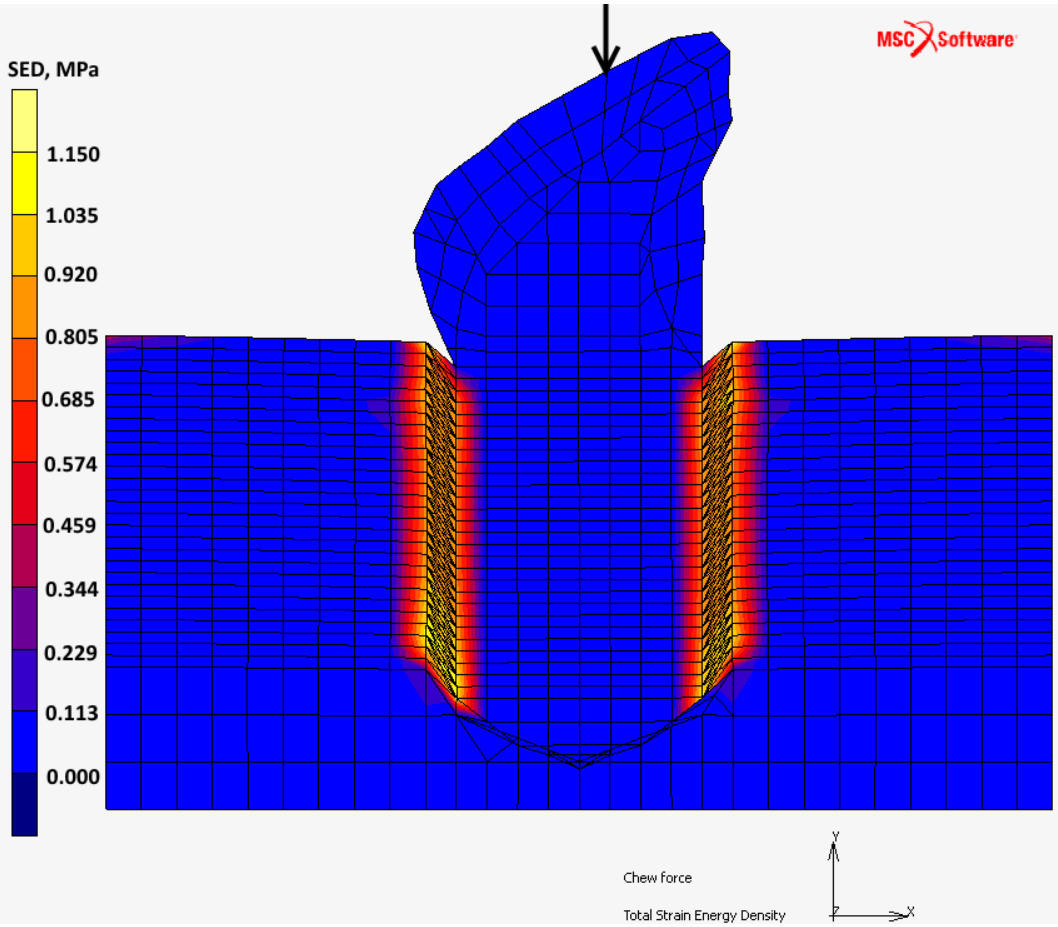

Slika 5.1: Distribution of SED for chew force

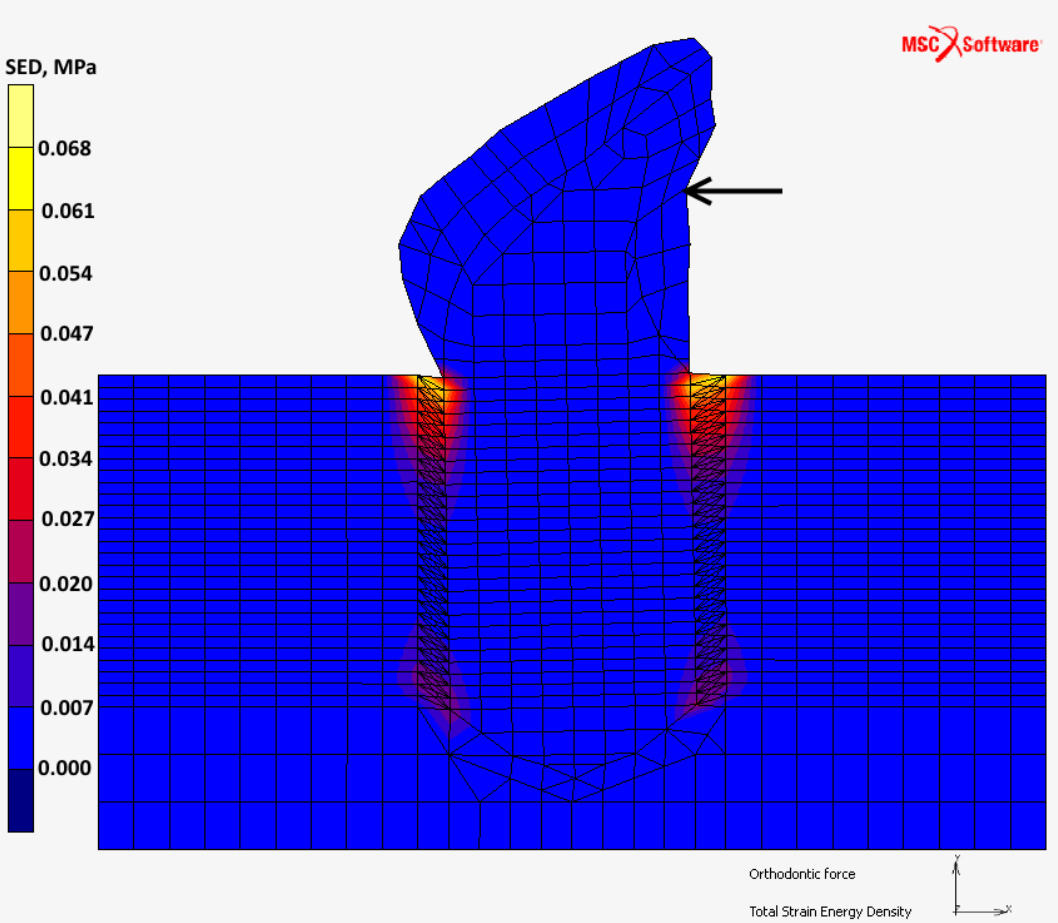

Slika 5.2: Distribution of SED for orthodontic force

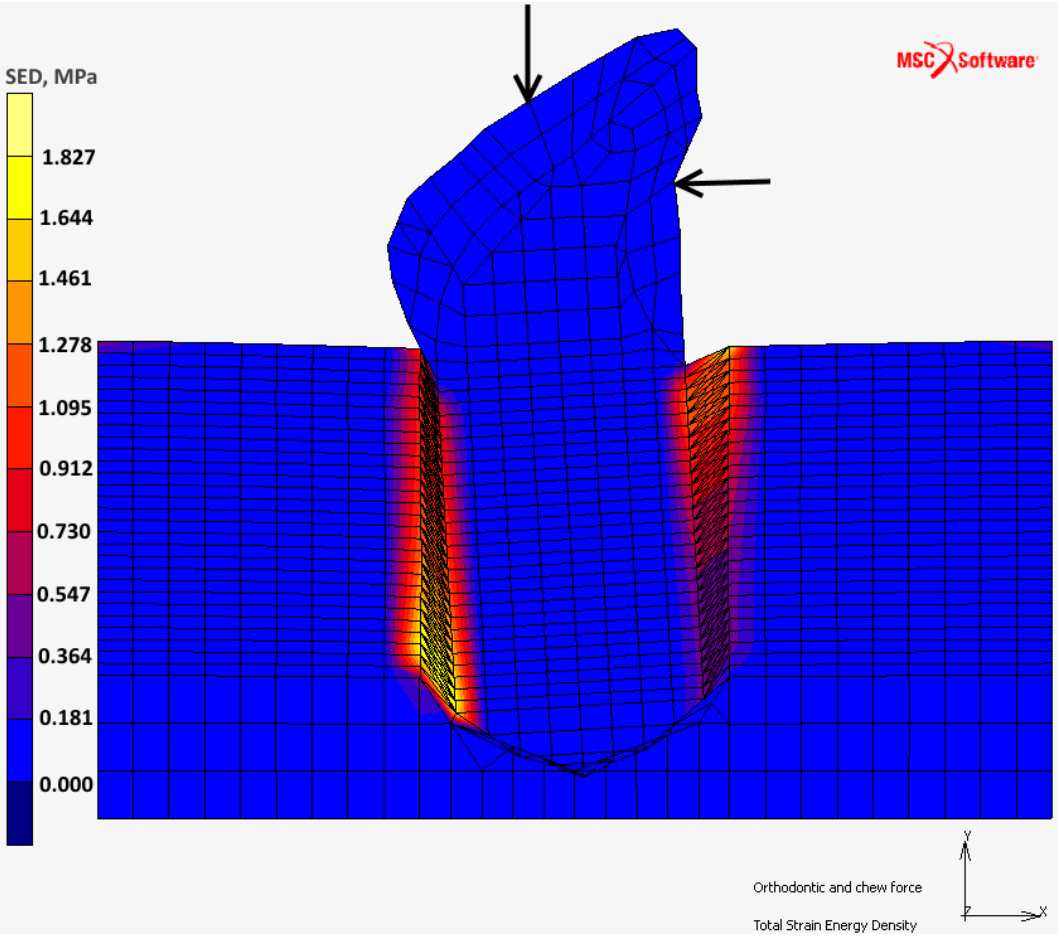

Slika 5.3: Distribution of SED for chew and orthodontic force

loading. Orthodontic loading is described by force or moment, or a combination of both, depending on the type of movement.

Since chewing force is applied vertically, the tooth is push down, which means that fibres are stretching, and these areas can be seen on the figure as a higher value of SED. Chewing force is a force with a high value, therefore its application influences the whole PDL, PDL fibres and matrix. The geometry of the tooth socket is not completely regular and it is not completely parallel with z axis (position of tooth is set in a way that in direction of z axis tooth and its socket are standing), therefore the areas that are showing higher values in SED distribution are not uniformly distributed as it could be seen in the 2D model. Higher values of SED can be seen on the lingual and labial sides of PDL, figure 5.4, and the highest value for SED in PDL is 2.384 MPa. On the figure 5.5 SED distribution in bone when chew force is is applied can be seen. As expected, areas with higher SED values are seen in the same places where there are on PDL, which is a result of stretched fibres pulling the bone, as shown on figure 5.5, and the highest values for SED for bone are 0.00769 MPa.

Orthodontic force is a light force when compared to chewing force, so the values of SED distribution are lower then when the tooth is under the impact of chewing force. In uncontrolled tipping, application of orthodontic force is in lingual direction, which means that the tooth is tilting in lingual direction, where the crown is directed lingually, and the root opposite, labially. The highest value for SED in PDL is 0.297 MPa, which is shown on Figure 5.6. This results in fibres stretching in lingual direction that are positioned nearer to crown, also as fibres put in near root on lingual side, as it can be seen on Figure 5.10 (a). With controlled tipping, which is applied in lingual direction, as a combination of force and moment, the tooth is tilting lingually around the centre of rotation which is now positioned atthe apex of the tooth. Consequently, on the labial side PDL fibres are stretching and on the lingual side they are unloaded and PDL matrix is compressed, shown on Figure 5.7 and Figure 5.10 (b). Maximum value for SED in this type of movement is 0.432 MPa. Figure 5.8 shows bodily movement. Bodily movement is translation movement, where the whole tooth moves parallel. Here, the tooth moves in lingual direction, where fibres on labial side are stretching, and on lingual side they are unloaded, but PDL matrix is compressed, as it Figure 5.10 shows. This type of movement is causing 6.6 MPa as highest value for SED. Rotation is a movement where the tooth rotates around its long axis, which is shown on Figure 5.9. These results with stretching the fibres on labial side, and unloading the fibres on lingual side, where PDL matrix is compressed. In this type of movement, values for SED are not above 0.00013 MPa.

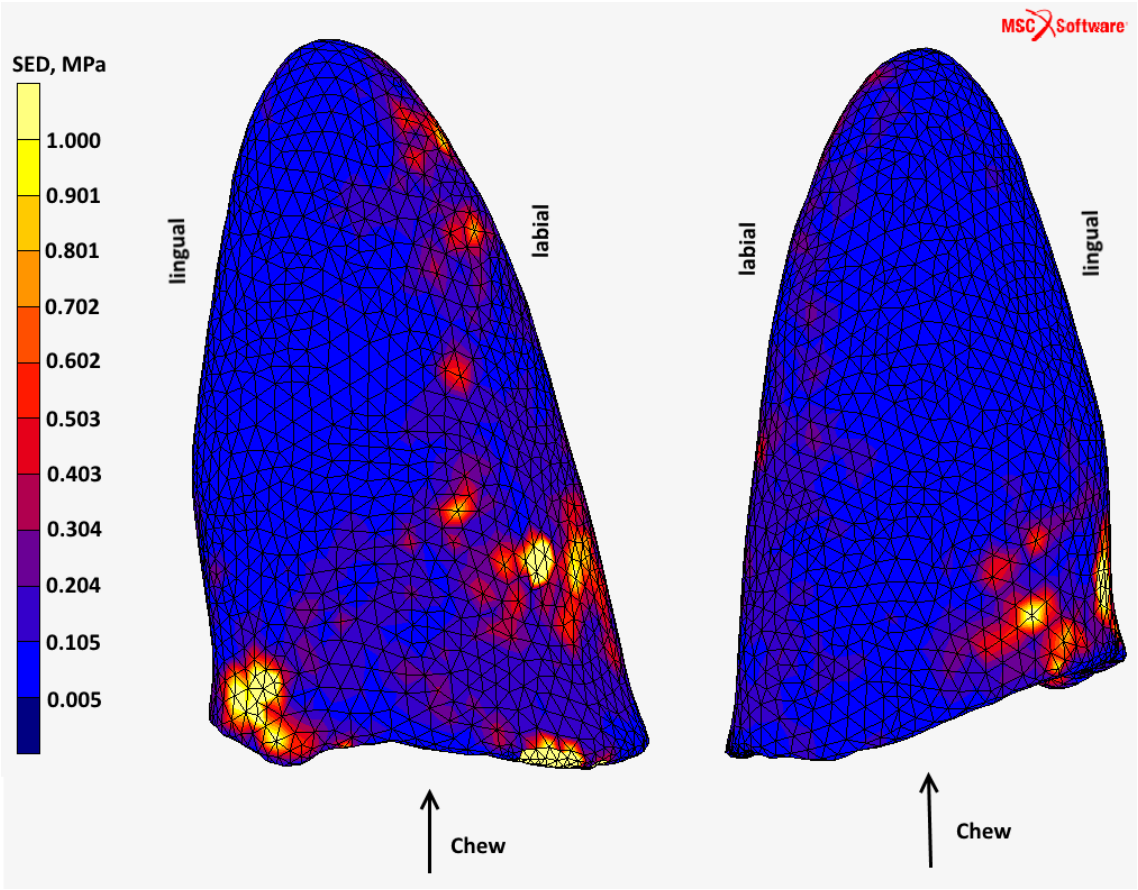

Slika 5.4: Distribution of SED for chew force in PDL

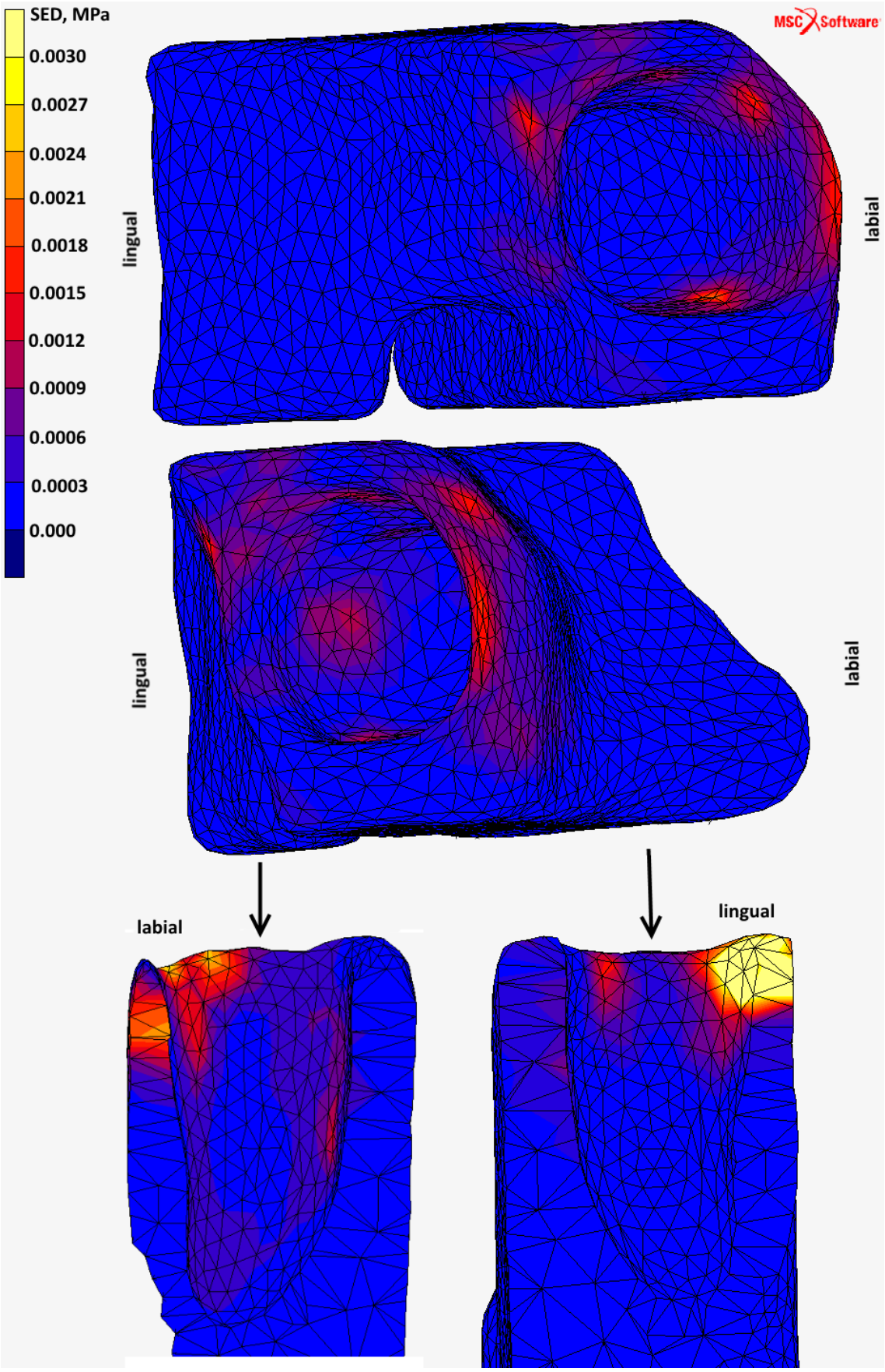

Slika 5.5: Distribution of SED for chew force in bone

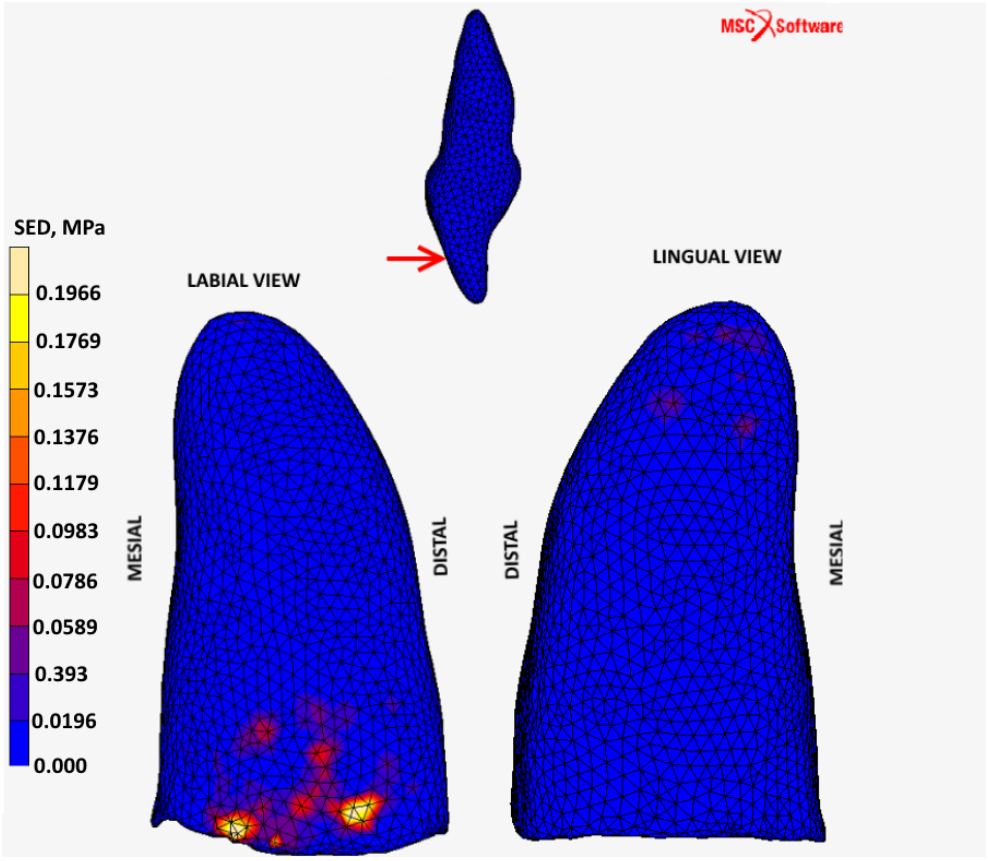

Slika 5.6: Uncontrolled tipping: distribution of SED for orthodontic force in PDL

Final analysis was with combination of both loading. In Figures 5.11, 5.12, 5.13 and 5.14 same characteristic areas as in application with orthodontic loading can be seen, but values for SED distribution are higher. As shown on figures 5.11, colour scale for uncontrolled tipping indicates that in the apical area, on the lingual side, SED refers to compressive loading, and on labial side on tensile loading. The cervical area, the area where the crown meets the root, on the labial sides also refers to overloading condition and on the lingual side refers to underloading condition. The reason for this is that orthodontic force is tilting the tooth in lingual direction, and together with chewing force it is making a moment that is causing higher rotation and in accordance with that, higher values of SED in that areas. At controlled tipping, Figure 5.12, underloading condition can be seen on the lingual side, both in the apical and cervical area, whereas on the labial side, overloading condition can be seen. The reason for this kind of loading distribution is that now the tooth is rotating around the centre of rotation which is now positioning in the apex of the root. Bodily movement, Figure 5.13, is causing tensile loading on the whole labial side, and on the lingual side there is compressive loading. With bodily movement the tooth translates to

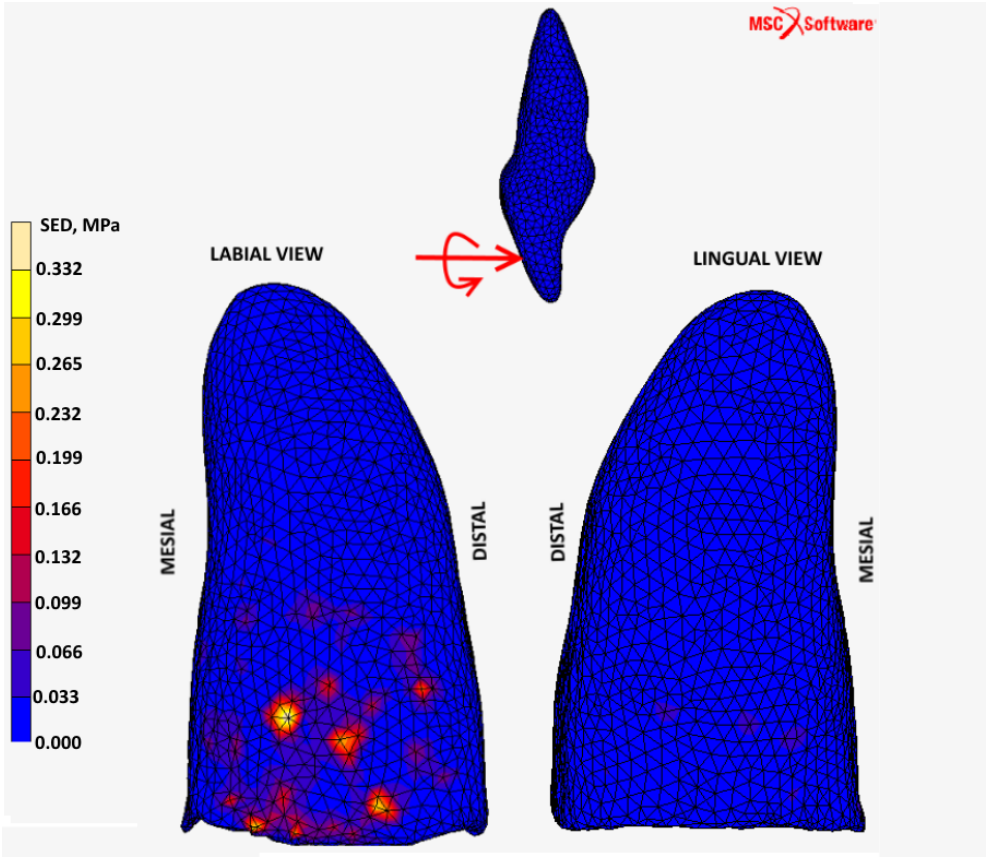

Slika 5.7: Controlled tipping: distribution of SED for orthodontic force in PDL

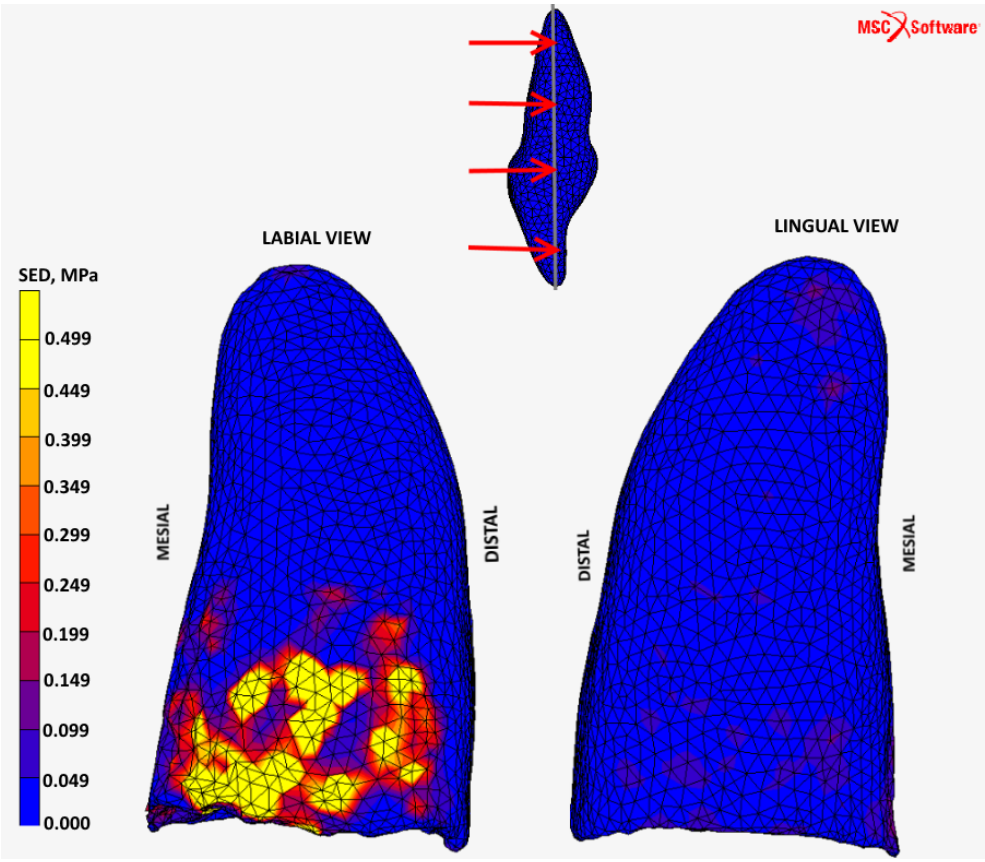

Slika 5.8: Bodily movement: distribution of SED for orthodontic force in PDL

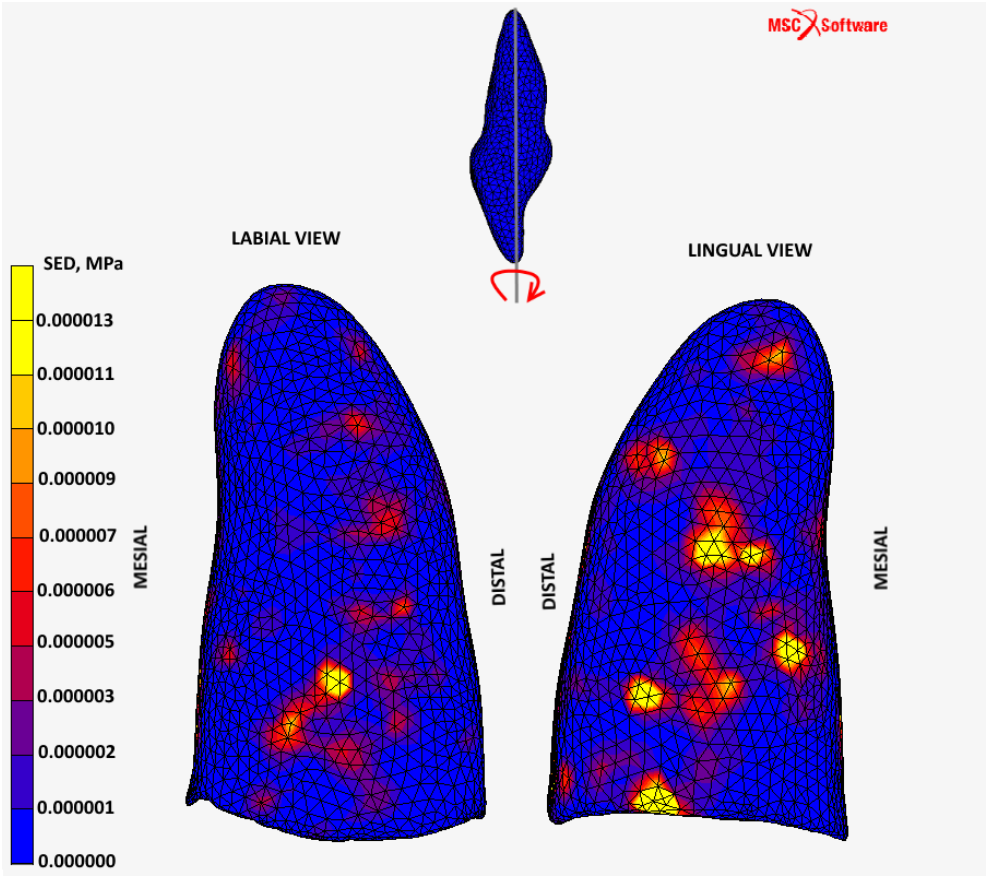

Slika 5.9: Rotation: distribution of SED for orthodontic force in PDL

lingual side to lingual side, compressing PDL matrix on that side, and stretching fibres on the other side. Rotation of tooth around its long axis causing fibre stretching on labial side, and PDL matrix compressing on lingual side is shown in Figure 5.14.

Results for 3D analyses are following the same representation as in 2D analyses. There are 4 characteristic areas where SED values are observed for analysis with chew force, orthodontic loading and chew and orthodontic loading together, Figure 5.20. Values are shown as percentage in boxes, blue box for orthodontic force and red for the combination of both forces, from referent value which is obtained from the analysis with chewing force. Negative values refer to underloading condition and positive values refer to overloading condition.

5.3 Bone remodelling algorithm

The final stage of this research was the implementation of bone remodelling algorithm. The bone remodelling algorithm was explained in Chapter 4.4.1. The algorithm follows bone remodelling theory developed by Huiskes *et al.* [11, 12, 13, 114, 113]. A schematic overview of algorithm is shown on Figure 4.11 and a schematic upgrade of the algorithm is shown on Figure 4.12. It can be seen that the main upgrade is in geometry, in which in this research the influence of the PDL is also used, and the role of the PDL in the hypothesis has already been explained.

Since bone remodelling algorithm is divided into two parts, reference run and remodelling run, the reference run was analyzed, in which only the influence of chewing force was taken into account. The value of chew force was the same as for all analyses, 100 N. Reference run was used to obtain referent value of SED, i.e. the referent value of stimulus. As mentioned before, density values were obtained from CT scans, leading to patient specific model, and these values are used as referent values of apparent density. Values are prescribed following Martin's approach 4.8, in which minimum apparent density was ρ_{min}=0.01 g/cm^3 and maximum ρ_{max}=1.73 g/cm^3. Values of apparent density are shown on Figure 5.15. During the reference run, values of apparent density remain the same.

Reference run is giving referent value of SED of each element. These values of SED, i.e. referent stimulus, S_{ref}, are later used to calculate the lazy zone, as well as bone formation and bone resorption. The value of the lazy zone used was 35%, similar to what was found

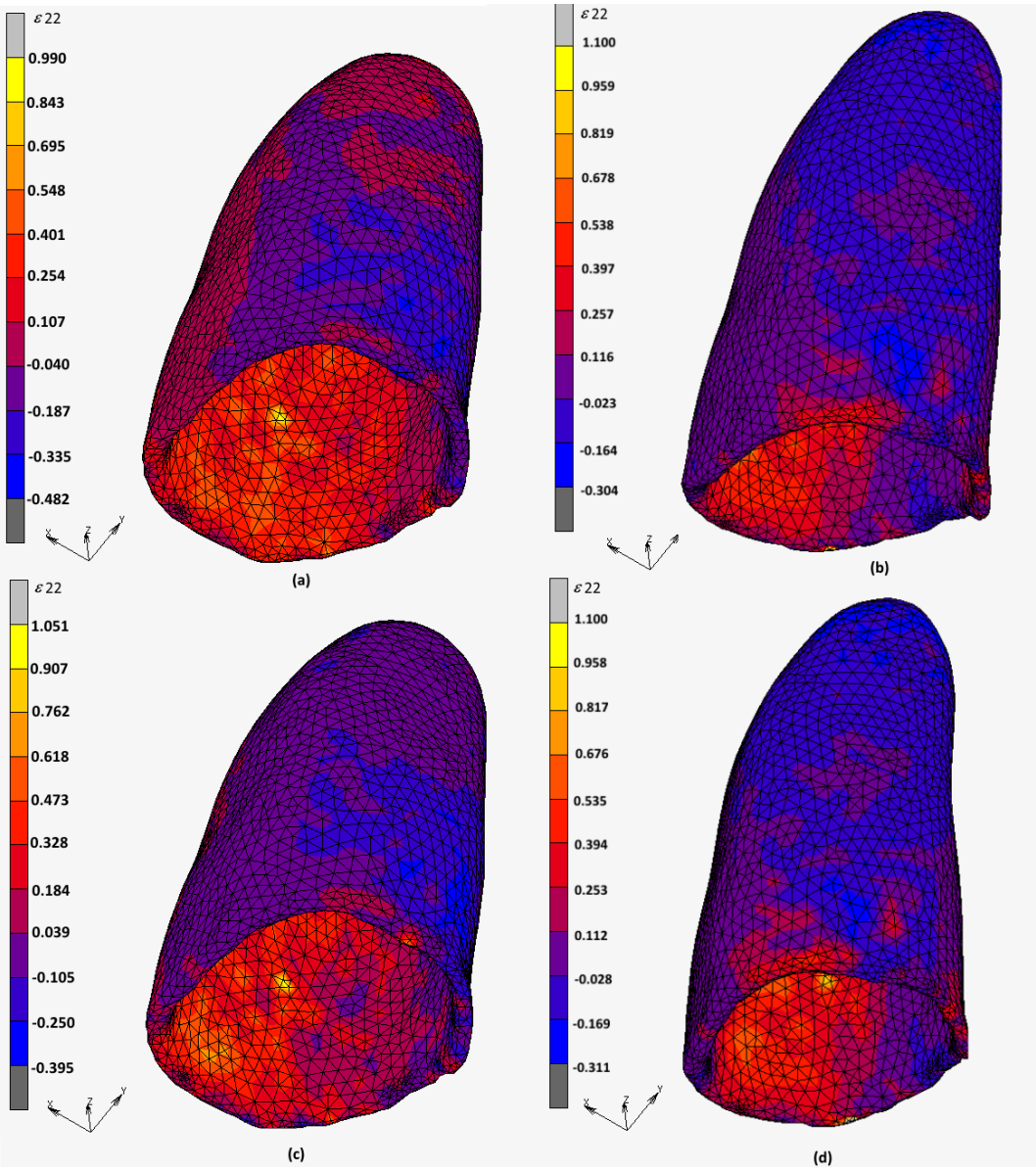

Slika 5.10: Distribution of axial strain for chew and orthodontic force in PDL for uncontrolled tipping (a), controlled tipping (b), bodily movement (c) and rotation (d)

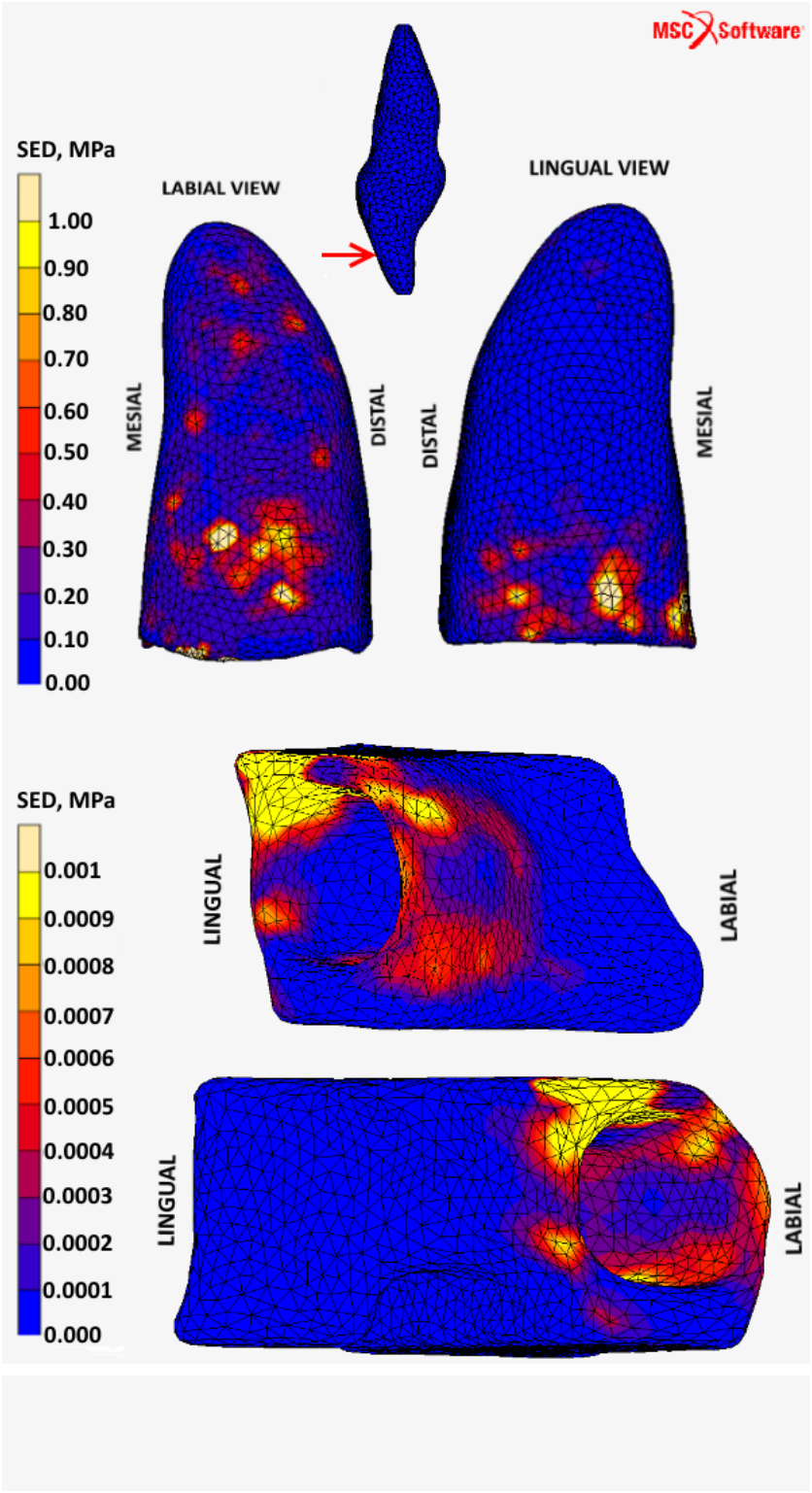

Slika 5.11: Distribution of SED for chew and orthodontic force in PDL and bone, uncontrolled tipping

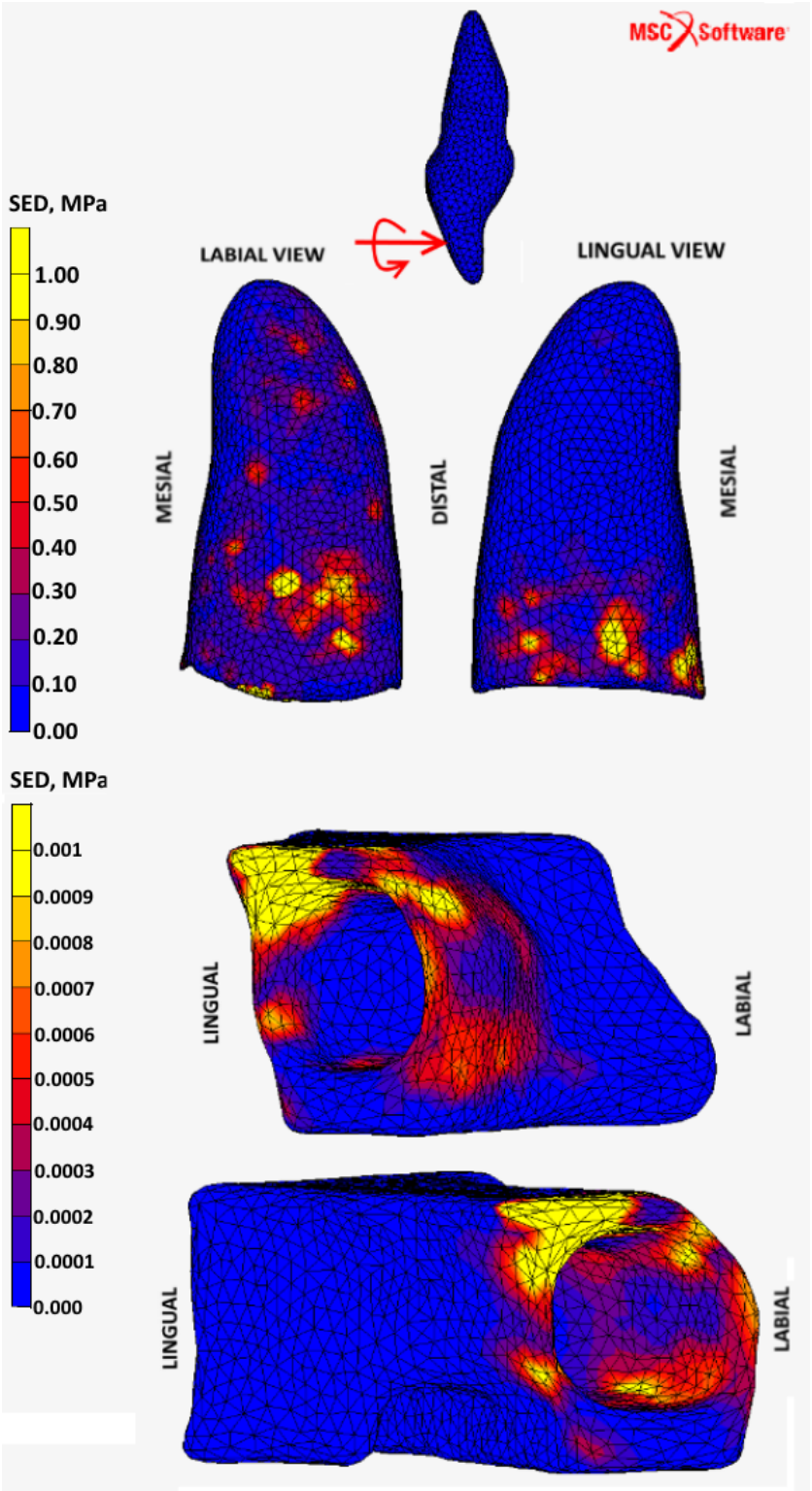

Slika 5.12: Distribution of SED for chew and orthodontic force in PDL and bone, controlled tipping

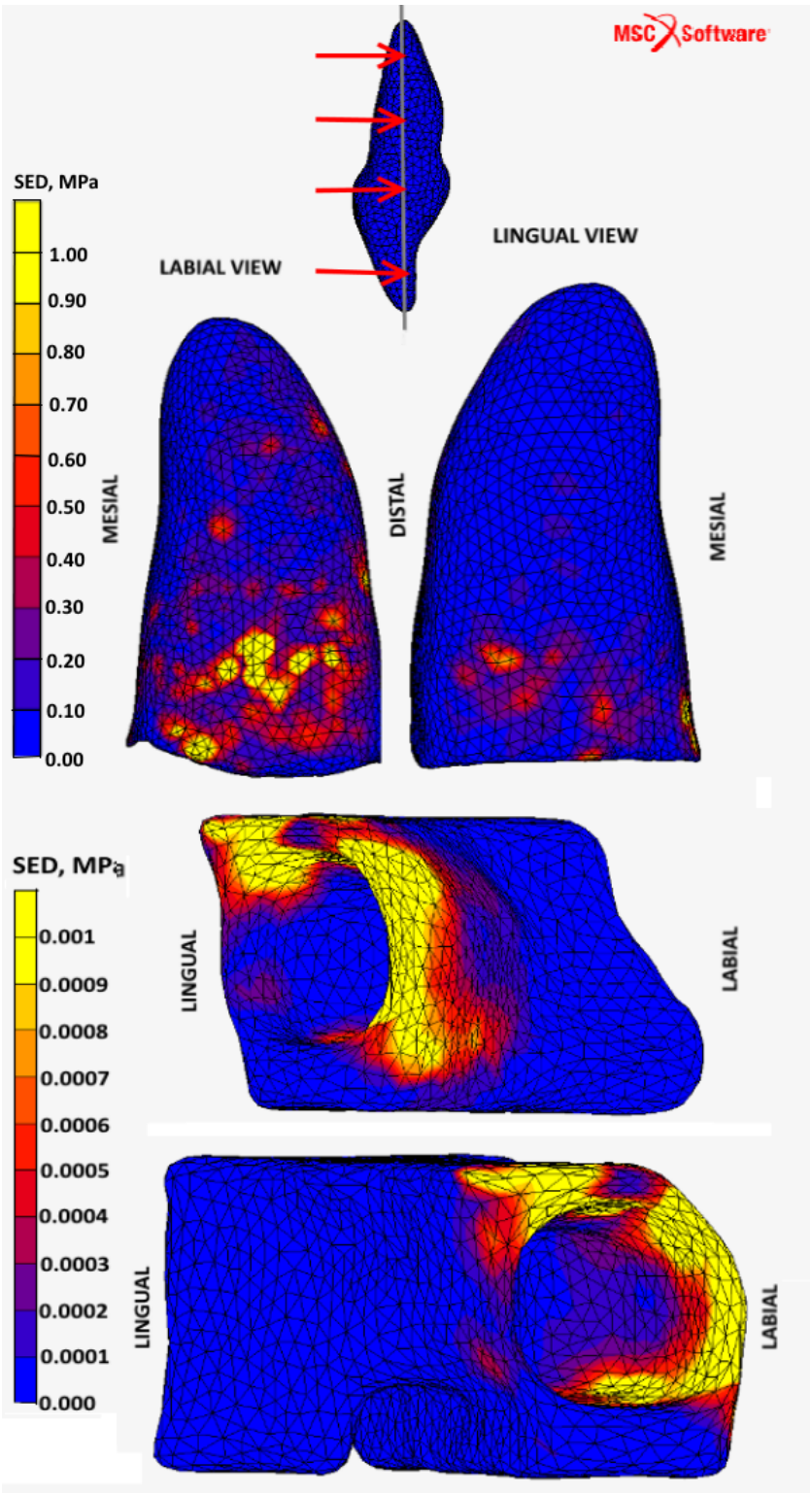

Slika 5.13: Distribution of SED for chew and orthodontic force in PDL and bone, bodily movement

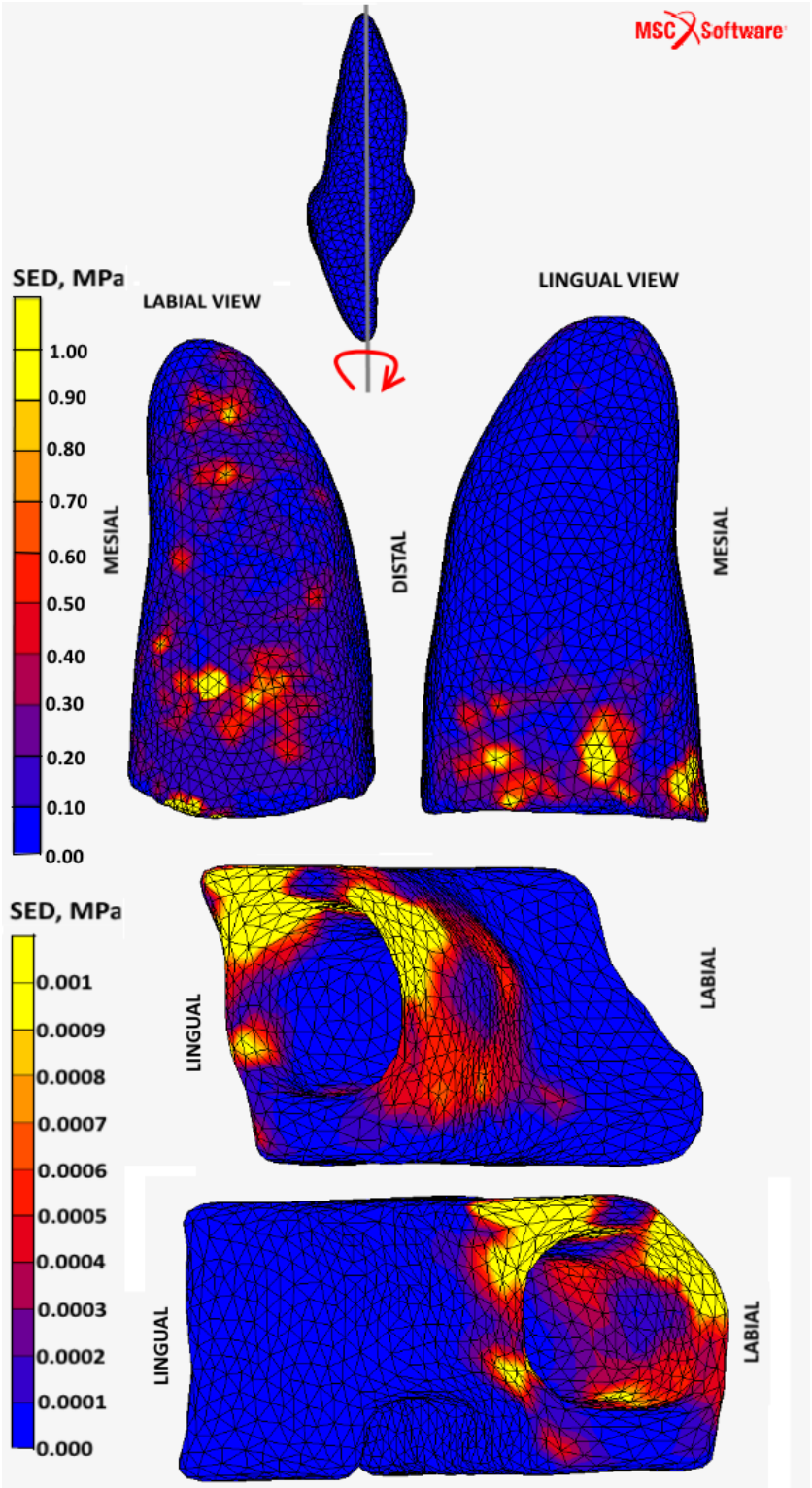

Slika 5.14: Distribution of SED for chew and orthodontic force in PDL and bone, rotation

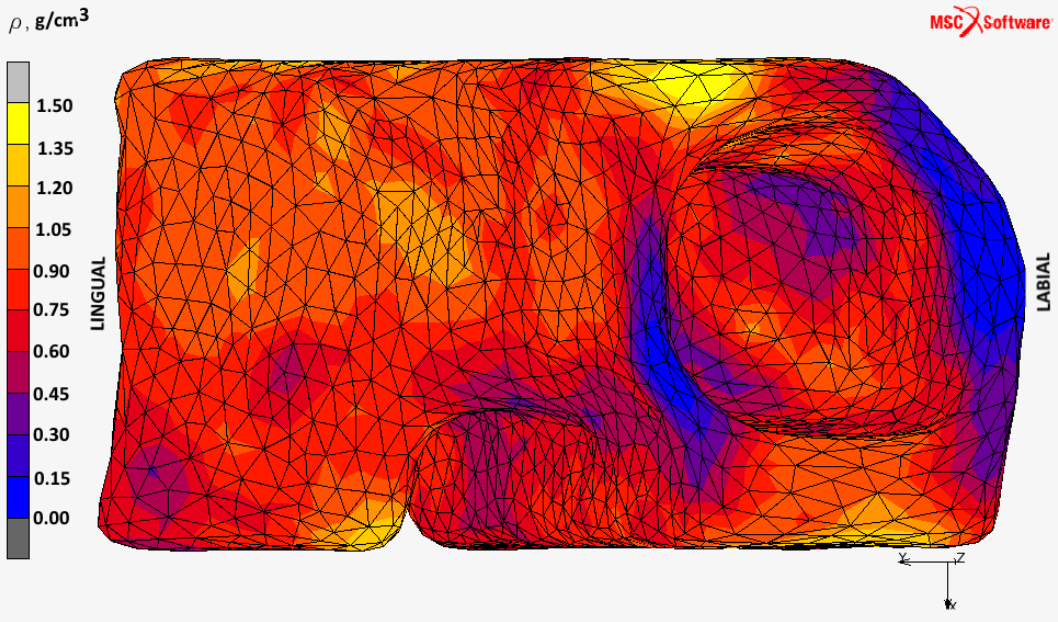

Slika 5.15: Distribution of apparent density for reference run

in literature [22]. 35% is half the length of the lazy zone. SED distribution for reference run is seen on Figure 5.16. The distribution is the same as it was for SED for chew force without the code, and this was expected.

The next step is getting new density values and showing bone formation and bone resorption. For a remodelling run, both chewing and orthodontic force are used. Values of new density are calculated at each iteration step for each element. Finite element used to describe bone is tetrahedron which has one iteration area and four nodes. All values that are calculated in integration area are extrapolated to nodal values, so the same approach was used to obtain new density. Figure 5.17 shows density distribution after a remodelling run was made. Changes in densities can be seen, especially in the labial and lingual cervical area, and also in the apical, both lingual and cervical, area. In uncontrolled tipping, most impact on bones occur in these areas, so, the changes in the apical and the cervical area in direction of orthodontic force application and opposite are expected.

A remodelling run also provides values of SED, as shown on Figure 5.18. SED distribution shows that changes, compared to Figure 5.16 can be seen in the apical and cervical area, both in lingual and labial direction, as expected. Cervical and apical areas, in lingual and labial direction, are showing the most changes in SED values, and therefore in stimulus as well.

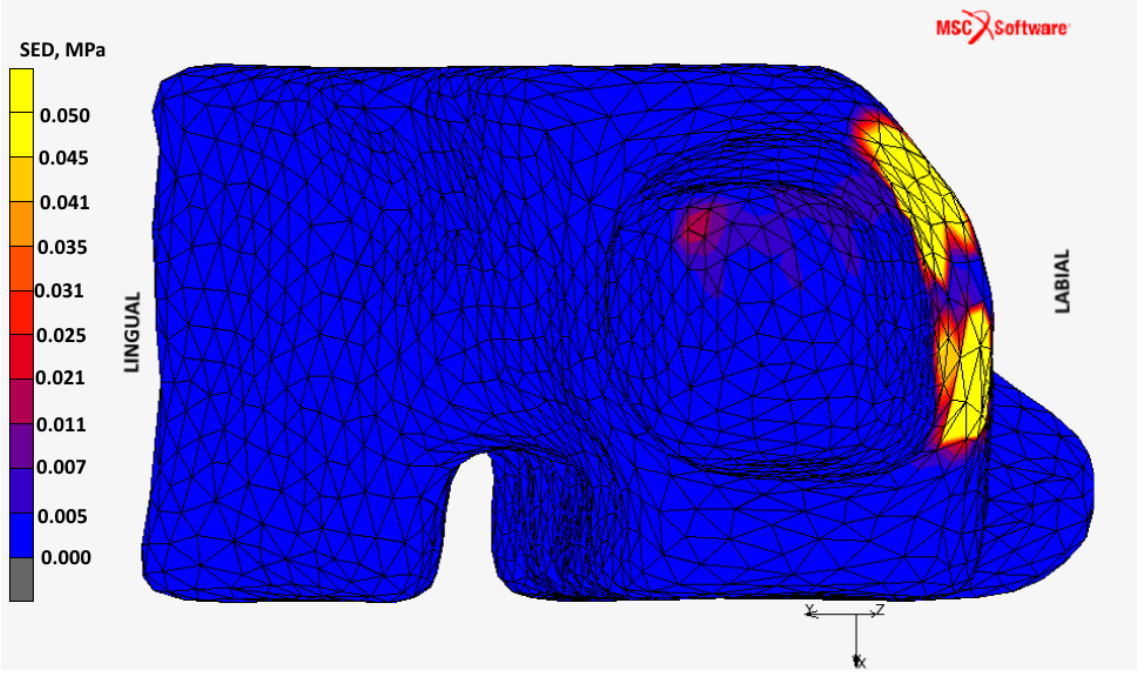

Slika 5.16: Distribution of SED for reference run

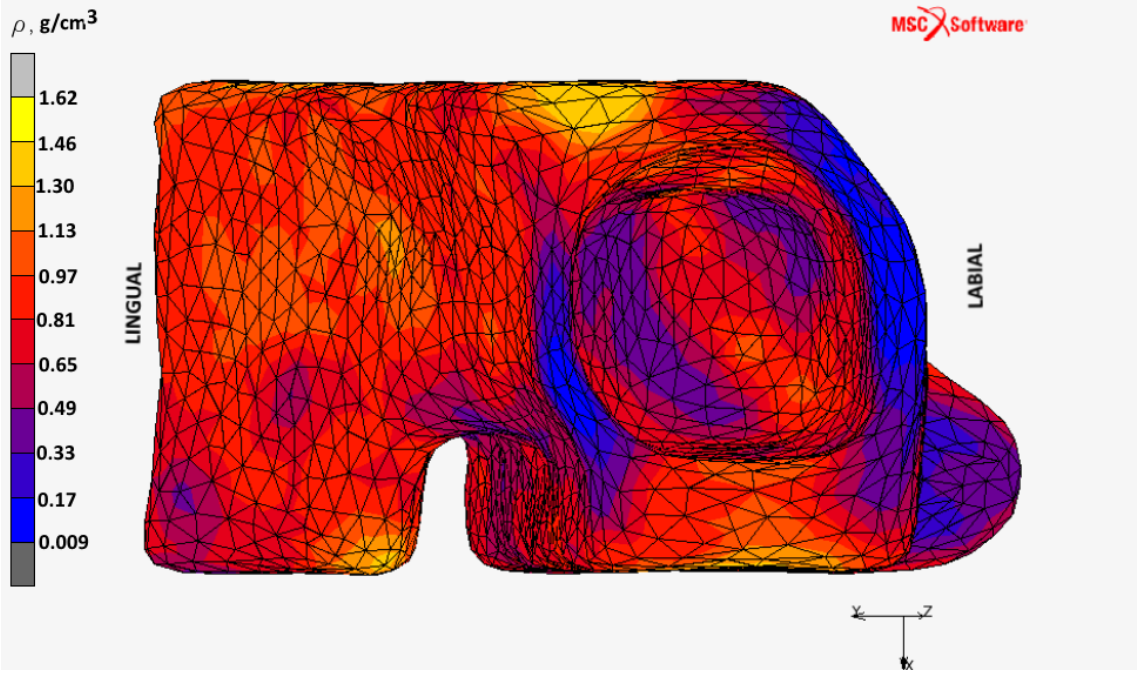

Slika 5.17: Distribution of apparent density for remodelling run

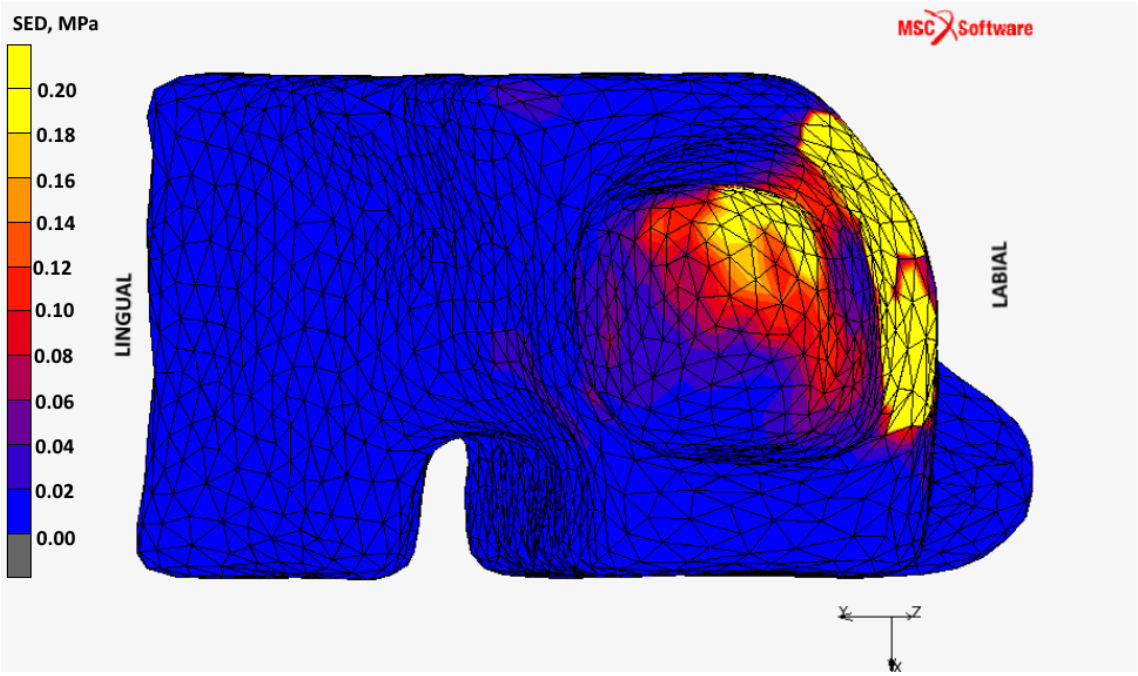

Slika 5.18: Distribution of SED for remodelling run

5.4 Discussion

In this research the biomechanical changes induced by chewing loading and orthodontic loading in the supporting apparatus of the tooth were analyzed. The results obtained here provide important information which could lend a hand in interpreting a complex biological reaction generated from complex loading. This study complements the previous FEM analyses of orthodontic bone remodelling by modelling the detailed periodontal and alveolar support, considering the orthodontic loading hardware and taking into account influence of chew loading. Furthermore, this research also uses a patient-specific approach. The study presented here has introduced a numerical model for orthodontic bone remodelling initiation that is based on the hypothesis set at the beginning of the research. The hypothesis states that the research will explain bone remodelling initiation induced by orthodontic forces without violating Wolff's Law. First, a 2D analysis was made to confirm the hypothesis, then afterwards a 3D analysis was made to confirm the hypothesis as well. 3D analyses included four different types of movement.

This research has taken into account the influence of chewing and orthodontic loading on the initiation of orthodontic bone remodelling. Application of chew force is seen as a referent value of daily loading level, so values of SED for other analyses are seen as a percentage of that referent value. Results are shown on Figure 5.19 for the 2D analysis and 5.21, 5.22, 5.23 and 5.24 for the 3D analysis. As explained above, four characteristic

areas where values for SED were observed can be seen here. In both figures, these values are shown as percentage of referent value.

Figure 5.19 shows results of 2D analyses. It can be seen that values for orthodontic force, blue boxes, are values of small amounts, as it can be expected because the force is quite small in value when compared to the to value of chewing force. Red boxes refer to values of SED in the analysis with chew and orthodontic loading together. It can be seen that on area 1 and 4 the values are negative, and on areas 2 and 3 the values are positive. As mentioned above, negative values refer to underloading condition. That means that on areas 1 and 4 PDL fibres are unloaded and PDL matrix is compressed. PDL matrix starts to reproduce osteoclast which are starting to resorb bone on these areas. Areas 2 and 3 show positive value, which refers to overloading conditions in these areas. That means that in these areas PDL fibres are stretched and pulling the bone. PDL reacts to that by increasing the osteoblasts production and in that way enables for bone formation to happen.

Figures 5.21, 5.22, 5.23 and 5.24 show results for 3D analyses for all four types of movement in four characteristic areas. Results are shown as a percentage of chewing force, where gray boxes refer to chew force, purple refer to orthodontic loading, blue refer to overloading condition which occurs under influence of chewing and orthodontic loading, and red boxes refer to underloading condition occurred under influence of chew and orthodontic loading. UT refers to uncontrolled tipping, CT refers to controlled tipping, BM refers to bodily movement and ROT refers to tooth rotation. Areas position for 3D model is shown on Figure 5.20. For all four types of movement at all four characteristic areas it can be seen that SED values, when orthodontic loading is applied, are values of low magnitude, just a small percentage of referent value. The reason for that is, as it is expected, the small value of orthodontic force and moment applied on the crown of the tooth. These small values of orthodontic loading cause changes in PDL matrix, but do not make noticeable changes in PDL fibres and surrounding bone. Even values of stresses in the capillary vessel are quite small [17], and the influence of orthodontic loading causes higher value stresses. This research has proved that this is not enough for triggering bone remodelling. Changes in stress and strain distribution in PDL matrix cause cell activity in PDL, but it does not cause bone remodelling since the influence on PDL fibres is negligible. To provoke bone remodelling, PDL fibres ought to be stretched on one side, and unloaded, together with PDL matrix compression, on the other side. When the orthodontic loading is applied by itself, this biological process cannot be quantified. On the other hand, when a combination of chewing force and orthodontic loading is applied, the biological process of bone remodelling can be seen in characteristic areas.

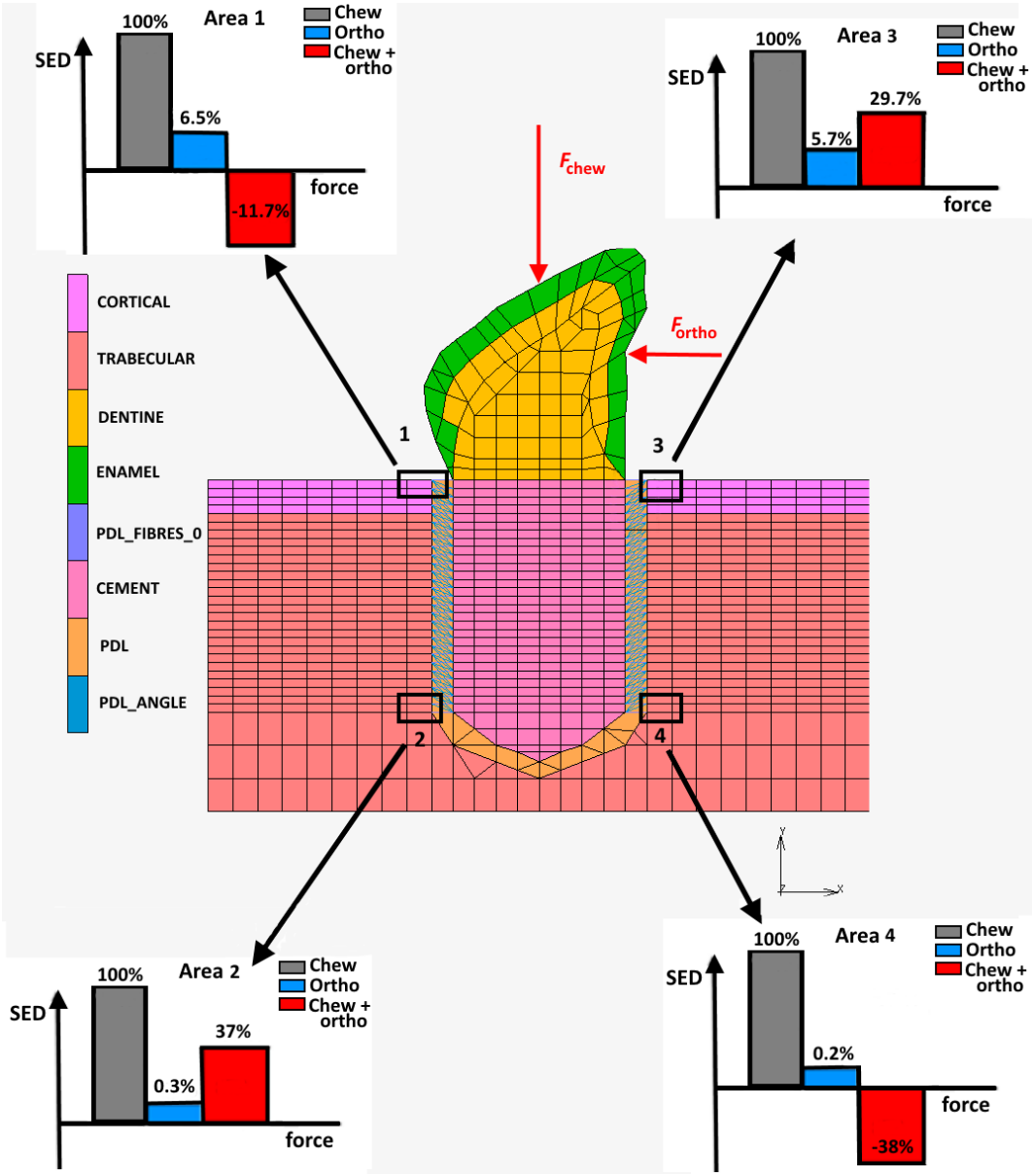

Slika 5.19: Results of 2D model

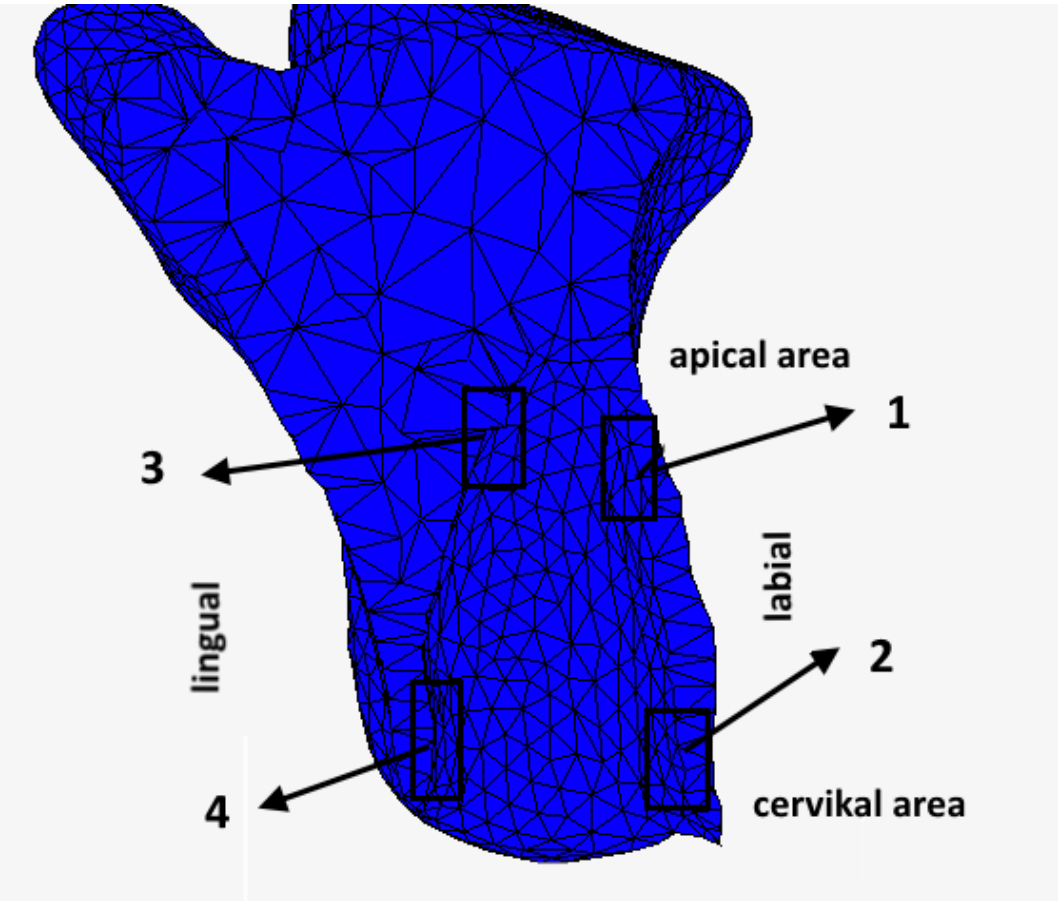

Slika 5.20: Characteristic area position for 3D model

Characteristic area 1 is area positioned on labial apical area. On diagram shown on Figure 5.21 it can be seen that only with uncontrolled tipping there is underloading condition which will lead to resorption, other movements have overloading here, and influence of only orthodontic force is negligible compared to referent value of daily loading level. On the diagram that shows results for area 2, Figure 5.22 it can be seen that in all four type of orthodontic movement studied here, there is overloading condition referring to bone formation. Also, values of orthodontic loading are higher than in area 1. The reason for that is that observed area 2 is in labial cervical area, and orthodontic force is applied, fibres in this area are stretching much more, since distance of applied force to the centre of rotation is higher, and then the value of M/F ratio is high, causing bigger tilting of the tooth. Compared to area 1, M/F ratio is much lower, which leads to lower tooth tilting, and lower fibres stretching, as it can be seen on Figure 5.10. Area 3 is also, shown on Figure 5.23, as area 1, on apical area, just on the opposite side, on lingual side. Here only for uncontrolled tipping there is overloading condition, and for other type of movement, there is underloading condition. For influence of orthodontic loading similar behaviour

can be seen as in area 1, which shows that orthodontic force almost has no any influence there on the surrounding tissue. In area 4, cervical lingual area, it can be seen that the tooth is under underloading condition. That is expected behaviour, because for all four orthodontic loadings, fibres are unloaded in this area, and PDL matrix is compressed. Again, the influence of orthodontic force in this area is unnoticeable.

When a combination of chew force and orthodontic loading is applied for all four tooth movements, SED distribution in analyses follows the biological respond in the PDL and the alveolar bone. When uncontrolled tipping movement is applied, the tooth tilts lingually around the centre of rotation, which is positioned at the centre of resistance. This type of movement is used the most in literature, because it nicely shows stress and strain distribution in bone by demonstrating bone formation and resorption. Therefore, in SED distribution it can be seen that in uncontrolled movement in apical area on lingual side overloading condition which refers to bone formation can be seen, and on labial apical side underloading condition which is leading to bone resorption can be seen. SED distribution in cervical area shows overloading on the labial side, and underloading on the lingual side. These results can be confirmed with similar analyses, but with different approach, in [18, 14, 15, 24, 16, 33, 30, 17, 22]. Others movements, even if they are not so numerically studied, also follow the expected biological respond. Numerical simulation of controlled tipping could not be found in literature, but results obtained in this research confirm the biological process, in which the tooth is rotating around the centre of rotation positioned in root apex, where on the lingual side there is underloading condition, and on the labial side there is overloading condition. The values in area 1 and 3 are different, since fibres in area of characteristic area 3 are stretching more than in the area where 1 is positioned, Figure 5.10. Bodily movement was analyzed by Mengoni *et. al.* [31], Penedo [17], Wang [22] and Cattaneo [24]. Results obtained in this research are in agreement with mentioned research, where underloading condition can be seen on the lingual side, in the direction force application and overloading condition can be seen on the labial side. Wang [22] and Mengoni [30, 31] were also analyzing rotation movement. Since the root is not symmetric around its main axis, at rotation movement, bone surrounding the tooth is or in overloading condition or underloading condition, considering moment application. Moment application here is in positive direction of z axis, on the lingual side there is underloaded condition and on labial there is overloaded condition which is in accordance with the results in literature [22, 30, 31].

As mentioned, in literature different approach can be seen to explain alveolar bone remodelling, and also, and according to that, results are shown differently in literature. Mengoni *et. al.* [30, 31] showed changes in density and stimulus also as displacement of

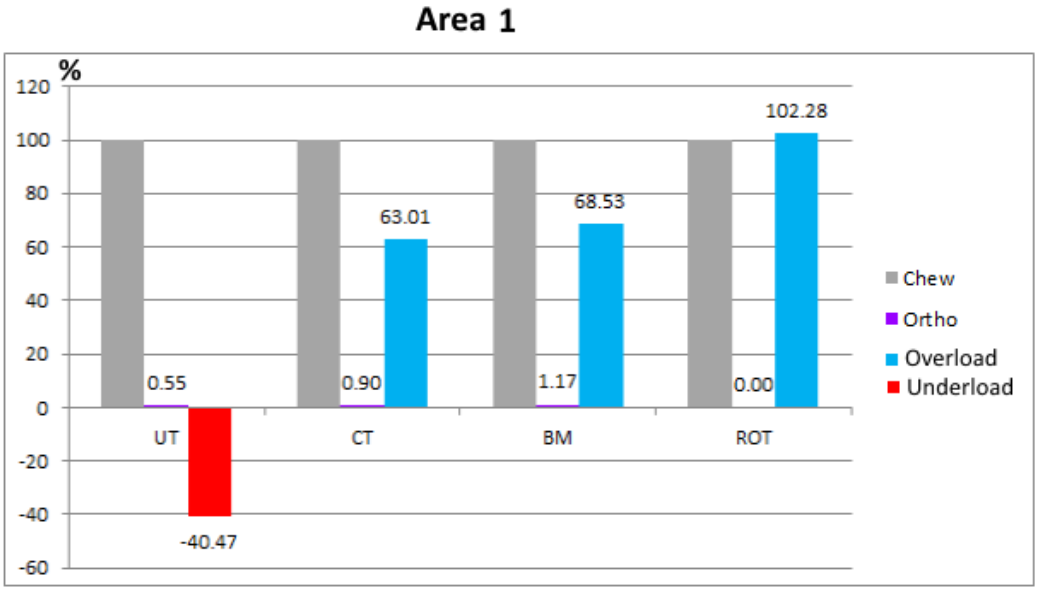

Slika 5.21: Results of 3D model, area 1

tooth. Wang *et. al.* [22] also showed changes in density and displacement of tooth through the centre of resistance. Bourauel *et. al.* [14, 15] showed translation and rotation of the tooth and also normal and shear strain in bone and the PDL. Penedo *et. al.* [17] showed displacement and axial stress. Field *et. al.* [16], Cattaneo *et. al.* [24], Ammar *et. al.* [18], Viecill *et. al.* [147] and Sansalone *et. al.* [148] showed principal stress in bone to confirm bone remodelling.

Figures 5.6 (b), 5.12 (b), 5.13 (b) and 5.14 (b) show strain in the PDL in the direction of applied orthodontic force. Strains are shown for analysis when chewing and orthodontic force are applied. In the direction of orthodontic force it can be seen positive values for strain, which refers to tensile loading on that areas in PDL, resulting stretching of PDL fibres. On opposite side, it can be seen negative values of strain in PDL which refers to compression in PDL as a result of tooth pressing that side of PDL. When it is looked on observed areas, expected behaviour can be seen. Therefore, on areas where resorption is expected, it can be seen that there is PDL compression, and on areas where bone formation is expected it can be seen PDL stretching in all observed types of movement, Figure 5.10. When results of strain in PDL are compared to Bourauel *et. al.* [14, 15] it can be seen that compression in PDL is in the same areas as in this research for uncontrolled tipping, also as areas of PDL stretching.

Bone remodelling algorithm calculates stimulus showing areas of bone remodelling initiation. Algorithm can differentiate between bone formation and bone resorption, also as the

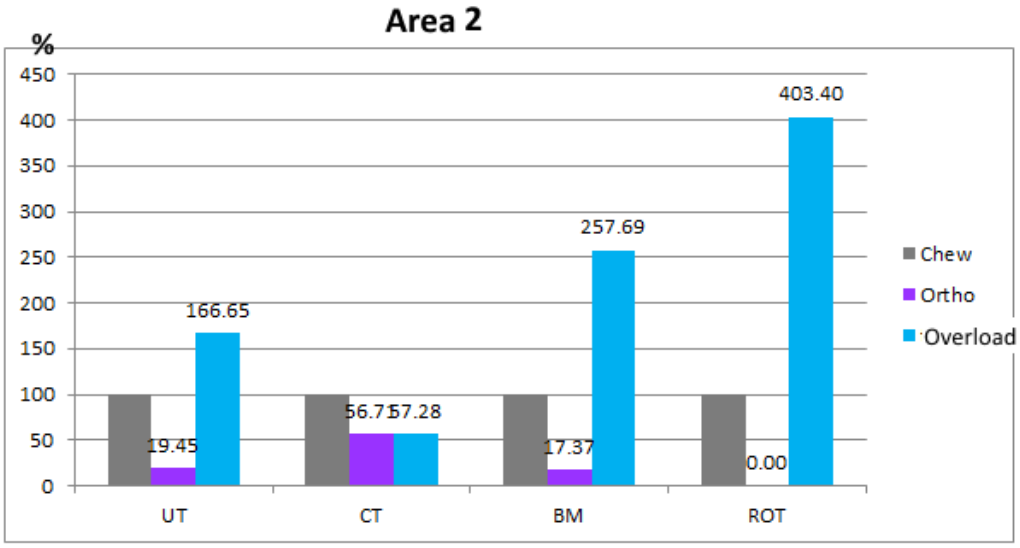

Slika 5.22: Results of 3D model, area 2

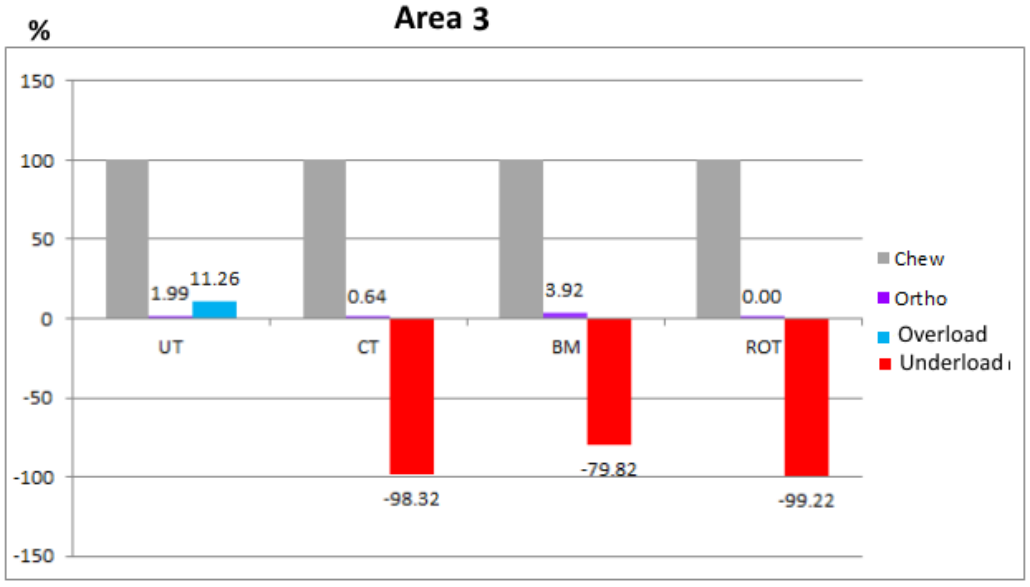

Slika 5.23: Results of 3D model, area 3

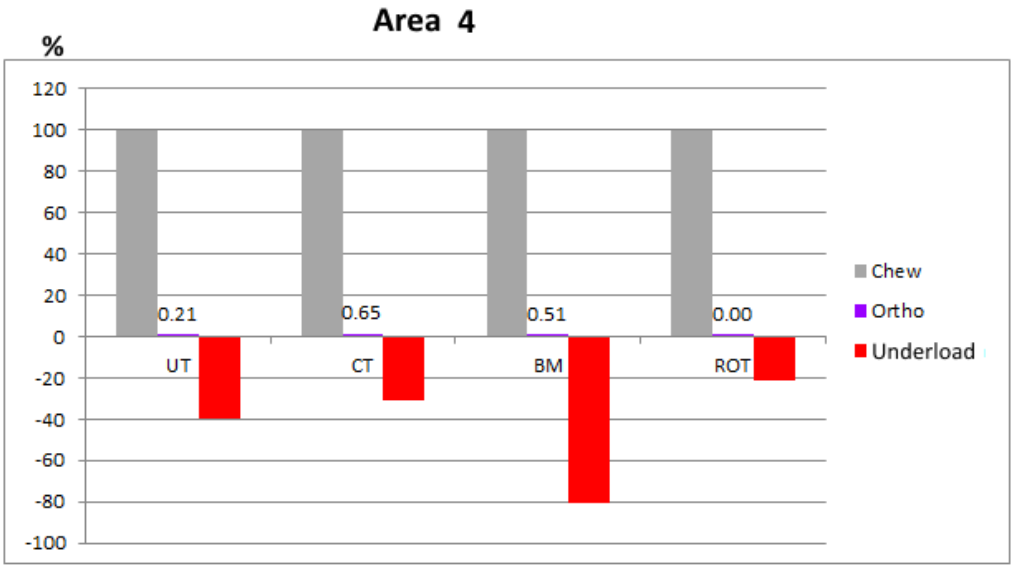

Slika 5.24: Results of 3D model, area 4

lazy zone. Algorithm takes referent value of SED and puts it as S_{ref} in first run, reference run, and afterwards, from it, calculates the length of the lazy zone. After the boundaries are set, obtained values of new SED (when chew and orthodontic forces are included) are compared with referent value. If new SED, now the stimulus S, is greater than referent value and is out of the boundaries of the lazy zone, then there is bone formation. Contrary, if new SED is lower than the referent one, and is out of boundaries of the lazy zone, there is bone resorption, following the Figure 3.2 (b).

Figure 5.25 shows the values of stimulus for uncontrolled tipping loading. Positive values means that there is bone formation, and negative values state that there is bone resorption. Zero values are when bone is in the lazy zone, where no bone remodelling takes place. It can be seen that last increment, at the end of bone remodelling, for the most of the bone, stimulus is positive, which means that new bone is formed. That is the result of continuous loading of chew and orthodontic force of whole bone. In labial cervical and lingual apical area positive values of stimulus can be seen, which means that more formation occurs in these areas, due to influence of orthodontic force which is pushing tooth on one side, and stretching fibres on opposite site, Figure 5.10. On the side where fibres are stretched, as result of overloading condition, there is bone formation. On other side, where PDL is compressed and in bone occur underloading condition, there is bone resorption.
Bone remodelling algorithm is also used to explain controlled typing, bodily movement and

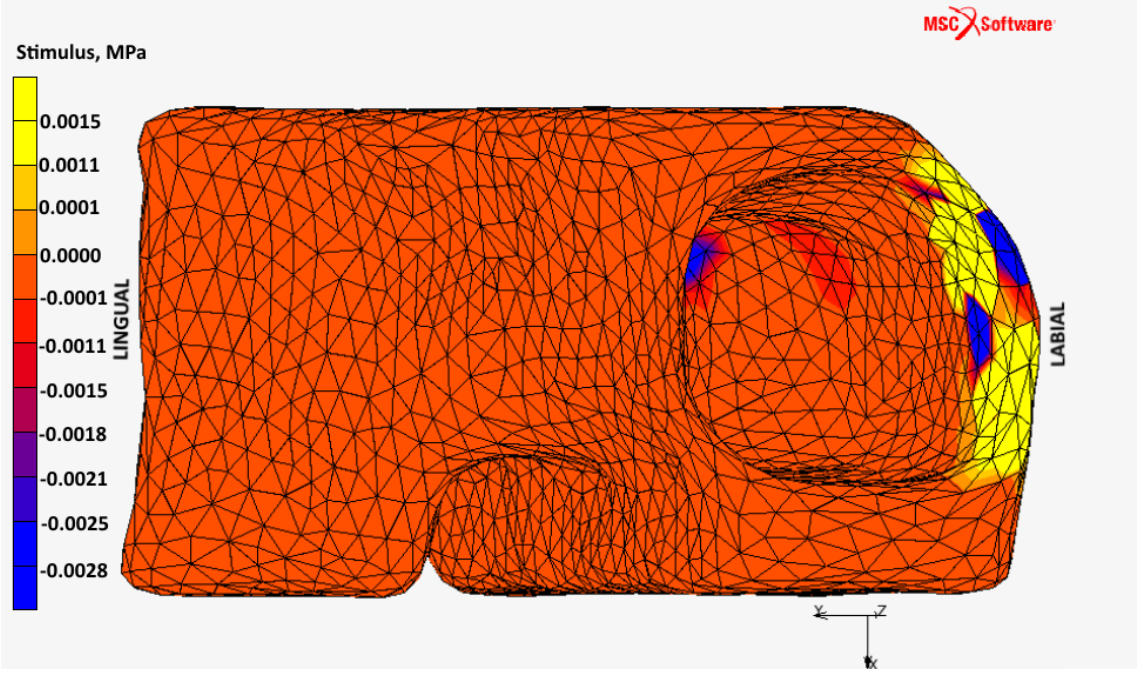

Slika 5.25: Distribution of stimulus for uncontrolled typing

rotation, shown on Figures 5.26, 5.27 and 5.28. In the whole analysis, the stimulus shows areas of formation and resorption as they could be seen in 3D model without the algorithm, Figures 5.11, 5.12, 5.13 and 5.14, and confirming the biological response. Therefore, in controlled typing, on the labial side there is formation, and on the whole lingual side, there is resorption, and the tooth rotates around the centre of rotation positioned in apex. In bodily movement, labial area is formed, and lingual area is resorbed, since tooth is moving in direction of force application. When rotation is applied, on labial area PDL fibres are stretched causing bone formation, and the lingual area PDL is compressed causing bone resorption, as it can be seen on Figure 5.10.

Results using bone remodelling algorithm are compared with literature where bone remodelling is described by user defined bone remodelling algorithm. This approach was used by Bourauel *et. al.* [14, 15] Mengoni *et. al.* [31] and Wang *et. al.* [22]. All of them have been simulating uncontrolled typing, showing changes in density, or stimulus or both. Differences between approaches are in using different stimulus and between using bone bending approach or compression-tension approach.
Comparing results from literature it can be seen that results obtained in this research follow density changes in Mengoni *et. al.* [31] and Wang *et. al.* [22] research. During bone remodelling induced by orthodontic and chewing force, most changes in density occur in the direction of tooth movement, and opposite areas. The reason for this is that bone

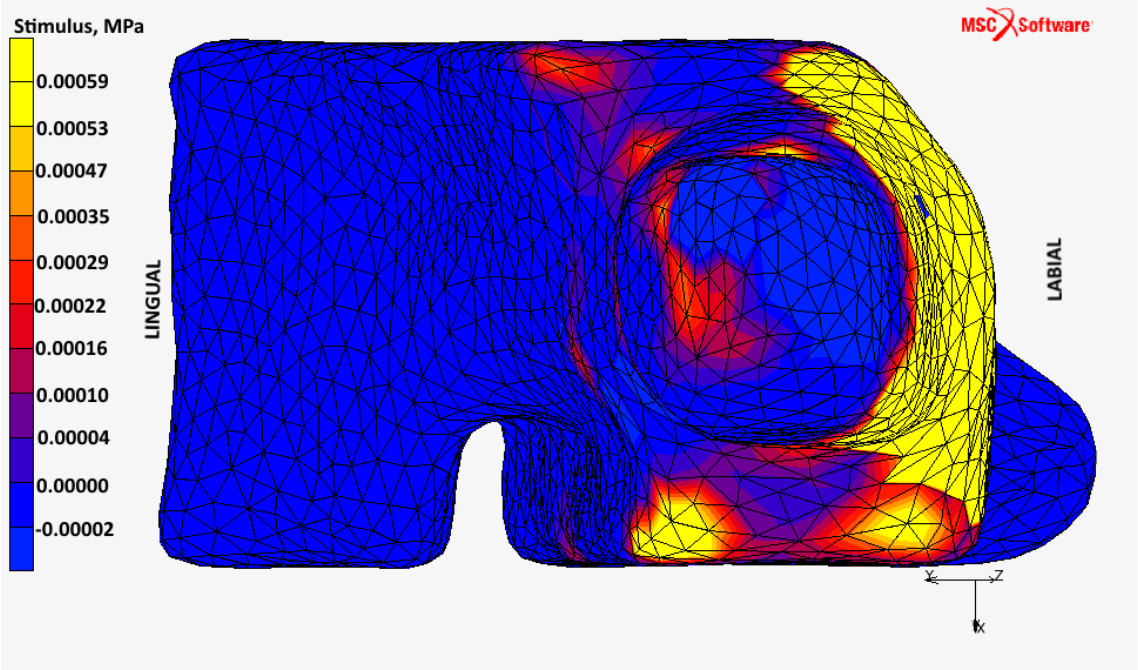

Slika 5.26: Distribution of stimulus for controlled typing

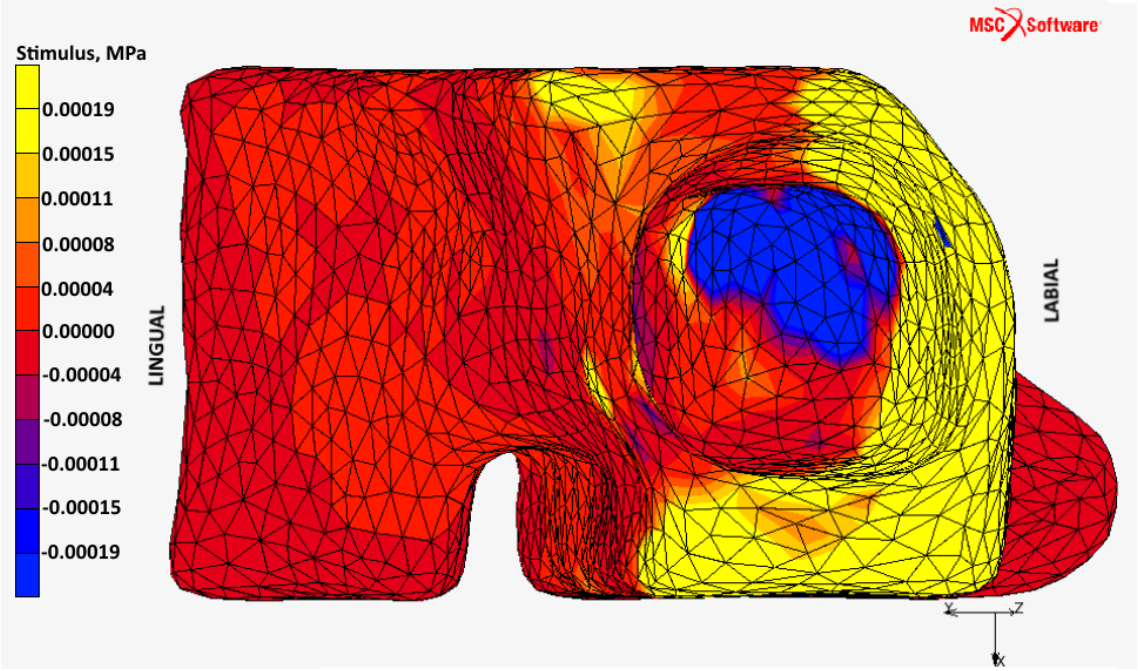

Slika 5.27: Distribution of stimulus for rotation

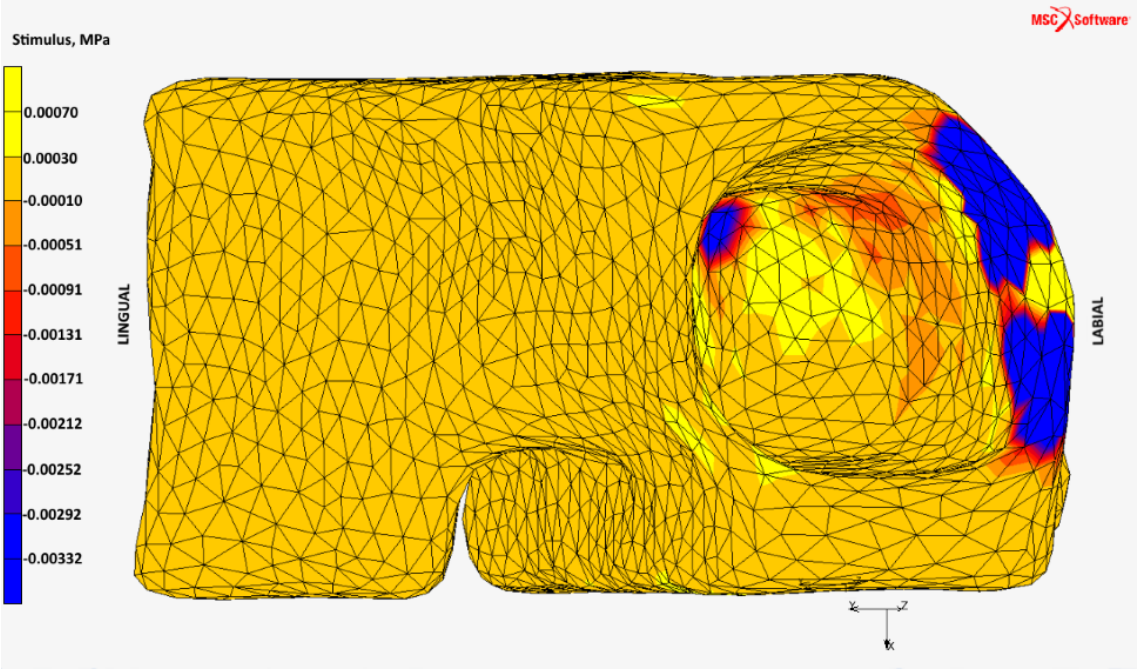

Slika 5.28: Distribution of stimulus for translation

needs to resorb in these directions, allowing tooth movement in that direction, and form in opposite direction. Therefore, where bone resorption occurs, values of density should be lower than in referent value, and where there is formation, higher values. Here, bone remodelling algorithm shows areas with higher values and lower values of density after analysis was made. So, areas where there is bone resorption can be seen, in which new density values are lower and in the areas where there is bone formation, is bone formation new values are higher.

Tables 5.1 and 5.2 are shows values stimulus and density for four characteristic areas of bone for four different types of movement. The first column in both tables shows referent values. In Table 5.1 it can be seen that some values are positive and some are negative, where positive values refer to bone formation and negative values refer to bone resorption. It can be seen that for uncontrolled tipping (UN) resorption appears in areas 1 and 4. For controlled tipping (CT) it can be seen that on areas 1 and 2 there is bone formation, and in other areas there is bone resorption. At bodily movement (BT) formation at areas 1 and 2, and resorption at areas 3 and 4 can be seen. Rotation (ROT) shows similar behaviour, on areas 1 and 2 there is formation, and 3 and 4 resorption.

In Table 5.2 changes in density in characteristic areas for all types of movement can be seen. If density is decreased then there is bone resorption, if it is increased, then there is bone formation. Compared to referent values, there is an increase for areas 2 and 3 for UT, which approves the values of stimulus, and in areas 1 and 4 there is a decrease in of

Tablica 5.1: Stimulus values for all four types of movements

Stimulus, 10^{-5} MPa					
Area	Referent value	UT	CT	BM	ROT
1	0.0125	-41.85	48.49	25.77	31.29
2	0.7796	147.80	277.78	460.3	25.0
3	0.0847	0.46	-5.29	-2.41	-38.33
4	0.0336	-1.81	-21.38	-11.75	-5.71

Tablica 5.2: Values of apparent density for all four types of movements

ρ, g/cm^3					
Area	Referent value	UT	CT	BM	ROT
1	0.64475	0.64321	0.64581	1.3039	0.64591
2	0.22735	0.22850	0.23345	1.2511	0.23780
3	0.62388	0.62474	0.62264	0.57918	0.62265
4	0.87433	0.62288	0.87340	0.84810	0.87415

bone density. For CT, BM and ROT an increase in bone density can be seen in areas 1 and 2, and decrease in areas 3 and 4. Values of density follow the behaviour of stimulus, showing bone resorption and bone formation.

Comparing the distribution of stimulus and density with Mengoni *et. al.* [30, 31] it can be seen that distribution of stimulus and density shows similar behaviour, bone formation and bone resorption. Most of the bone is at the end in the lazy zone, and that is expected, since remodelling is finished, or the same parts of the bone were not under influence of chew and orthodontic force. These areas are mostly on other bone surface, or on bone on which it is in contact with PDL, and bone remodelling is finished there.
Bone remodelling algorithm has showed expected biological behaviour, confirming the hypothesis presented at the beginning of research. Therefore, it can be concluded that chewing force has influence on bone remodelling, since it is daily loading in mouth, and alveolar bone is under influence of chew force constantly. The combination of daily loading, chewing force, with orthodontic force, causes bone remodelling which enables tooth movement in desirable direction.

In published literature, various data can be confusing and it does not even confirm the biological response of orthodontic bone remodelling and orthodontic tooth movement.

Since each author used a different approach of showing bone remodelling n the end the results are shown in different way (in literature results showing bone remodelling are expressed as SED, HMH stresses, axial stresses, normal strains, shear strains, equivalent strain and principal strain), magnitudes of orthodontic force are different, therefore it is not easy to compare results. There is no experimental research done on humans so that the results could be compared to it. The main advantage of the research that was carried out is that each movement that was studied and numerically analyzed here has its confirmation in biological response, and in some numerical analyses found in literature. This certainly gives additional ”weight” to the results and their future use.

6 Conclusion

The main goal in orthodontic treatment is to move the tooth to the desired position, no matter whether the initial problem was pathological or aesthetic in nature. This can be achieved only by an irreversible process in the alveolar bone called bone remodelling.
In this thesis the focus was on testing whether tooth movement resulting from orthodontic force application can be predicted using load adaptive bone remodelling theories developed in earlier studies in orthopeadic biomechanics when applied to the alveolar bone. The hypothesis investigated here is that the tooth is 'hanging' in the fibrous PDL when loaded by chewing forces, and that orthodontic loading would reduce the loading in the fibres on the side to which the tooth is pushed and increase the loading in the fibres on the other side.
The hypothesis set out in this thesis is based on the assumption that patient-specific model that uses finite element analyses can predict the initiation of orthodontic bone remodelling and, hence, orthodontic tooth movement, which would result in personalized orhtodontic treatment. Such simulation tool needs to model the biological and mechanical reactions of all tissues and materials involved. During orthodontic tooth movement, two tissues have a major influence, the alveolar bone and the periodontal ligament. When orthodontic loading is applied, bone and the PDL react mechanically and biologically to the loading, and bone and PDL reactions are closely linked as well. This coupling can be treated as model, and in the research carried out here, the focus was on the mechanics and the phenomenological aspect of biology. Finite Element Method (FEM) was selected in order to describe the mechanics of bone remodelling initiation. FEM involves a series of computational procedures to calculate the stress and strain in each element. Strain energy density, SED, is used as a mechanical stimulus for the bone, following the earlier theories developed in orthopeadic biomechanics. Since SED is associated with bone density changes according to bone remodelling theories, in this research the remodelling of the alveolar bone was monitored by observing changes in the strain energy density.

In the research presented first a 2D model was developed, which was consisted of tooth, bone and the PDL. The main focus was on describing the PDL and connecting it to other parts of the model. Finite element analyses of the 2D model were made by using the software Marc Mentat. After preliminary analyses were made, it was concluded that the PDL described as a continuum would not lead to a realistic description of a biological problem. The next step was to include PDL fibres into the model. This approach offered more realistic results. The 2D model highlighted the significant role of the PDL in bone remodelling, and its numerical description. Even the 2D model is a drawing that represents tooth, the PDL and bone was a clear enough representation to confirm to confirm the hypothesis and to continue onto the 3D model.

One of the main contributions of this research is including chew force into analyses and recognizing its influence on bone remodelling due to orthodontic treatment. Chewing force represents daily loading in the mouth. Strain energy density obtained from the analysis with chew force is referent value of stimulus. Another influence of chewing force that it makes a larger moment on tooth after application of orthodontic force which tilts the tooth. Other forces, like muscle forces, swallowing forces etc., that can be found in the mouth were neglected because their magnitude is much lower.

The next step was to introduce a 3D model developed from CT scans made on CBCT. The scans were obtained from a patient to whom orthodontic treatment was recommended. Geometry was made in the software Mimics, which allows for a precise geometry of the system tooth-ligament-bone and enables to define bone density read from CT images.

Afterwards, the 3D model was imported in Marc Mentat, in which the same approach was made as in the 2D model, but also, four different types of orthodontic tooth movement were analyzed: uncontrolled tipping, controlled tipping, bodily movement and rotation. The first analysis was made with chew force in order to obtain the referent value of strain energy density. Then, the analyses were made with four different orthodontic loading. The 3D model also confirmed the hypothesis that was set out at the beginning of the research. Despite the simplification of material properties, the proposed description of bone remodelling initiation specified for the alveolar bone is able to indicate underloading condition and overloading condition, which leads to bone resorption and bone formation for four different types of orthodontic loading mimicking biological response.

The next step was the implementation of bone remodelling algorithm made in in the programming language Fortran into Marc Mentat by special user subroutine. Bone remodelling algorithm was able to predict bone remodelling initiation in areas in which bone remodelling initiation should occur. Bone remodelling algorithm has three main subroutines that are called by Marc Mentat and these subroutines were able to calculate

referent SED, new apparent density and objective function. Objective function is used to calculate if there is bone formation or bone resorption following the remodelling rate scheme made by Huiskes *et al.*

The methodology employed here, however, has some limitations which should be discussed. First, it is assumed that root resorption does not occur in the presented study. Second, mechanical properties of tooth, bone and the PDL are assumed to be isotropic and linear elastic. And third, strong dependence on the boundary conditions has been seen to affect bone remodelling. The next step in future research is to try to solve these limitations.

In conclusion, although the current method has limitations mentioned above, the consequence of orthodontic treatment can be predicted numerically by FEM. Using a SED as a mechanical stimulus for bone remodelling, the various types of orthodontic loading that transfer its influence on the surrounding bone result in different modes of tooth movement and morphology of bone. Therefore, analyzing tooth movement associated with mechanical loading can be used to predict clinical consequences and to help in the planning of orthodontic therapies. The most important contribution of the research is the development of a numerical model of bone remodelling initiation which includes:

- *influence of chew force* - including the influence of chew force in bone remodelling as a daily loading stimulus and its influence in orthodontic tooth movement,
- *fibrous periodontal ligament* - describing the PDL as matrix and fibres has provided a more realistic description of the problem,
- *patient-specific geometry* - including the geometry based on real-patient data is a step towards personalization of the numerical modelling,
- *SED* - as mechanical stimulus for bone remodelling,
- *bone remodelling initiation* - can be simulated using load adaptive bone remodelling theories developed in orthopeadic biomechanics.

Future research, based on the results obtained in this research, will expand to multi-tooth geometry and will attempt to explain bone remodelling when more teeth are involved. Also, the next step is to explain and numerically confirm orthodontic tooth movement generated from orthodontic force applied on tooth. These steps should be compared with CBCT images of patients to whom orthodontic treatment is recommended.

A Introduction to Contact Problem in Marc Mentat

The simulation of many physical problems requires the ability to model the contact phenomena. The analysis of contact behavior is complex because of the requirement to accurately track the motion of multiple geometric bodies, and the motion due to the interaction of these bodies after contact occurs. This includes representing the friction between surfaces and heat transfer between the bodies if required. The numerical objective is to detect the motion of the bodies, apply a constraint to avoid penetration, and apply appropriate boundary conditions to simulate the frictional behavior and heat transfer. Two numerical procedures to simulate these complex physical problems have been implemented in Marc Mentat, namely a node-to-segment and a segment-to-segment procedure. Since for both procedures the model set up is very similar, switching from one procedure to the other only involves minor effort [145].

There are two types of contact bodies in Marc Mentat – deformable and rigid. Deformable body is a meshed body consisting of finite element. Rigid body is a geometric body consisting of curves (2D) and surfaces (3D). The algorithm used to establish the contact is based on the fact that nodes on the boundary are on element edges or faces that belong to only one element. As all nodes on free surfaces are considered contact nodes (node-to-segment procedure) or all edges/faces defining the free surfaces are considered contact segments (segment-to-segment procedure).

In contact analysis, a distinction is made between touching and glue conditions. In structural analysis, a touching condition triggers the local application of a nonpenetration constraint still allowing relative sliding of the bodies in the contact interface. The nonpenetration constraint is applied through a tying or boundary condition on the displacement components normal to the contact surfaces. A glue condition suppresses all relative motions between bodies through tyings or boundary conditions applying them to all displacement degrees of freedom of the nodes in contact. Unless a flag has been set, nodes in contact via the glue option are not allowed to separate.

Two solids are potentially in contact with boundary Γ_c^1 (solid 1) and Γ_c^2 (solid 2). The equations that represent the mechanical equilibrium can be written using the principle of virtual work such that [149]

$$W^{int}(\overline{\mathbf{u}}, \overline{\delta\mathbf{u}}) + W^{ext}(\overline{\mathbf{u}}, \overline{\delta\mathbf{u}}) + W^{c}(\overline{\mathbf{u}}, \overline{\delta\mathbf{u}}) = 0, \tag{A.1}$$

where $\overline{u}$ and $\overline{\delta\mathbf{u}}$ are respectively the real and the virtual displacement field. Moreover, $W^{int}(\overline{\mathbf{u}})$ is the virtual work associated to the internal forces and $W^{ext}(\overline{\mathbf{u}})$ is the virtual work related to external forces expect the contact ones. The virtual work connected to the contact is noted $W^{c}(\overline{\mathbf{u}})$.
This last one can be written as:

$$W^{c}(\overline{\mathbf{u}}, \overline{\delta\mathbf{u}}) = \int_{\Gamma_c^1} (\delta\xi^{\beta} t_{t_\beta} + \delta g t_n) d\Gamma_c^1. \tag{A.2}$$

Here, Greek letter β can take values 1 or 2. On contact boundary Γ_c^1, the field of virtual relative displacement between the two interfaces is split in the normal direction, δg and the tangential plane, $\delta\xi^{\beta}$. In the same way, the contact stress is projected on the normal direction (normal contact stress, t_n) and on the tangential plane (tangential contact stress, $\overline{\mathbf{t_t}} = \overline{\mathbf{t_{t_1}}} + \overline{\mathbf{t_{t_2}}}$). The contact's laws are the unilateral contact (A.3) and the Coulomb's friction

$$g \leq 0, t_n \geq 0, g t_n = 0 \tag{A.3}$$

$$\Phi = \overline{||t_t||} - \mu t_n \leq 0, \zeta \geq 0, \Phi\zeta = 0 \tag{A.4}$$

where ζ is the absolute rate of sliding, g is the distance between the two boundaries and μ is the Coulomb's friction coefficient. The relation between the rate of sliding and the speed of sliding ($\overline{\mathbf{v_t}}$) is given by:

$$\overline{\mathbf{v_t}} - \zeta \frac{\overline{\mathbf{t_t}}}{\overline{||\mathbf{t_t}||}}. \tag{A.5}$$

Several numerical methods exist to solve the contact problem. Figure A.1 presents the global picture of the Penalty Method used in this work.

The contact surface tractions are computed using a node-to-segment algorithm. The equations of contact are solved for every integration point to each element on the contact surface Γ_c^1, called slave surface. So, the contact surface tractions are known through their values at integration points. The link between one point of the slave surface and the master surface Γ_c^2 is done by orthogonal projection on the closer element of the boundary Γ_c^2. The projection is performed for each integration point of each element of the slave surface so that we can compute the virtual work of the contact forces for each element of this surface.
The penalty method ensures a continuous relation between the contact surface tractions

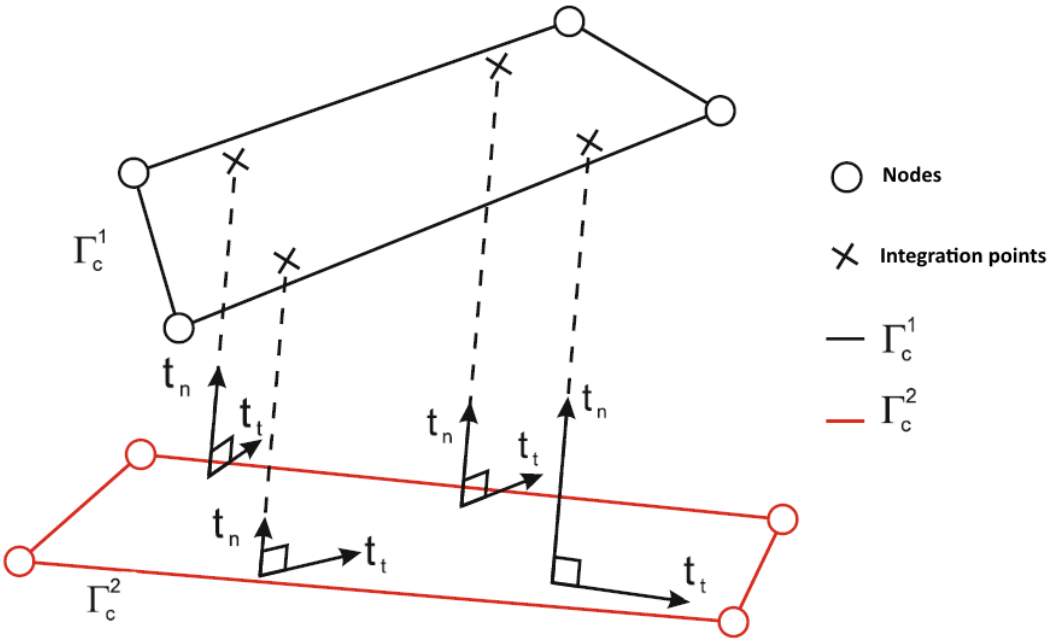

Slika A.1: Orthogonal projection for the detection of contact between two surfaces [149]

and the displacements. The idea is to regularize the contact laws allowing penetration of the two bodies provided that the contact surface tractions are proportional to the normal gap.

The penalty method needs some non-zero penetration to generate a normal contact force (this penetration can be physically described in terms of an elastic deformation of the contact surface), as well as some tangential motion to generate the tangential forces, even if the contact is sticking (here again, this might correspond to some elastic shear deformation of the asperities produced by the tangential forces).

B Getting fibres

When the 3D model of tooth, PDL and bone was made, next challenge was to put the fibres that describe PDL fibres and which should connect bone and tooth. Fibres are chosen to be described as a liner spring elements. Since connecting the nodes from tooth and bone is not easy to be done in 3D model, special algorithm in Matlab was made. Marc Mentat's function procedure can read Matlab's algorithm and make linear elements.
Between tooth and bone there is space that is filled with PDL matrix, and in that space PDL fibres should be put. In mouth PDL fibres are embedded in tooth and bone and filling the periodontal space, therefore, length of fibres is as thickness of periodontal space. Average thickness of PDL matrix in model was 1 mm. Fibres are connecting nodes from bone and the one from tooth, hence, which nodes belong to tooth and which to bone should be known.
The Matlab algorithm is able to read face nodes of bone and tooth. When all face nodes from bone and tooth are read, next step is to find the distance between the nodes. Average distance between nodes that are in contact with PDL matrix is 1 mm, as average thickness of PDL matrix, therefore, length of 1 mm is put as a maximum distance between face nodes of bone and tooth. Next step in algorithm is checking the distance between nodes. If the distance is 1 mm or less then the Marc Mentat puts linear element. If distance is more then 1 mm, nodes are skipped. Therefore, when code reads all nodes, next step was comparing the distance of nodes. When all nodes that have distance 1 mm or less are found, algorithm stops. In this way, fibres are put horizontally and under different angles. The flow chart of Matlab code is shown on Figure B.1.

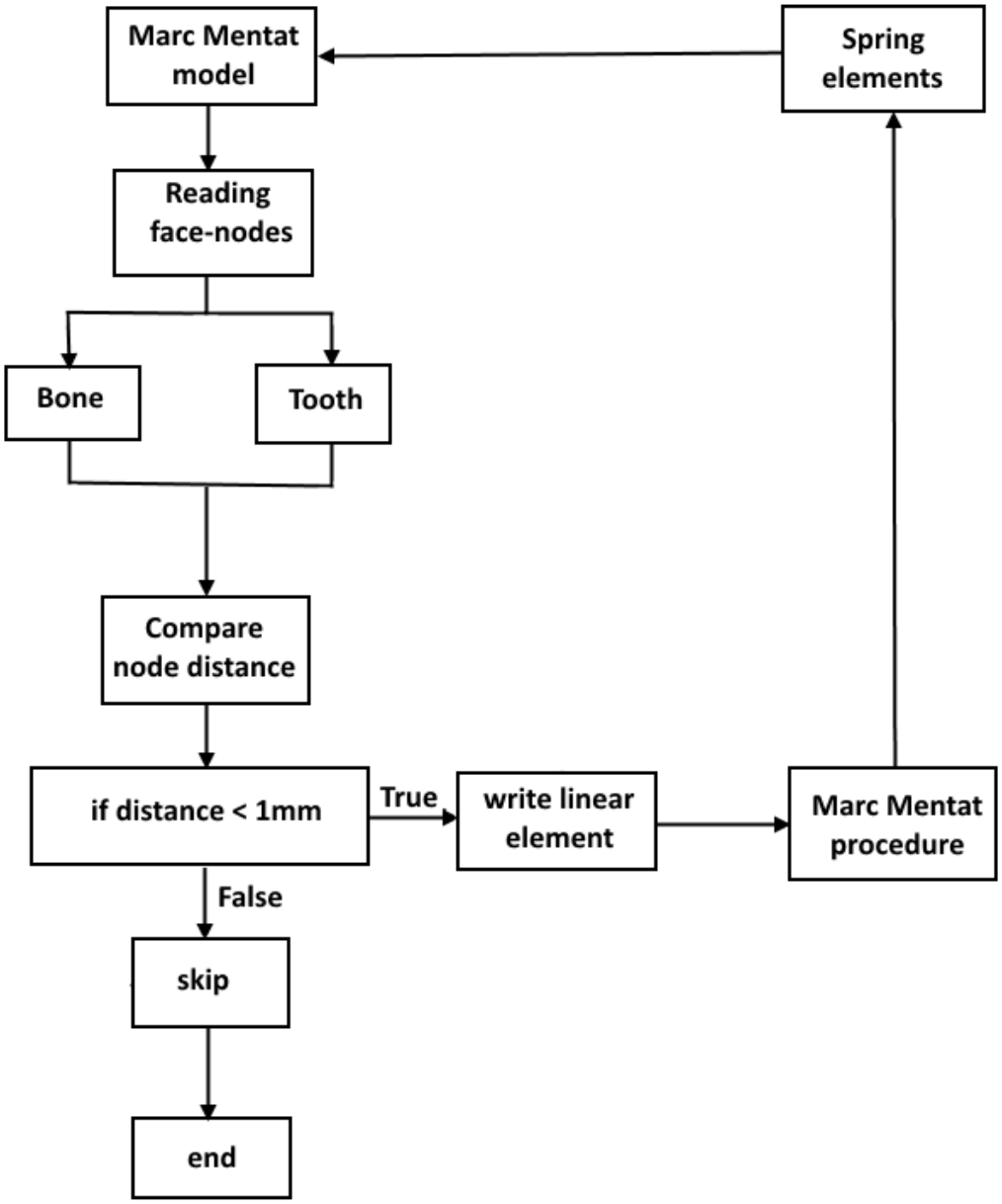

Slika B.1: Flow chart of getting PDL fibres

C Životopis

Jasna Leder Horina je rođena 24. kolovoza 1984. u Pakracu. Odrasla je u Daruvaru, gdje je završila osnovnu i srednju školu, Gimnaziju Daruvar. Akademske godine 2003./2004. upisuje Fakultet strojarstva i brodogradnje, studij strojarstva. Na drugoj godini studija se odlučuje za smjer Dizajn konstrukcija, te na trećoj godini studija na usmjerenje Dizajn medicinskih konstrukcija. Na tom usmjerenju je završila preddiplomski studij, te također i diplomski studij. Diplomski studij je završila 2008. pod mentorstvom prof. Tanje Jurčević Lulić i prof. Ivice Smojvera.

Po završetku studija zapošljava se u tvrtci Instrumentaria d.d. kao razvojni inženjer i konstruktor. U svibnju 2009. godine se zapošljava kao znanstvena novakinja na Fakultetu strojarstva i brodogradnje, Zavodu za tehničku mehaniku, Katedra za biomehaniku i ergonomiju. Iste godine upisuje doktorski studij na istom fakultetu, smjer Teorija konstrukcija. Prilikom zapošljavanja na fakultetu aktivno sudjeluje u izvođenju nastave na matičnom zavodu i katedri, te je uključena u znanstveni projekt Virtualna trodimenzijska primijenjena antropologija.

Dobitnica je stipendije za akademsku mobilnost Erasmus te stipendije potpore mobilnosti Institucijskog financiranja znanstvene djelatnosti. Obje stipendije je odradila na Fakultetu za Biomedicinsko inženjerstvo, Tehničkog sveučilišta u Eindhovenu, grupa ortopedska biomehanika pod mentorstvom prof. Berta van Rietbergena.

Aktivno sudjeluje u izvođenju nastave kolegija Katedre, te je također uključena u ostale znanstvene i stručne djelatnosti Katedre za biomehaniku i ergonomiju. Do sada je kao autor ili koautor objavila 8 znanstvenih radova u raznim časopisima i zbornicima radova u zemlji i inozemstvu. Članica je Hrvatskog društva za mehaniku, Europskog društva za biomehaniku i Hrvatskog ergonomijskog društva.

D Biography

Jasna Leder Horina was born on 24 August 1984 in Pakrac, Croatia. She grew up in Daruvar, where she finished elementary school and high school "Gimnazija Daruvar". In 2003 she enrolled in the BA program in Mechanical Engineering at the Faculty of Mechanical Engineering and Naval Architecture, University of Zagreb. In her second year she attended the course „Design of medical devices". She obtained her BA degree and continued her education in the same group . In 2008 she received her Mag. Ing. Mech. degree under the supervision of Prof. Tanja Jurčević Lulić and Prof. Ivica Smojver.

After finishing her studies, she started working in Instrumentaria d.d. as a designer and a development engineer. In May 2009 she started working as a research assistant at the Faculty of Mechanical Engineering and Naval Architecture at the Department of Applied Mechanics in the Chair of Biomechanics and Ergonomics. In 2009 she enrolled in the postgraduate program in Theory of Structures and Design.

During her work at the Faculty she has participated in teaching and has done research on the scientific project of the Chair.

She received the Erasmus mobility grant and the mobility support of the University of Zagreb. Both grants were used for her stay as visiting researcher at Eindhoven University of Technology, Netherlands. There she pursued research under the supervision of Prof. Bert van Rietbergen in the group for Orthopaedic Biomechanics at the Department of Biomedical Engineering.

So far she has published eight scientific papers in journals and proceedings as author and co-author. She is a member of the Croatian Society of Mechanics, the European Society of Biomechanics and the Croatian Ergonomics Society.

Bibliography

[1] J. C. Crockett, M. J. Rogers, F. P. Coxon, L. J. Hocking, and M. H. Helfrich. Bone remodelling at a glance. *Cell Science at a Glance* 124(7):991–998, 2011.

[2] S. C. Cowin. Wolff's law of trabecular architecture at remodeling equilibrium. *Journal of Biomechanical Engineering* 108(1):83–88, 1986.

[3] H. M. Frost. Bone mass and the mechanostat: A proposal. *The Anatomical Record* 219(1):1–9, 1987.

[4] H. M. Frost. Skeletal structural adaptations to mechanical usage (SATMU): 2. Redefining Wolff's Law: The remodeling problem. *The Anatomical Record* 226(4):414–422, 1990.

[5] H. M. Frost. Skeletal structural adaptations to mechanical usage (SATMU): 1. Redefining Wolff's Law: The bone modeling problem. *The Anatomical Record* 226(4):403–413, 1990.

[6] H. M. Frost. Wolff's law and bone's structural adaptations to mechanical usage: an overview for clinicians. *The Angle Orthodontist* 64(3):175–188, 1994.

[7] D. R. Carter. Mechanical loading histories and cortical bone remodeling. *Calcified Tissue International* 36(1):19–24, 1984.

[8] D. R. Carter. Mechanical loading history and skeletal biology. *Journal of Biomechanics* 20(11–12):1095–1109, 1987.

[9] G. S. Beaupré, T. E. Orr, and D. R. Carter. An approach for time-dependent bone modeling and remodeling-application: A preliminary remodeling simulation. *Journal of Orthopaedic Research* 8(5):662–670, 1990.

[10] G. S. Beaupre, T. E. Orr, and D. R. Carter. An approach for time-dependent bone modeling and remodeling-theoretical development. *Journal of Orthopaedic Research* 8(5):651–661, 1990.

[11] R. Huiskes, H. Weinans, H. Grootenboer, M. Dalstra, B. Fudala, and T. Slooff. Adaptive bone-remodeling theory applied to prosthetic-design analysis. *Journal of Biomechanics* 20(11–12):1135–1150, 1987.

[12] R. Huiskes, H. Weinans, and M. Dalstra. Adaptive bone-remodeling theory and biomechanical design considerations for noncemented total hip arthroplasty. *Journal of Orthopedics Research* 12(9):1255–1267, 1989.

[13] R. Huiskes, H. Weinans, and B. van Rietbergen. The relationship between stress shielding and bone resorption around total hip stems and the effects of flexible materials. *Clinical Orthopaedics and Related Research* 1(274):124–134, 1992.

[14] C. Bourauel, D. Freudenreich, D. Vollmer, D. Kobe, D. Drescher, and A. Jäger. Simulation of orthodontic tooth movements. a comparison of numerical models. *Journal of Orofacial Orthopedics / Fortschritte der Kieferorthopädie* 60:136–151, 1999.

[15] C. Bourauel, D. Vollmer, and A. Jäger. Application of bone remodeling theories in the simulation of orthodontic tooth movements. *Journal of Orofacial Orthopedics / Fortschritte der Kieferorthopädie* 61(4):266–279, 2000.

[16] C. Field, I. Ichim, M. V. Swain, E. Chan, M. A. Darendeliler, W. Li, and Q. Li. Mechanical responses to orthodontic loading: A 3-dimensional finite element multi-tooth model. *American Journal of Orthodontics and Dentofacial Orthopedics* 135(2):174–181, 2009.

[17] N. D. Penedo, C. N. Elias, M. C. T. Pacheco, and J. P. de Gouvêa. 3D simulation of orthodontic tooth movement. *Dental Press Journal of Orthodontics* 15:98–108, 2010.

[18] H. H. Ammar, P. Ngan, R. J. Crout, V. H. Mucino, and O. M. Mukdadi. Three-dimensional modeling and finite element analysis in treatment planning for orthodontic tooth movement. *American Journal of Orthodontics and Dentofacial Orthopedics* 139(1):59–71, 2011.

[19] M. Mengoni and J. Ponthot. An enhanced version of a bone-remodelling model based on the continuum damage mechanics theory. *Computer Methods in Biomechanics and Biomedical Engineering* 18(12):1367–1376, 2014.

[20] J. Tominaga, P. C. Chiang, H. Ozaki, M. Tanaka, Y. Koga, C. Bourauel, and N. Yoshida. Effect of play between bracket and archwire on anterior tooth movement

in sliding mechanics: A three-dimensional finite element study. *Journal of Dental Biomechanics* 3, 2012.

[21] A. V. Schepdael, J. V. Sloten, and L. Geris. Mechanobiological modeling can explain orthodontic tooth movement: Three case studies. *Journal of Biomechanics* 46(3):470–477, 2013.

[22] C. Wang, J. Han, Q. Li, L. Wang, and Y. Fan. Simulation of bone remodelling in orthodontic treatment. *Computer Methods in Biomechanics and Biomedical Engineering* 17(9):1042–1050, 2012.

[23] L. Borák, Z. Florian, S. Bartáková, P. Prachár, and N. Murakami. Bilinear elastic property of the periodontal ligament for simulation using a finite element mandible model. *Dental Materials Journal* 30(4):448–454, 2011.

[24] P. M. Cattaneo, M. Dalstra, and B. Melsen. Moment-to-force ratio, center of rotation, and force level: A finite element study predicting their interdependency for simulated orthodontic loading regimens. *American Journal of Orthodontics and Dentofacial Orthopedics* 133(5):681–689, 2008.

[25] P. M. Cattaneo, M. Dalstra, and B. Melsen. Strains in periodontal ligament and alveolar bone associated with orthodontic tooth movement analyzed by finite element. *Orthodontics and Craniofacial Research* 12:120–128, 2009.

[26] C. G. Provatidis. A comparative fem-study of tooth mobility using isotropic and anisotropic models of the periodontal ligament. *Medical Engineering and Physics* 22(5):359–370, 2000.

[27] C. G. Provatidis. An analytic model for stress analysis of a tooth in translation. *International Journal of Engineering Science* 39:1361–1381, 2001.

[28] C. T. Rubin and L. E. Lanyon. Regulation of bone formation by aplied dynamic loads. *The Journal of Bone and Joint Surgery* 66(3):397–402, 1984.

[29] L. E. Lanyon and C. T. Rubin. Static vs dynamic loads as an influence on bone remodelling. *Journal of Biomechanics* 17(12):897–905, 1984.

[30] M. Mengoni and J. Ponthot. Isotropic continuum damage/repair model for alveolar bone remodeling. *Journal of Computational and Applied Mathematics* 234(7):2036–2045, 2010.

[31] M. Mengoni, V. d'Otreppe, and J. Ponthot. A fully nonlinear finite element model for orthodontic tooth movement prediction. *10th International Symposium on Biomechanics and Biomedical Engineering*, 2012.

[32] A. N. Natali. *Dental Biomechanics*. CRC Press, 2003.

[33] B. Melsen. Tissue reaction to orthodontic tooth movement a new paradigm. *The European Journal of Orthodontics* 23(6):671–681, 2001.

[34] B. Melsen. Biological reaction of alveolar bone to orthodontic tooth movement. *The Angle Orthodontist* 69(2):151–158, 1999.

[35] A. V. Schepdael, J. V. Sloten, and L. Geris. A mechanobiological model of orthodontic tooth movement. *Biomechanics and Modeling in Mechanobiology* 12(2):249–265, 2012.

[36] J. H. Marangalou, F. Ghalichi, and B. Mirzakouchaki. Numerical simulation of orthodontic bone remodeling. *American Journal of Orthodontics and Dentofacial Orthopedics* 68:64–71, 2009.

[37] M. Doblaré and J. García. Anisotropic bone remodelling model based on a continuum damage-repair theory. *Journal of Biomechanics* 35(1):1–17, 2002.

[38] V. Krishnan and Z. Davidovitch. Cellular, molecular, and tissue-level reactions to orthodontic force. *American Journal of Orthodontics and Dentofacial Orthopedics* 129(4):469–469, 2006.

[39] S. Henneman, J. W. V. den Hoff, and J. C. Maltha. Mechanobiology of tooth movement. *The European Journal of Orthodontics* 30(3):299–306, 2008.

[40] S. Besdo. Determination of dynamically adapting anisotropic material properties of bone under cyclic loading. *Journal of Biomechanics* 44(2):272–276, 2011.

[41] K. Noel. *Synopsis of human anatomy and physiology*. Wm. C. Brown Publishers, USA, 1997.

[42] `http://myampgoesto11.tumblr.com/post/17081738326/daily-anatomy-anatomical-planes`. accessed: 2014-11-20.

[43] Gnatologija@net, 2001, `http://gnato.sfzg.hr/`.

[44] J. C. Nickel, P. Yao, P. M. Spalding, and L. R. Iwasaki. Validated numerical modeling of the effects of combined orthodontic and orthognathic surgical treatment on TMJ loads and muscle forces. *American Journal of Orthodontics and Dentofacial Orthopedics* 121(1):73–83, 2002.

[45] S. J. Nelson and M. M. Ash. *Wheeler s dental anatomy, physiology, and occlusion*. Sounders, Elsevier, St. Louis, Missouri, USA, 2010.

[46] `http://www.dentalhealth.ie/dentalhealth/teeth/toothtypes.html`. accessed: 2014-11-25.

[47] `http://medical-dictionary.thefreedictionary.com/accessional+teeth`. accessed: 2014-11-05.

[48] S. C. Cowin. *Bone Mechanics Handbook, Second Edition*. CRC Press, 2001.

[49] S. Cowin and D. Hegedus. Bone remodeling i: theory of adaptive elasticity. *Journal of Elasticity* 2(3):313–326, 1976.

[50] `http://www.anatomiahumana.ucv.cl/kine1/top2.html`. accessed: 2014-11-15.

[51] M. Bergomi. *Experimental and numerical investigations on the fluid contribution to the tensile-compressive mechanical behavior of the bovine periodontal ligament*. Ph.D. thesis, École polytechnique ́fedérale de Lausanne, 2008.

[52] R. van Oers. *Simulation of bone remodeling at the cellular scale*. Ph.D. thesis, University of Eindhoven, the Netherlands, 2010.

[53] D. J. Hadjidakis and I. I. Androulakis. Bone remodeling. *Annals of the New York Academy of Sciences* 1092:385–396, 2006.

[54] L. J. Raggatt and N. C. Partridge. Cellular and molecular mechanisms of bone remodeling. *The Journal of Biological Chemistry* 285:25103–25108, 2010.

[55] U. Kini and B. Nandeesh. Physiology of bone formation, remodeling, and metabolism. *Radionuclide and Hybrid Bone Imaging*, pp. 29–57. Springer Berlin Heidelberg, 2012.

[56] `https://imueos.wordpress.com/2010/09/29/bone-physiology/`. accessed: 2014-11-27.

[57] A. Nanci and D. D. Bosshardt. Structure of periodontal tissues in health and disease. *Periodontology 2000* 40(1):11–28, 2006.

[58] H. F. Wolf, K. H. Rateitschak, and E. M. Rateitschak-Plüss. *Parodontologija*. Naklada Slap, 2009.

[59] W. Beertsen, C. A. G. McCulloch, and J. Sodek. The periodontal ligament: a unique, multifunctional connective tissue. *Periodontology 2000* 13(1):20–40, 1997.

[60] G. Singh. *Textbook of Orthodontics*. Jaypee Brothers Medical Publishers, New Delhi, India, 2007.

[61] `http://dentalandspa.com/samopouzdanje_i_zadovoljstvo_uz_lijep_i_pravilan_osmijeh.html`. accessed: 2014-12-20.

[62] R. Nanda. *Biomechanics and esthetic strategies in clinical orthodontics*. Sounders, Elsevier, St. Louis, Missouri, USA, 2005.

[63] M. Hinterkausen, C. Bourauel, G. Siebers, A. Haase, D. Drescher, and B. Nellen. In vitro analysis of the initial tooth mobility in a novel optomechanical set up. *Medical Engineering and Physics* 20(1):40–49, 1998.

[64] S. R. Toms and A. W. Eberhardt. A nonlinear finite element analysis of the periodontal ligament under orthodontic tooth loading. *American Journal of Orthodontics and Dentofacial Orthopedics* 123(6):657–665, 2003.

[65] B. Melsen, P. M. Cattaneo, M. Dalstra, and D. C. Kraft. The importance of force levels in relation to tooth movement. *Seminars in Orthodontics* 13(4):220–233, 2007.

[66] R. S. Nanda and Y. S. Tosun. *Biomechanics in Orthodontics: Principles and Practice*. Quintessence Publishing Co Inc, 2010.

[67] Y. Ren, J. C. Maltha, and A. M. Kuijpers-Jagtman. Optimum force magnitude for orthodontic tooth movement: A systematic literature review. *Angle Orthodontist* 73(1):86–92, 2003.

[68] Y. Ren, J. C. Maltha, M. A. V. Hof, and A. M. Kuijpers-Jagtman. Optimum force magnitude for orthodontic tooth movement: A mathematic model. *American Journal of Orthodontics and Dentofacial Orthopedics* 25(1):71–77, 2004.

[69] R. S. Quinn and D. K. Yoshikawa. A reassessment of force magnitude in orthodontics. *American Journal of Orthodontics* 88(3):252–260, 1985.

[70] E. H. Hixon, H. Atikian, G. E. Callow, H. W. McDonald, and R. J. Tacy. Optimal force, diferential force, and anchorage. *American Journal of ORTHODONTICS* 55(1):437–457, 1969.

[71] G. Andreasen and P. Johnson. Experimental findings on tooth movements under two donditions of applied force. *Angle Orthod* 37(9):9–12, 1967.

[72] D. Vollmer, C. Bourauel, and K. Maier. Determination of the centre of resistance in an upper human canine and idealized tooth model. *The European Journal of Orthodontics* 21:633–648, 1999.

[73] `http://www.dentalpedia.ca/biomechanics/physics-in-orthodontics/tooth-movements/`. accessed: 2014-12-21.

[74] A. C. Kak and M. Slaney. *Principles of Computerized Tomographic Imaging*. Society for Industrial and Applied Mathematics, 2001.

[75] V. d'treppe de Bouvette. *From medical imaging to finite element simulations: a contribution to mesh generation and locking-free formulations for tetrahedra*. Ph.D. thesis, Université de Liége, 2012.

[76] J. Zhang, C. Yan, C. Chui, and S. Ong. Fast segmentation of bone in ct images using 3d adaptive thresholding. *Computers in Biology and Medicine* 40(2):231–236, 2010.

[77] T. Hangartner. Thresholding technique for accurate analysis of density and geometry in qct, pqct and μct images. *Journal of Musculoskelet Neuronal Interact* 7(1):9–16, 2007.

[78] G. N. Hounsfield. Computes medical imaging, Nobel Lecture, December 8, 1979. *Journal of Computer Assisted Tomography* 4(5):665–674, 1980.

[79] A. Katsumata, A. Hirukawa, S. Okumura, M. Naitoh, M. Fujishita, E. Ariji, and R. P. Langlais. Effects of image artifacts on gray-value density in limited-volume cone-beam computerized tomography. *Oral Surgery, Oral Medicine, Oral Pathology, Oral Radiology, and Endodontology* 104(6):829–836, 2007.

[80] Mimics. Materialise, 2014, `http://biomedical.materialise.com`. 2014-12-27.

[81] J. J. Schreiber, P. A. Anderson, H. G. Rosas, A. L. Buchholz, and A. G. Au. Hounsfield Units for Assessing Bone Mineral Density and Strength: A Tool for Osteoporosis Management. *The Journal of Bone and Joint Surgery* 11(93):1057–1063, 2011.

[82] P. Mah, T. E. Reeves, and W. D. McDavid. Deriving hounsfield units using grey levels in cone beam computed tomography. *Dentomaxillofacial Radiology* 39(6):323–335, 2009.

[83] M. O. L. Vich. *Analysis of Skeletal and Dental Changes with a Tooth-Borne and a Bone-Borne Maxillary Expansion Appliance assessed through Digital Volumetric Imaging*. Ph.D. thesis, University of Alberta, 2009.

[84] D. A. Miles. *Atlas of cone beam imaging for dental applications*. Quintessence Publishing Co, Inc, 2013.

[85] W. C. Scarfe, A. G. Farman, and P. Sukovic. Clinical applications of cone-beam computed tomography in dental practice. *Journal of Canadian Dental Association* 72(1):75–80, 2006.

[86] T. Lauc. 3D diagnostics in orofacial region. *Rad hrvatske akademije znanosti i umjetnosti, knjiga 514*, pp. 127–152. Hrvatska akademija znanosti i umjetnosti, 2012.

[87] T. Lauc. Suvremene elektrodijagnostičke metode i njihova primjena u osoba s temporomandibularnim poremećajima. *Kompjuterska tomografija bazirana na koničnoj zraci u dijagnostici antropoloskih varijacija i poremećaja temporomandibularnog zgloba*, pp. 59–73. Hrvatska akademija znanosti i umjetnosti, 2014.

[88] E. Hamed, Y. Lee, and I. Jasiuk. Multiscale modeling of elastic properties of cortical bone. *Acta Mechanica* 213(1-2):131–154, 2010.

[89] S. C. Cowin. *Tissue Mechanics*. Springer, 2006.

[90] J. Currey. Incompatible mechanical properties in compact bone. *Journal of Theoretical Biology* 231(4):569–580, 2004.

[91] J. H. Marangalou, K. Ito, M. Cataldi, F. Taddei, and B. van Rietbergen. A novel approach to estimate trabecular bone anisotropy using a database approach. *Journal of Biomechanics* 46:2356–2362, 2013.

[92] D. C. Newitt, S. Majumdar, B. van Rietbergen, G. von Ingersleben, S. T. Harris, H. K. Genant, C. Chesnut, P. Garnero, and B. MacDonald. In vivo assessment of architecture and micro-finite element analysis derived indices of mechanical properties of trabecular bone in the radius. *International Osteoporosis Foundation and National Osteoporosis Foundation* 13:6–17, 2002.

[93] D. C. Newitt, B. van Rietbergen, and S. Majumdar. Processing and analysis of in vivo high-resolution mr images of trabecular bone for longitudinal studies: Reproducibility of structural measures and micro-finite element analysis derived mechanical properties. *International Osteoporosis Foundation and National Osteoporosis Foundation* 13:278–287, 2002.

[94] P. K. Zysset. A review of morphology elasticity relationships in human trabecular bone: theories and experiments. *Journal of Biomechanics* 36(10):1469–1485, 2003.

[95] M. Doblaré and J. García. Application of an anisotropic bone-remodelling model based on a damage-repair theory to the analysis of the proximal femur before and after total hip replacement. *Journal of Biomechanics* 34(9):1157–1170, 2001.

[96] U. Wolfram, H. J. Wilke, and P. K. Zysset. Rehydration of vertebral trabecular bone: Influences on its anisotropy, its stiffness and the indentation work with a view to age, gender and vertebral level. *Bone* 46(2):348–354, 2010.

[97] H. S. Hosseini, D. H. Pahr, and P. K. Zysset. Modeling and experimental validation of trabecular bone damage, softening and densification under large compressive strains. *Journal of the Mechanical Behavior of Biomedical Materials* 15(0):93–102, 2012.

[98] M. Charlebois, M. Jirsásek, and P. K. Zysset. A nonlocal constitutive model for trabecular bone softening in compression. *Biomechanics and Modeling in Mechanobiology* 9:597–611, 2010.

[99] J.-Y. Rho, L. Kuhn-Spearing, and P. Zioupos. Mechanical properties and the hierarchical structure of bone. *Medical Engineering and Physics* 20(2):92–102, 1998.

[100] R. Schneider, G. Faust, U. Hindenlang, and P. Helwig. Inhomogeneous, orthotropic material model for the cortical structure of long bones modelled on the basis of clinical ct or density data. *Inhomogeneous, orthotropic material model for the cortical structure of long bones modelled on the basis of clinical CT or density data* 198(27–29):2167–2174, 2009.

[101] E. Hamed, E. Novitskaya, J. Li, P.-Y. Chen, I. Jasiuk, and J. McKittrick. Elastic moduli of untreated, demineralized and deproteinized cortical bone: Validation of a theoretical model of bone as an interpenetrating composite material. *Acta Biomaterialia* 8:1080–1092, 2012.

[102] A. A. Abdel-Wahab, K. Alam, and V. V. Silberschmidt. Analysis of anisotropic viscoelastoplastic properties of cortical bone tissues. *Journal of the Mechanical Behavior of Biomedical Materials* 4:807–820, 2011.

[103] L. Duchemin, V. Bousson, C. Raossanaly, C. Bergot, J. Laredo, W. Skalli, and D. Mitton. Prediction of mechanical properties of cortical bone by quantitative computed tomography. *Medical Engineering ad Physics* 30:321–328, 2008.

[104] E. Novitskaya, P. Y. Chen, S. Lee, A. C.-C. na, G. Hirata, V. A. Lubarda, and J. McKittrick. Anisotropy in the compressive mechanical properties of bovine cortical bone and the mineral and protein constituents. *Acta Biomaterialia* 7:3170–3177, 2011.

[105] M. Szabó and P. Thurner. Anisotropy of bovine cortical bone tissue damage properties. *Journal of Biomechanics* 46:2–6, 2013.

[106] B. Helgason, E. Perilli, E. Schileo, F. Taddei, S. Brynjolfsson, and M. Viceconti. Mathematical relationships between bone density and mechanical properties: A literature review. *Clinical Biomechanics* 23:135–146, 2008.

[107] S. Boutroy, B. V. Rietbergen, E. Sornay-Rendu, F. Munoz, M. L. Bouxsein, and P. D. Delmas. Finite element analysis based on in vivo hr-pqct images of the distal radius is associated with wrist fracture in postmenopausal women. *Journal of Bone and Mineral Research* 23(3):392–399, 2008.

[108] E. Dall'Ara, R. Schmidt, D. Pahr, P. Varga, Y.Chevalier, J. Patsch, F. Kainberger, and P. Zysset. A nonlinear finite element model validation study based on a novel experimental technique for inducing anterior wedge-shape fractures in human vertebral bodies in vitro. *Journal of Bone* 43:2374–2380, 2010.

[109] E. Dall'Ara, B. Luisier, R. Schmidt, F. Kainberger, P. Zysset, and D. Pahr. A nonlinear qct-based finite element model validation study for the human femur tested in two configurations in vitro. *Bone* 52:27–38, 2013.

[110] D. Pahr, J. Schwiedrzik, E. Dall'Ara, and P. Zysset. Clinical versus pre-clinical fe models for vertebral body strength predictions. *Journal and the Mechanical Behavior of Biomedical Materials* 33:76–83, 2014.

[111] H. M. Frost. Bone's mechanostat: A 2003 update. *The Anatomical Record Part A: Discoveries in Molecular, Cellular, and Evolutionary Biology* 275(2):1–10, 2003.

[112] C. Hernandez, G. Beaupré, T. Keller, and D. Carter. The influence of bone volume fraction and ash fraction on bone strength and modulus. *Bone* 29(1):74–78, 2001.

[113] H. Weinans, R. Huiskes, and H. Grootenboer. The behavior of adaptive bone-remodeling simulation models. *Journal of Biomechanics* 25(12):1425 – 1441, 1992.

[114] B. van Rietbergen, R. Huiskes, H. Weinans, D. Sumner, T. Turner, and J. Galante. The mechanism of bone remodeling and resorption around press-fitted tha stems. *Journal of Biomechanics* 26(4–5):369–382, 1993.

[115] C. R. Jacobs. The mechanobiology of cancellous bone structural adaptation. *Journal of Rehabilitation Research and Development* 37(2):209–216, 2000.

[116] C. R. Jacobs, J. C. Sirno, G. S. Beaupré, and D. R. Carter. Adaptive bone remodeling incorporating simultaneous density and anisotropy considerations. *Journal of Biomecanics* 30(6):603–613, 1997.

[117] P. J. Prendergast and D. Taylor. Prediction of bone adaptation using damage accumulation. *Journal of Biomechanics* 27(8):1067–1076, 1994.

[118] L. M. McNamara and P. J. Prendergast. Bone remodelling algorithms incorporating both strain and microdamage stimuli. *Journal of Biomechanics* 40:1381–1391, 2006.

[119] J. R. Fernandez, J. M. Garcia-Aznar, R. Martinez, and J. Viano. Numerical analysis of a strain-adaptive bone remodelling problem. *Computer Methods in Applied Mechanics and Engineering* 199:1549–1557, 2010.

[120] J. R. Fernandez, J. M. Garcia-Aznar, and R. Martinez. Numerical analysis of a diffusive strain-adaptive bone remodelling theory. *International Journal of Solids and Structures* 49:2085–2093, 2012.

[121] A. Idhammad and A. Abdali. On a new law of bone remodeling based on damage elasticity: A thermodynamic approach. *Theoretical Biology and Medical Modelling* -:51–62, 2012.

[122] A. Idhammad, A. Abdali, and N. Alaa. Computational simulation of the bone remodeling using the finite element method: An elastic-damage theory for small displacements. *Theoretical Biology and Medical Modelling* 10:10–21, 2013.

[123] J. Currey. The effect of porosity and mineral content on the young's modulus of elasticity of compact bone. *Journal of Biomechanics* 21(2):131–139, 1988.

[124] P. Pivonka, J. Zimak, D. W. Smith, B. S. Gardiner, C. R. Dunstan, N. A. Sims, T. J. Martin, and G. R. Mundy. Model structure and control of bone remodeling: A theoretical study. *Bone* 43:249–263, 2008.

[125] P. Pivonka, P. R. Buenzli, S. Scheiner, C. Hellmich, and C. R. Dunstan. The influence of bone surface availability in bone remodelling - a mathematical model including coupled geometrical and biomechanical regulations of bone cells. *Engineering Structures* 47:134–147, 2013.

[126] T. Adachi, Y. Kameo, and M. Hojo. Trabecular bone remodelling simulation considering osteocytic response to fluid-induced shear stress. *Philosophical Transactions of the Royal Society A: Mathematical, Physical and Engineering Sciences* 368:2669–2682, 2010.

[127] R. Ruimerman, P. Hilbers, B. van Rietbergen, and R. Huiskes. A theoretical framework for strain-related trabecular bone maintenance and adaptation. *Journal of Biomechanics* 38:931–941, 2005.

[128] R. Ruimerman and R. Huiskes. Development of a unifying theory for mechanical adaptation and maintenance of trabecular bone. *Theoretical Issues in Ergonomics Science* 6:225–238, 2005.

[129] R. Ruimerman, B. van Rietbergen, P. Hilbers, and R. Huiskes. The effects of trabecular-bone loading variables on the surface signaling potential for bone remodeling and adaptation. *Annals of Biomedical Engineering* 33:71–78, 2005.

[130] E. Verhulp, B. van Rietbergen, and R. Huiskes. Comparison of micro-level and continuum-level voxel models of the proximal femur. *Journal of Biomechanics* 39:2951–2957, 2006.

[131] E. Verhulp, van Rietbergen, R. Müller, and R. Huiskes. Indirect determination of trabecular bone effective tissue failure properties using micro-finite element simulations. *Journal of Biomechanics* 41, 2008.

[132] E. Verhulp, B. van Rietbergen, and R. Huiskes. Load distribution in the healthy and osteoporotic human proximal femur during a fall to the side. *Bone* 42:30–35, 2008.

[133] S. Scheiner, P. Pivonka, and C. Hellmich. Coupling systems biology with multiscale mechanics, for computer simulations of bone remodeling. *Computer Methods in Applied Mechanics and Engineering* 254:181–196, 2013.

[134] C. Field, Q. Li, W. Li, and M. V. Swain. Biomechanical response in mandibular bone due to mastication loading on 3-unit fixed partial dentures. *Journal of Dental Biomechanics* 1(1):1–11, 2010.

[135] C. Field, Q. Li, W. Li, and M. Swain. Influence of tooth removal on mandibular bone response to mastication. *Archives of Oral Biology* 53(12):1129–1137, 2008.

[136] J. Reinaa, J. Garcá-Aznar, J. Domíngueza, and M. Doblaré. Numerical estimation of bone density and elastic constants distribution in a human mandible. *Journal of Biomechanics* 40:828–836, 2007.

[137] C. Field, Q. Li, W. Li, M. Thompson, and M. Swain. Prediction of mandibular bone remodelling induced by fixed partial dentures. *Journal of Biomechanics* 43(9):1771–1779, 2010.

[138] A. Natali, P. Pavan, E. Carniel, and C. Dorow". A transversally isotropic elasto-damage constitutive model for the periodontal ligament. *Computer Methods in Biomechanics and Biomedical Engineering* 6(5–6):329–336, 2006.

[139] G. Pietrzak, A. Curnier, J. Botsis, S. Scherrer, A. Wiskott, and U. Belser. A nonlinear elastic model of the periodontal ligament and its numerical calibration for the study of tooth mobility. *Computer Methods in Biomechanics and Biomedical Engineering* 2(5):91–100, 2010.

[140] G. Limbert, C. van Lierde, O. L. Muraru, X. F. Walboomers, M. Frank, S. Hansson, J. Middleton, and S. Jaecques. Trabecular bone strains around a dental implant and associated micromotions a microct-based threedimensional finite element study. *Journal of Biomechanics* 43:1251–1261, 2010.

[141] M.-Z. Su, H.-H. Chang, Y.-C. Chiang, J.-H. Cheng, L.-J. Fuh, C.-Y. Wang, and C.-P. Lin. Modeling viscoelastic behavior of periodontal ligament with nonlinear finite element analysis. *Journal of Dental Sciences* 8(2):121–128, 2013.

[142] R. Aversa, D. Apicella, L. Perillo, R. Sorrentino, F. Zarone, M. Ferrari, and A. Apicella. Non-linear elastic three-dimensional finite element analysis on the effect of endocrown material rigidity on alveolar bone remodeling process. *Dental Materials* 25:678–690, 2009.

[143] S. R. Toms, G. J. Dakin, J. E. Lemons, and A. W. Eberhardt. Quasi-linear viscoelastic behavior of the human periodontal ligament. *Journal of Biomechanics* 35:1411–1415, 2001.

[144] H. Qian, J. Chen, and T. R. Katona. The influence of pdl principal fibers in a 3-dimensional analysis of orthodontic tooth movement. *American Journal of Orthodontics and Dentofacial Orthopedics* 120(3):272–279, 2001.

[145] Marc mentat, `http://www.mscsoftware.com/`. 2014-12-27.

[146] B. Martin. The effects of geometric feedback in the development of osteoporosis. *Journal of Biomechanics* 5:447–455, 1972.

[147] R. F. Viecilli, T. R. Katona, J. Chen, J. K. Hartsfield, and W. E. Roberts. Three-dimensional mechanical environment of orthodontic tooth movement and root resorption. *American Journal of Orthodontics and Dentofacial Orthopedics*, 2008.

[148] V. Sansalone, A. A. Kachi, and S. Naili. A finite element study of two orthodontic treatment steps. *IFMBE Proceedings*, vol. 31, 2010.

[149] P. Bussetta, D. Marceau, and J.-P. Ponthot. The adapted augmented lagrangian method: a new method for the resolution of the mechanical frictional contact problem. *Computational Mechanics* 49:259–275, 2012.